The PHILOSOPHICAL MAGAZINE

FIRST PUBLISHED IN 1798

. 43 SEVENTH SERIES No. 347 December, 1952

A Journal of Theoretical Experimental and Applied Physics

PRICE 15s. 0d.
Annual Subscription £8 0s. 0d. payable in advance

AND PUBLISHED BY TAYLOR & FRANCIS LTD., RED LION COURT, FLEET ST., LONDON, E.C.4.

ADVANCES IN PHYSICS

A QUARTERLY SUPPLEMENT OF THE PHILOSOPHICAL MAGAZINE

On 1st January, 1952, the first number of this new Quarterly Supplement to the Philosophical Magazine was published. The aim of this Supplement will be to give those interested in physics comprehensive and authoritative accounts of recent important developments. It is felt by the Editor that in view of the rapid advances in many branches of physics, scientists will welcome a journal devoted to articles of this type.

CONTENTS FOR VOLUME 1, 1952 NOS. 1-4

PRICE *per part* **15/-** *plus postage* **PRICE** *per annum* **£2 15s. 0d.** *post free*

Printed and Published by
TAYLOR & FRANCIS, LTD., RED LION COURT, FLEET ST., LONDON, E.C.4

CXXIII. *Some Properties of Lines on Divergent-beam X-ray Photographs*

By A. G. Peace and G. E. Pringle
Department of Inorganic and Physical Chemistry, University of Leeds*

[Received August 25, 1952]

Summary

The quantitative aspect of x-ray extinction is reconsidered in its particular relation to divergent-beam photography. Special consideration is given to the optical resolution obtainable with the usual experimental arrangements, and some experimental data on unresolved lines are discussed. This leads to a determination of the mosaic spread of crystals previously conditioned by liquid air treatment to minimize primary extinction effects, but in general quantitative conclusions are hampered by the usual doubt as to how much of the observed extinction is primary and how much secondary.

List of Symbols

a=spacing of reflecting planes.
$A=\sqrt{(A'A'')}$.
$A'=q\times$number of reflecting planes intersected by a line parallel to the reflected beam.
$A''=q\times$number of reflecting planes intersected by incident ray.
c=ratio in which absorption is diminished by Borrmann effect.
C_1=Euler's constant.
C_2=a constant, approximately 0·25.
$G(u)$=the partition of Q as a function of u.
$G'(u)$=the partition of Q' as a function of u.
$G_1(u)=G(u)$ modified by Borrmann effect.
I_0=Bessel function of imaginary argument, order zero.
I_1=Bessel function of imaginary argument, order 1.
J_0=Bessel function of order zero.
J_1=Bessel function of order 1.
K=ratio of white radiation intensity to characteristic.
m=variable number of multiple reflections.
q=amplitude of beam reflected by one plane when the incident beam has unit amplitude.
Q=volume reflecting power for given set of planes.
$Q'=Q$ diminished by primary extinction.
$\mathscr{R}(x)$=intensity of reflected beam at position x in direction of incidence.

---

* Communicated by Professor E. G. Cox.

$\mathscr{S}(z)$=function defined by Darwin, expressing the integrated reflection by transmission through a mosaic (§ 3).

$\mathscr{T}(x)$=intensity of emergent beam at position x.

t=depth in crystal.

t'=depth in crystal measured obliquely in direction of reflection.

t''=depth in crystal measured obliquely in direction of incidence.

T, T', T''=final values of t, t', t'' respectively at exit surface.

x=fractional coordinate of point of exit.

y=$(1-x)$.

z=argument of functions $\mathscr{S}$ and I_0.

β=factor expressing source size.

$$\delta=\frac{2\pi}{\lambda}\frac{ua\cos\theta}{q}\sqrt{\left(\frac{\sin\overline{\phi-\theta}}{\sin\overline{\phi+\theta}}\right)}.$$

$$\epsilon=\frac{\mu+G'}{G'}\frac{T'-T''}{2\sqrt{(T'T'')}}.$$

λ=wavelength of characteristic radiation.

η=mosaic spread in given plane.

θ=Bragg angle.

ϑ=angular half width of divergent-beam line for monochromatic radiation.

ϕ=inclination of reflecting planes to crystal surface.

μ=ordinary absorption coefficient of characteristic radiation.

σ=contrast of divergent-beam line against neighbouring background.

σ_m=contrast in absence of white radiation.

ξ=diffraction width.

Υ=absorption ratio for white radiation/absorption ratio for characteristic.

$\omega(u)$=weighting function expressing source shape.

§ 1. Introduction

Methods of producing transmission photographs of crystalline specimens with wide divergent x-ray beams have been described by various authors (e.g. Borrmann 1941, Lonsdale 1943, May 1949). Amongst many physically important applications is the study of extinction effects and the textural investigation of single crystals (e.g. Lonsdale 1947 a and b). One of the differences from parallel-beam photography in practice is that divergent-beam photographs can often be obtained in a matter of a few seconds and this recommends them as a means of sorting a batch of crystals into grades of different microscopic texture. In deciding whether the information so used can be pursued to quantitative conclusions, we have first to consider the adequacy of extinction theory and its relevance to the divergent-beam arrangement. On this basis (§ 2) we can attempt to correlate extinction coefficients with measurements of line width (§ 3). The further step (§ 5) of converting results of measurement into knowledge of primary extinction factors and of block

dimensions is hampered by uncertainty of the theoretical factors for finite blocks, and by the difficulty of separating primary extinction effects from secondary.

§ 2. Resolution and Line Structure

In Darwin's paper (1922) the relevant theory is presented for parallel beams of x-rays which are unlimited in lateral extent. The arrangement for producing divergent-beam photographs, such as the one we have

Fig. 1

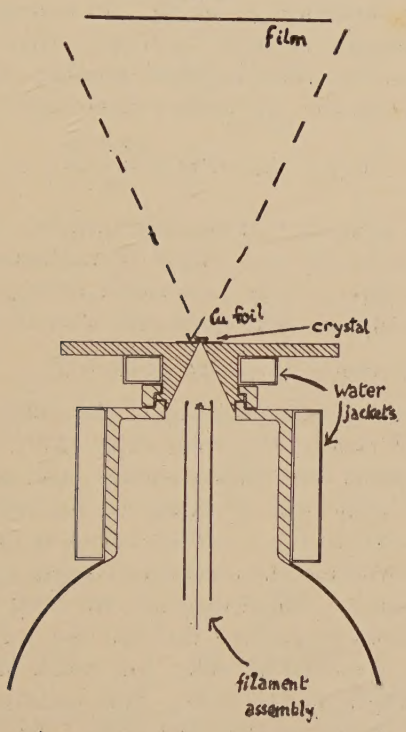

Siemens tube fitted with transmission target as used for divergent-beam photography.

used (fig. 1) depends for its success on employing a small x-ray source, smaller than the slab of crystal covering it, so that the simple theory can be supplemented for this case by studying the behaviour of a narrow beam of x-rays passing through a single crystal, assumed in what follows to be a plate with parallel faces. Without recourse to differential equations we can see from the theory of secondary extinction (Darwin *loc. cit.*) that, ignoring rays reflected back into the beam, the apparent attenuation of a given monochromatic primary ray incident on a mosaic crystal at an angle differing by a small amount u from a reflecting angle is

$$\exp\left[-\{\mu+G'(u)\}t'\right], \quad . \quad . \quad . \quad . \quad . \quad . \quad . \quad . \quad (2.1)$$

where μ is the ordinary true linear absorption coefficient, t' is the variable path length in the crystal at depth t and $G'(u)$ is the partition of Q' the volume reflection coefficient for the planes in question, i.e.

$$G'(u)=G'(0)\exp(-u^2/2\eta^2)=\frac{Q'}{\eta\sqrt{(2\pi)}}\exp(-u^2/2\eta^2). \quad . \quad . \quad (2.2)$$

The argument of G' will usually be omitted for brevity in what follows. Corresponding unprimed quantities G and Q refer to the ideal mosaic conditions with negligible primary extinction. The exponential expression (2.1) can be regarded as a ' probability of survival ' of a packet of energy. Pursuing a statistical argument, we equate the probability of reflection per unit length of path to $G'(u)$; then the probability of arrival at the exit surface after an even number of reflections, m, can easily be shown to be, in the ' symmetric Laue case '

$$\exp[-(\mu+G')T']\frac{(G'T')^m}{m!},$$

where T' is the final value of t' at the exit surface. For the moment we confine our discussion to this case, which is mathematically the simplest because $\exp(-\mu T')$ appears only as a factor throughout. The primary beam together with all even reflections give a total of

$$\exp[-(\mu+G')T']\cosh G'T'$$

whereas the ' reflected ' beam, consisting of the sum of the odd reflections gives $\exp[-(\mu+G')T']\sinh G'T'$; total $\exp(-\mu T')$. In a certain sense therefore, the two beams are complementary, and the power deficiency of the transmitted beam will be equal to the reflected power if the background proportional to $\exp(-\mu T')$ is taken as the level of reference.

In order to decide whether the constituent terms comprising these two beams are, experimentally, added together, we need to know the lateral spread of the reflections in passing through the crystal. We find that the beam does tend to spread laterally, but much more slowly than the first power of the depth in the slab. This conclusion follows from a statistical argument similar to that just used. Adapting this argument to the geometry of fig. 2 where x and y $(=1-x)$ are fractional co-ordinates of the point of exit in the range BC, we find that the intensities of multiple reflections issuing at the point x when unit power is incident in the form of a sufficiently narrow beam on the first surface can be expressed for the general Laue case as

(*a*) Mosaic crystal

$$\left.\begin{aligned}
&\text{Transmitted,} \quad \mathscr{T}(x)=\exp[-(\mu+G')(xT'+yT'')] \\
&\qquad\qquad G'\sqrt{\left(\frac{yT''}{xT'}\right)}I_1[2G'\sqrt{(xyT'T'')}]\operatorname{cosec}2\theta. \\
&\text{Reflected,} \quad \mathscr{R}(x)=\exp[-(\mu+G')(xT'+yT'')] \\
&\qquad\qquad G'I_0[2G'\sqrt{(xyT'T'')}]\operatorname{cosec}2\theta.
\end{aligned}\right\} \quad (2.3)$$

(*b*) Perfect non-absorbing crystal; in this case, incident intensity × (width)^2 is equated to unity.

$$\left.\begin{aligned}\text{Transmitted,}\quad & \mathscr{T}(x)=\left\{\frac{q}{2a\cos\theta}\sqrt{\left(\frac{yT''}{xT'}\right)}J_1[2\sqrt{(xyA'A'')}]\right\}^2.\\ \text{Reflected,}\quad & \mathscr{R}(x)=\left\{\frac{q}{2a\cos\theta}J_0[2\sqrt{(xyA'A'')}]\right\}^2,\end{aligned}\right\}\quad (2.4)$$

where T' and T'' are the two extreme path lengths in the crystal:

$$T'=T\ \text{cosec}\ (\phi+\theta),$$
$$T''=T\ \text{cosec}\ (\phi-\theta),$$

Fig. 2

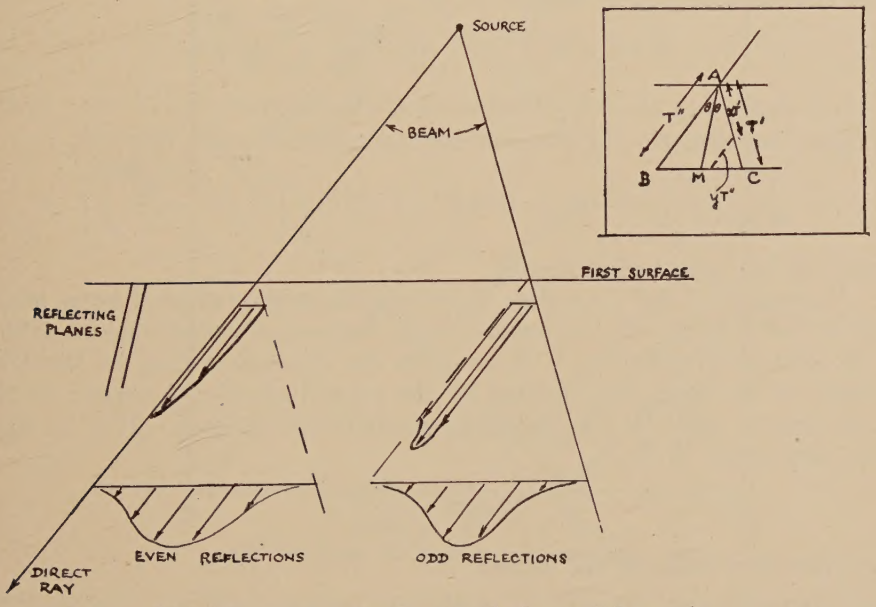

Multiple x-ray reflections in thick crystal mosaic.

where T is the true thickness of the crystal plate, and similarly A', A'' are the numbers of reflecting planes intersected by T' and T'', multiplied by q, the reflecting power of one plane; if a is the spacing of the reflecting planes

$$A'=qT'\sin\theta/a,$$
$$A''=qT''\sin\theta/a.$$

J_0 and I_0 are Bessel functions of zero order of real and imaginary argument; J_1 and I_1 are of the first order. In these expressions we assume no limit to the maximum possible number of secondary reflections: if this were done we should have to curtail the power-series development of 2.3 and 2.4 at the appropriate stage.

By integrating the reflected amplitude for the perfect crystal over the range of values of x and making allowance for phase, we recover Waller's formula (1926) for the power of the reflected beam

$$\sin^2 A\sqrt{(1+\delta^2)}/1+\delta^2,$$

where $A=\sqrt{(A'A'')}$

and $$\delta=\frac{2\pi}{\lambda}\frac{ua\cos\theta}{q}\sqrt{\left(\frac{\sin\overline{\phi-\theta}}{\sin\overline{\phi+\theta}}\right)}.$$

The corresponding formula for the mosaic crystal is

$$\exp\left[-(\mu+G')\left(\frac{T'+T''}{2}\right)\right]\sqrt{\left(\frac{T''}{T'}\right)}\sinh B\sqrt{(1+\epsilon^2)}/\sqrt{(1+\epsilon^2)}$$

for the reflected power where

$$B=G'\sqrt{(T'T'')}, \qquad \epsilon=\frac{\mu+G'}{G'}\frac{T'-T''}{2\sqrt{(T'T'')}},$$

which reduces to Darwin's formula in the symmetric case ($\epsilon=0$); in the slightly asymmetric case we obtain a fair approximation by

$$\frac{1}{2}\sqrt{\left(\frac{T''}{T'}\right)}\{1-\exp[-(G')(T'+T'')]\}\exp\left[-\mu\left(\frac{T'+T''}{2}\right)\right],$$

neglecting ϵ^2 and higher powers.

Formulae 2.3 and 2.4 enable us to find where the reflected beam issues from the crystal. In accordance with Borrmann's observations (1950) on calcite, the beam tends to issue, in the symmetric case, at the mid-point of the range as if guided by the crystal planes; however, in the asymmetric case the corresponding result is not obvious. If G' is large we may write

$$I_0(z)\approx\frac{e^z}{\sqrt{(2\pi z)}},$$

so that $\mathscr{R}(x)$ contains the factors

$$1/\sqrt[4]{(xyT'T'')}\exp[-\mu(xT'+yT'')]\exp\{-(G')[\sqrt{(xT')}-\sqrt{(yT'')}]^2\};$$

if therefore μ exerts only a minor influence, the maximum reflection will issue where

$$xT'=yT'',$$

that is, as if the beam were constrained to follow the crystal planes. Evidently in practice the multiple reflections will emerge over a range not exceeding BC, gradually becoming, with increasing thickness, relatively more and more concentrated towards the point M. The total spread of the emergent beam, counting the direct ray, is therefore not less than

$$BM=\frac{T''\sin\theta}{\sin\phi}=\frac{T\sin\theta}{\sin\phi\sin\overline{\phi-\theta}}.$$

The range of values of ϕ and θ under typical experimental conditions is shown in fig. 3. It appears that at least in the case where a typical Laue pair of lines, light and dark, is present, ϕ will not be far from 90°; in such a case the separation of the deficiency line from the centre of its concomitant reflections will be of order $T \tan\theta$ but tending to be smaller if there is less secondary extinction. Strong absorption can shift the reflections in either direction according to the sign of θ, if there is any obliquity ($\phi \neq 90°$). In the case of a specimen 1 mm thick, if θ is of

Fig. 3

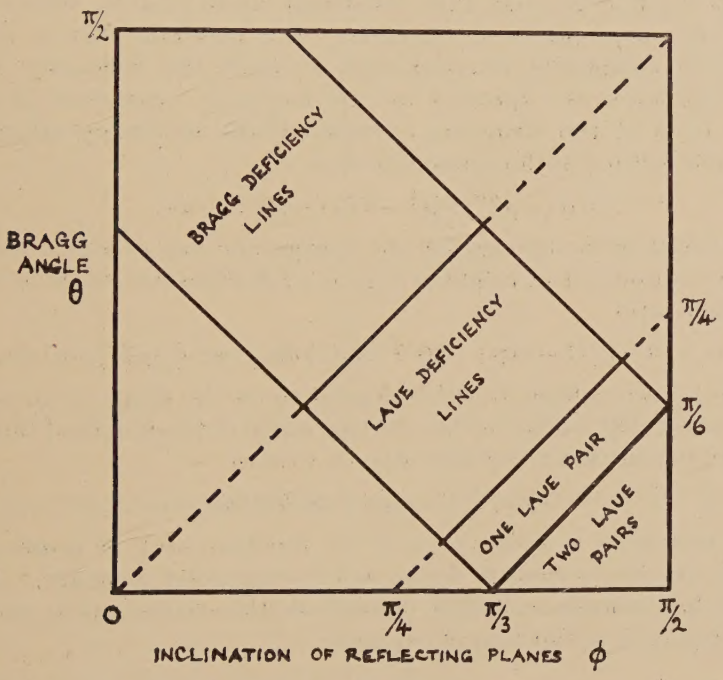

Geometrical conditions limiting production of deficiency and reflection lines with typical experimental layout.

order 10° say, $T \tan\theta$ is about $\frac{1}{6}$ mm. This gives an idea of the conditions to be fulfilled in order that the direct beam shall be either resolved or observed only in company with its multiple reflections, for each element of the source will give a repetition of the fundamental pattern, and the overlapping will determine the question of resolution. A reasonable source would be about $\frac{1}{4}$ mm in diameter, and $\frac{1}{10}$ mm would be practicable, but smaller sources would generally tend to require long exposures of the film. A similar condition is imposed if one attempts to resolve the angular structure of the beam. The most favourable condition for this is to place the film far from the crystal. Whether the minimum distance for resolution is practicable depends on the actual mosaic spread of the

crystal in the plane of incidence. In some cases the mosaic spread is of the order of 1 minute of arc, so that at a distance of one metre, the angular structure will be represented by a width of order 0·3 mm, so that resolution will begin at about this distance ; actually the line width is often considerably greater than the mosaic spread, so that conditions are then more favourable. However, even at 1 m the exposure is already 100 times greater than at 10 cm, and at this smaller distance, resolution of angular structure will not occur with a source $\frac{1}{4}$ mm diameter, especially if allowance is made for the further blurring due to the multiple reflections. We may make a broad distinction between ' resolved ' and ' unresolved ' divergent beam lines, and this distinction must also be observed in choosing the appropriate mathematics. We conclude that it is only adequate in completely resolved lines to treat the deficiency of the transmitted beam as expressed by the factor in expression (2.1). If actually none of the structure is resolved, the deficiency relative to background will be, in the symmetric case,

$$\exp(-\mu T')\int \tfrac{1}{2}(1-\exp[-2G'T'])\,du.$$

The contrast of the line against the background due to monochromatic radiation transmitted in neighbouring non-reflecting directions is due to an intensity ratio

$$\exp(-\mu T')\int \tfrac{1}{2}(1-\exp[-2G'T'])\omega(u)\,du/\int \exp(-\mu T')\omega(u)\,du,$$

where $\omega(u)$ is a weighting function depending on the shape of the source. If $\omega(u)$ varies only a little in the effective range of the weighted function, the centre-line intensity contrast may be written

$$(1/\beta)\int \tfrac{1}{2}(1-\exp[-2G'T'])\,du,$$

where β represents a mean range of the function $\omega(u)$, or source mean diameter, and for a circular source is $(2/\pi)\times$angular diameter. Actual photographic contrast will also depend on the characteristic curve of film blackening as a function of exposure.

§ 3. The Line Width

It is natural to attempt to measure the mosaic spread directly by divergent beam photography, and to expect the results to correspond to the magnitude of secondary extinction, since the extinction coefficient g_2 is equal to $1/2\eta\sqrt{\pi}$ for a Gaussian mosaic.

The experimental basis of such an attempt is to take photographs at different distances from the crystal, and to rely on the rate of increase of the width of lines with distance. We assume that the finite source diameter is an additive contribution given by the intercept of the graph on the width axis ; the mean angular half-width (ϑ) will be the slope of the graph. Referring to fig. 4 we see that the contrast for a line with resolved angular structure depends on the power ratio, given in the symmetric case by

$$\tfrac{1}{2}(1-\exp[-2G'T']),$$

closely resembling a step-function if $G'T'$ is reasonably large as we shall assume. A good estimate of half-width will therefore be given by

$$\tfrac{1}{2}2\vartheta=\tfrac{1}{2}\int_{-\infty}^{\infty}(1-\exp[-2G'T'])\,du$$

$$=Q'T'-\frac{Q'^2T'^2}{2\eta\sqrt{\pi}}+\ldots.$$

or

$$\vartheta=\eta\mathscr{S}\left(\frac{Q'T'}{\eta}\right), \text{ defining } \mathscr{S}. \quad . \quad . \quad . \quad . \quad . \quad (3.1)$$

Fig. 4

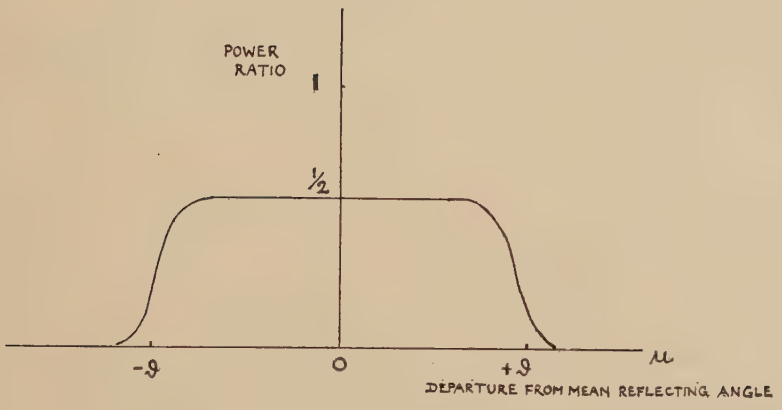

Angular distribution of secondary extinction in the symmetric Laue case.

Thus in general the apparent line width depends upon the amount of secondary extinction instead of being simply proportional to the mosaic spread. The contrast σ_m in unresolved lines for monochromatic radiation, in the range of linear film response will be

$$\sigma_m=\frac{\eta}{\beta}\mathscr{S}\left(\frac{Q'T'}{\eta}\right)=\frac{\vartheta}{\beta}. \quad . \quad . \quad . \quad . \quad . \quad . \quad (3.2)$$

In some measurements on a pentaerythritol crystal, we measured ϑ from the slope of the width graph, after first correcting for the inhomogeneity of the CuKα line. Contrast σ was measured with a Cambridge microdensitometer and corrected for white background by calculation as referred to below, § 4. The table of values (1) refers to these corrected contrasts on (002) and (110) deficiency lines photographed at a distance of 6 cm in the symmetric Laue position.

These results are consistent with our assumption that the lines on which σ_m was measured were completely unresolved. Knowing Q from independent measurements (Llewellyn, Cox and Goodwin 1937), and T, we can deduce η from eqn. (3.2) and a knowledge of the function $\mathscr{S}$,

graphed in fig. 5. This function has been expressed alternatively as the power series already given, or in the asymptotic form

$$\mathscr{S}(z)=\sqrt{(2\ln\sqrt{(2/\pi)z})}\left(1+\frac{C_1}{2\ln\sqrt{(2/\pi)z}}-\frac{C_2}{(\ln\sqrt{(2/\pi)z})^2}+\ldots.\right) \quad (3.3)$$

where C_1 is Euler's constant ($\sim 0{\cdot}577\ldots.$) and $C_2 \sim 0{\cdot}25$.

Table 1

(hkl)	(002)	(110)
ϑ	$4{\cdot}8\ 10^{-4}$	$2{\cdot}2\ 10^{-4}$
β	$2{\cdot}62\ 10^{-3}$	$2{\cdot}62\ 10^{-3}$
σ_m	$0{\cdot}172\pm0{\cdot}010$	$0{\cdot}082\pm0{\cdot}006$
σ_m calc. $\left(=\frac{\vartheta}{\beta}\right)$	$0{\cdot}183$	$0{\cdot}084$
η	$1{\cdot}75\ 10^{-4}=0{\cdot}60'$	$1{\cdot}4\ 10^{-4}=0{\cdot}48'$

Fig. 5

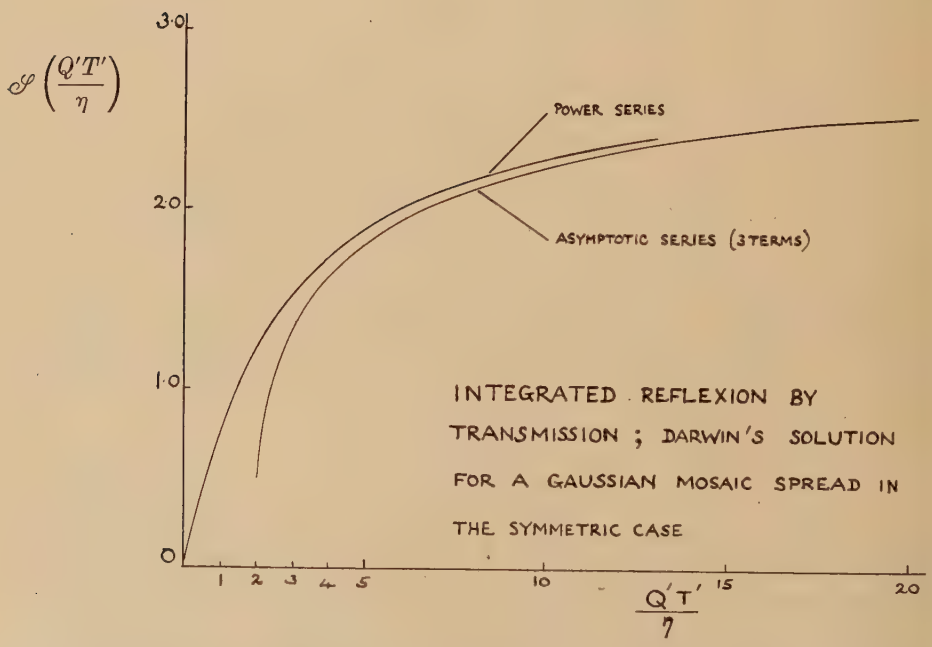

The latter form shows that for heavy secondary extinction the line contrast of unresolved lines or width of resolved lines increases very slowly with Q.

Since η is defined as the r.m.s. of random small rotations about a common axis, it is to be expected that it will behave as a symmetric tensor of the second rank and will not as a rule be the same for different lines of the same crystal.

§ 4. Effect of Continuous Radiation

If in addition to the characteristic line there is energy amounting to K times as much in the white radiation, the contrast, σ, of lines on the photograph is reduced. If in the neighbourhood of the line a typical background measurement is obtained free from any selective effects of diffraction, the line contrast is simply reduced in the ratio

$$\sigma=\sigma_m/(1+KY),$$

where Y is the weighted mean absorption ratio $\exp(-\mu T'')$ for white radiation divided by the ordinary absorption ratio for the characteristic radiation. The weighting function is the spectral intensity multiplied by sensitivity of the film to the radiation. Both may be represented, the one fairly well and one rather roughly, by powers of μ so that the averaging can be performed with the aid of incomplete Γ-functions. This was done in our experiments so as to find the approximate value of $(1+KY)$; the estimated value was 1·49 for the circumstances of table 1, and was used to obtain σ_m from measured values of σ.

To estimate K accurately was not practicable, but an attempt was made to apply existing data obtained by Ulrey (1918) and Unnewehr (1923) on ordinary x-ray tubes of that time, together with the white-radiation formulae of Kramers (1923) and Davis (1918). Photographic sensitivity was taken to be within limits proportional to exposure (Charlesby 1940) and its variation with wavelength according to a curve obtained by smoothing out the effects of absorption edges in Seeman's data (1950).

A further consequence of the admixture of white radiation is that instead of increasing indefinitely with crystal thickness, the contrast passes through a maximum (Lonsdale 1947 a). Detailed calculation showed that the optimum thickness should be slightly different for resolved and unresolved lines, but was not critical except as to order of magnitude, and did not greatly exceed the simplest estimate $(1/\mu_\alpha)$ obtained from the linear absorption μ_α of the characteristic radiation in the crystal.

§ 5. Primary Extinction

Since eqn. (3.2) can always be solved for η, given Q', it does not suffice to determine these quantities uniquely. Only in the case of weak secondary extinction does the attempt to measure η directly succeed; in this case the width of line is more closely connected with mosaic spread than in the case of strong secondary extinction.

For the present purpose we can express the effect of primary extinction by means of a factor which diminishes the value of Q to some value Q'. This value is only known as a function of block size for very special cases; for reflection from or through an infinite plate of non-absorbing crystal (fig. 6), or by reflection from thick plates of slightly absorbing crystal. Neglect of the slight absorption introduces errors of order 18% (Darwin *loc. cit.*). It is not to be expected that the extinction factor even for finite rectangular blocks can be obtained by simple interpolation but

such a procedure may give approximate indications. We may perhaps regard as the appropriate interpolation ratio s_1/s_2 in the diagram (fig. 7). However, for comparison with experiment we have kept the two extreme cases apart, and the results of calculation are plotted as values of σ_m against block size, with η assumed to be constant for each line (fig. 8).

Fig. 6

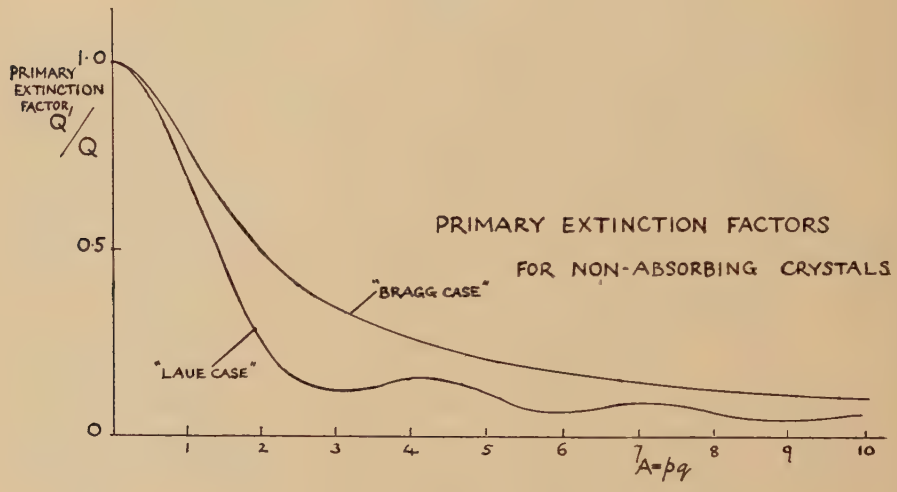

Fig. 7

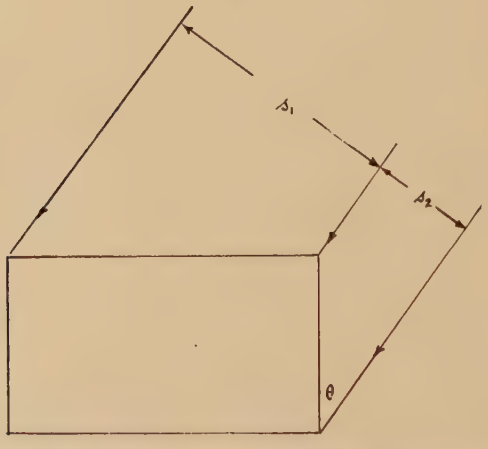

Choice of interpolation factor for rectangular block (§ 5).

In a series of tests in which a crystal of pentaerythritol was repeatedly immersed in liquid air, line contrast was found to have changed at first after each immersion, but before complete disintegration the contrast had reached a more or less settled value for each line. It is the final values that appear in table 1. In view of their agreement with the measurements of ϑ, we may regard the factor $(1+KY)$ as having been

determined with reasonable accuracy, and similarly η (last line of table 1), on the assumption that primary extinction was negligible at this stage. It then transpires that the measurements at the earlier stages on the two strong lines of pentaerythritol can be explained by using a common abscissa scale in fig. 9. It happens that the spacing of the two sets of planes is also the same; but the block dimensions could in principle have quite a different meaning for the two lines and for the Bragg and

Fig. 8

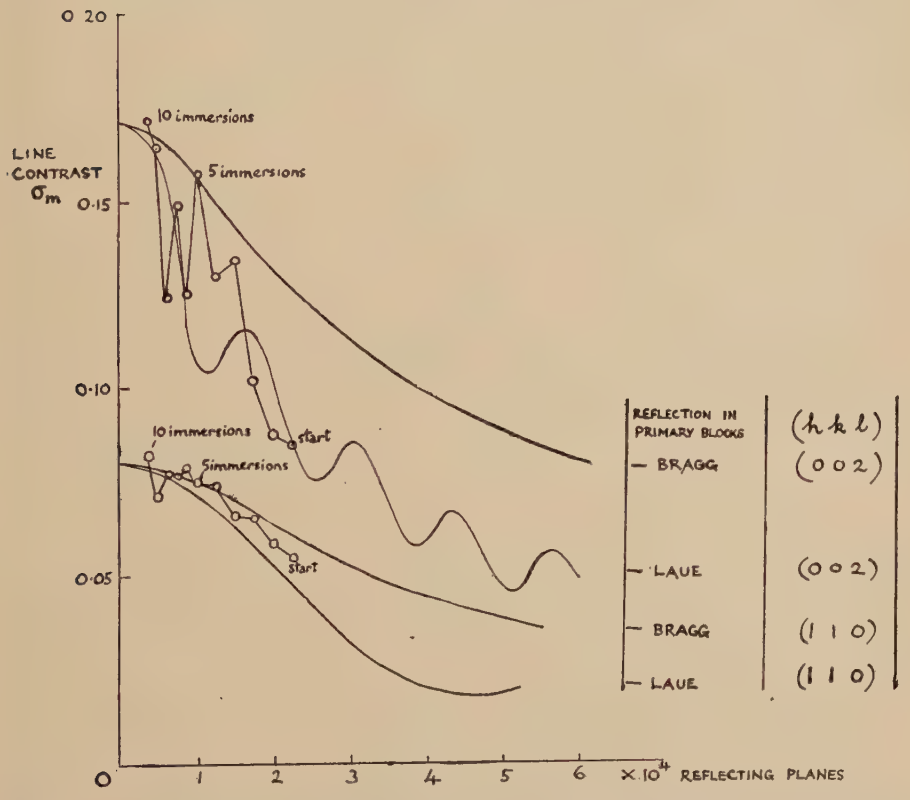

Changes produced in the contrast of two lines of pentaerythritol on liquid air immersion. — Calc. effect of primary extinction. ○ Experimental points plotted on the basis of fig. 9.

Laue cases. In the Bragg case the relevant dimension is parallel to the crystal face, in the Laue case perpendicular; only in the latter case is a block dimension common to both lines involved. It seems that the results are at least consistent with the view that during most of the experiment the blocks were of such a shape that the Laue case was the more relevant. This is probable for (110) from the tetragonal symmetry, since θ in fig. 7 is fairly small.

The estimated values of η for the two lines are, not unexpectedly, somewhat different though the larger value was observed for (002) contrary to a remark by Llewellyn, Cox and Goodwin (*loc. cit.*). Had we attributed the contrast changes purely to changes in η, we should have had to assume an increase from 0·3′ to 0·6′ for (002) and from 0·24′ to 0·48′ for (110). If, on the other hand, the changes were purely due to splitting of blocks, the initial mean block dimension is determined to order of magnitude as about 50–60 μ. Although this is an appreciable fraction of the crystal thickness it is probable that the extinction formulae remain substantially applicable. An attempt to detect such blocks microscopically was unsuccessful.

Fig. 9

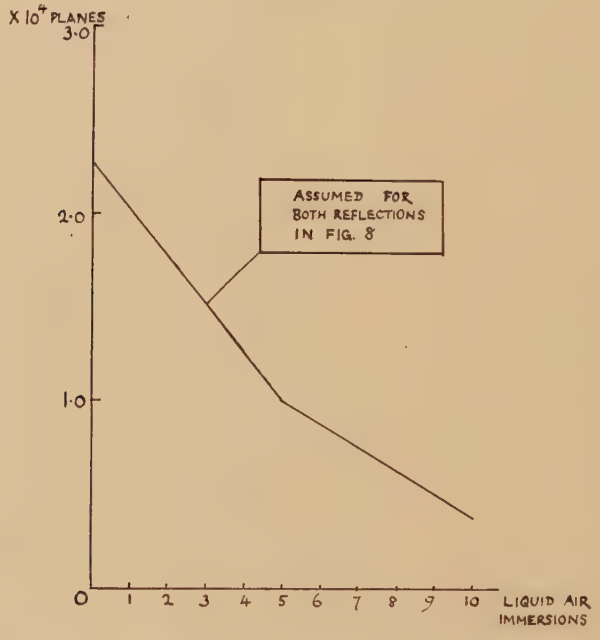

Block dimensions assumed, to fit curves in fig. 9.

§ 6. The Borrmann Effect

It has been observed by Borrmann (1950) and theoretically confirmed by von Laue (1949) that an abnormally low absorption can occur in perfect crystals in the case of an x-ray beam at the reflecting angle. This reduction is likely to be incomplete in small blocks, but we may investigate the effect in mosaics by supposing μ reduced to some unknown smaller value $c\mu$, taking this to apply as a mean in the reflection range.

A transmitted ray spends a fraction $\xi G/Q$ of its path in blocks oriented so as to reflect, where ξ denotes the diffraction width ; different values of

u are distributed almost uniformly within that range so we may conclude that the apparent absorption neglecting multiple reflections is

$$\mu_s=\mu\left(1-\frac{\xi G}{Q}\right)+c\mu\frac{\xi G}{Q}+G$$
$$=\mu+\left(1-\frac{\xi\mu(1-c)}{Q}\right)G=\mu+G_1 \text{ say.} \quad . \ . \ . \ . \ (6.1)$$

The effect therefore resembles a small fractional change in $G(u)$ independent of u and therefore acts in the same sense as primary extinction. The transmission is now seen to be in the symmetric case

$$\sigma_m=1-\exp(-G_1T')\cosh GT'.$$

If GT' is large, the condition for line reversal, the ' deficiency ' becoming negative, reduces to

$$\mu T'>\frac{\sqrt{(2\pi)\ln 2}}{1-c}\frac{\eta}{\xi},$$

this demands a very much greater thickness than for a perfect crystal, for which the analogous inequality is

$$\mu T'>\frac{\ln 2}{1-c},$$

having regard to the probably much smaller c in the second case.

Further calculations have shown that for organic crystals it would be difficult to notice the effect on the contrast of lines, though it would become more important for weak lines than for strong ones, and more important for more strongly absorbing substances.

§ 7. Further Experimental Points

Lonsdale (1947 b) in a reference to Ehrenberg mentions that source dimensions may have an influence in blurring divergent beam lines. Detailed calculations (§ 3) have shown that this effect may be crucial for their visibility. In the first place we have shown that β, the effective source dimension, appears in the denominator of the contrast of unresolved lines. It will also determine the distance beyond which different parts of a Laue pair will, through inhomogeneity of the characteristic line, increasingly overlap and so suffer partial cancellation. Illustrating these points, we found first that a source with diameter 0·23 mm gave better lines than one with 0·3 mm. From several crystals of ammonium dihydrogen phosphate however, only one specimen gave even faint lines ; others gave none even after having been immersed in liquid air. However, with a hole of 0·06 mm diameter accurately drilled in a tantalum plate, fairly well defined lines were obtained after $1\frac{1}{2}$ hours from a crystal 0·25 mm thick ; with the larger source this specimen gave none.

Calculation shows that with a given experimental arrangement the contrast passes through a maximum as a function of η and is small for small values of η. This conclusion is relevant to the interpretation of the results of liquid air immersion. This treatment is known to be

effective in diminishing the effect of extinction on integrated reflection (e.g. Llewellyn, Cox and Goodwin 1937) and has also been found by Lonsdale to be often effective in producing divergent beam lines. Success is usually attributed to the effect of sudden cooling in producing innumerable cracks and so, by reducing the blocks to a finer texture, diminishing extinction and increasing the reflecting power Q'. The process does not always succeed, however. Lonsdale has shown (1947 a) that the texture of both mosaic and perfect diamonds is apparently immune to any change except by much more drastic treatment. Whilst other crystals may also have the thermal and mechanical properties to simulate the resistant behaviour of diamonds, this cannot be deduced directly from the contrast on a single divergent-beam photograph, without careful consideration of the resolution. If the mosaic spread is extremely small the unresolved lines will probably be faint or absent, and this cannot be taken as a direct proof that primary extinction is operating, without detailed calculation. So then, if treatment results in no improvement, it may be because the texture is already fine enough to prevent primary extinction. Again, we may safely assume that the mosaic spread will be either unchanged by immersion, or increased, perhaps by the release of internal strains previously present in the crystal. The resulting effect on contrast will then depend on which domain of angles includes η, and will be favourable or unfavourable to line production according as η is below or above the angular subtense of the source.

Acknowledgments

We wish to thank Professor E. G. Cox for suggesting the enquiry and for constant advice and criticism, Professor K. Lonsdale for helpful discussion at a later stage, and Professor R. Whiddington and Dr. G. E. Brindley for the use of a microdensitometer.

References

Borrmann, G., 1941, *Phys. Z.*, **42,** 157 ; 1950, *Z. Phys.*, **127,** 297.
Charlesby, A., 1940, *Proc. Phys. Soc.*, **52,** 657.
Darwin, C. G., 1922, *Phil. Mag.*, **43,** 800.
Davis, B., 1918, *Phys. Rev.*, **11,** 433.
Kramers, H. A., 1923, *Phil. Mag.*, **46,** 836.
Laue, M. von, 1949, *Acta Cryst.*, **2,** 106.
Llewellyn, F. J., Cox, E. G., and Goodwin, T. H., 1937, *Chem. Soc.*, **183,** 883.
Lonsdale, K., 1943, *Nature, Lond.*, **151,** 53 ; 1947 a, *Phil. Trans.* A, **817,** 240, 219 ; 1947 b, *Min. Mag.*, **28,** 14.
May, W., 1949, *Nature, Lond.*, **163,** 569.
Seeman, H. E., 1950, *Rev. Sci. Instrum.*, **21,** 314.
Ulrey, G. T., 1918, *Phys. Rev.*, **11,** 401.
Unnewehr, E. C., 1923, *Phys. Rev.*, **22,** 529.
Waller, I., 1926, *Ann. Phys.*, **79,** 261.

CXXIV. *Programming a Digital Computer to Learn*

By Anthony G. Oettinger*
University Mathematical Laboratory, Cambridge†

[Received June 11; revised August 20, 1952]

Abstract

Techniques for programming a digital computer to perform simple learning tasks are discussed with reference to two concrete examples. These examples have a particular bearing on questions proposed by Turing (1950) and by Wilkes (1951). By the application of the techniques described, digital computers can be made to serve as models in the study of the functions and of the structures of animal nervous systems.

§ 1. Introduction

In recent publications, Turing, Wilkes, Shannon, von Neumann and others examine in theoretical fashion several facets of the problem of the design of machines having properties usually associated only with the nervous systems of living organisms.‡ Turing (1950), writing on 'Computing Machinery and Intelligence', examines the question 'Can Machines Think?' and, finding this question too vague to be answerable as such, proposes that it be replaced by a related but less ambiguous question based on an *imitation game* played with a machine and a human interrogator. In addition, he suggests that the term 'machine' be restricted to mean 'universal digital computer', since such machines have the important property of being able, when provided with a suitable *programme*, to mimic arbitrary machines in a very general class. Wilkes (1951 a) discusses the possibility of giving a digital computer the ability to learn. Stating that under special conditions "it is easy to see how a machine could be programmed so that it appeared to learn", he then poses the more speculative question of "whether it would in principle be possible to construct a generalized learning programme which would enable an operator, if he had sufficient patience, to 'teach' the machine any subject he chose". Shannon (1950) outlines the requirements for a machine capable of playing chess, on the assumption that the rules of the game and the necessary principles of strategy are made known to the machine from the start. von Neumann

* Communicated by the Author.

† Now at the Computation Laboratory of Harvard University, Cambridge, Mass.

‡ A comprehensive bibliography of the literature about this subject is appended.

(1951) expresses the feeling that " it is unlikely that we could construct automata of a much higher complexity than the ones we now have, without possessing a very advanced and subtle theory of automata and information " ; he describes some of the difficulties to be faced when designing complex automata, and briefly sketches some potential components of a general theory.

In spite of the wealth of conjectures now available in the literature, attempts to produce concrete realizations of these conjectures have been sparse. Ashby (1948) and Grey Walter (1950) have reported the construction of some electro-mechanical devices specially built to perform a limited number of the functions of living organisms. The theoretical importance of universal digital computers has been discussed by the writers quoted earlier. This paper describes some practical techniques by which a universal digital computer can be made to exhibit a variety of modes of animal-like behaviour. Two concrete examples which have a particular bearing on the questions proposed by Turing and by Wilkes are described in detail. In each of these examples a machine modifies its behaviour on the basis of experience acquired in the course of operation. The techniques employed may be of interest to all those who are concerned with the non-numerical applications of digital computers, and to those who, like psychologists and neurophysiologists, are interested in the potentialities of existing digital computers as models of the structure and functions of animal nervous systems.

A brief description of those properties of universal digital computers which are important in the present application will be given as a preliminary. In that description particular reference will be made to the properties of the Edsac,* the machine used for these experiments, but this entails no essential loss of generality. Information, coded in the form of holes on standard teleprinter tape, is introduced into the Edsac from the outside by a tape reader which, by means of light beams and photocells, transcribes sequences of holes into trains of electrical pulses. The pulse trains formed in this fashion are held in the machine's *store*, sometimes called its memory. The store is divided into bins or *storage locations*, each capable of holding seventeen pulses. The pulses are usually interpreted as binary digits, the presence and absence of a pulse in a given position representing 1 and 0 respectively. For easy identification the storage locations are numbered serially. Information can be extracted from the store and sent to the *arithmetic unit*, where operations are performed on it ; the result may then be returned to an appropriate storage location. Finally, information held in the machine can be sent to the outside world by using the electrical pulses to actuate a teleprinter or a tape punch. All these procedures are carried out under the direction of a *control unit*. The solution of a given problem

* The Edsac (Electronic Delay Storage Automatic Calculator) is in operation at the University Mathematical Laboratory, Cambridge.

proceeds step by step as a series of elementary operations, each of which is specified by an *order*. When a mathematician assembles the set of orders required to work out the solution of a problem he is said to be *programming* this problem for the machine. Eight of the twenty orders available on the Edsac are listed in table 1, together with their respective functions.

Table 1. Selected Edsac Orders

A n	Add $C(n)$* to $C(Acc)$†.
S n	Subtract $C(n)$ from $C(Acc)$.
T n	Transfer $C(Acc)$ to storage location n, and clear the accumulator.
U n	Transfer $C(Acc)$ to storage location n, and do not clear the accumulator.
E n	If $C(Acc) \geqslant 0$, execute next the order which stands in storage location n ; otherwise proceed serially.
C n	Collate the number in storage location n with the number in the multiplier register and add the result into the accumulator : that is, add a ' 1 ' into the accumulator in digital positions where both numbers have a ' 1 ', and add a ' 0 ' in other digital positions.
I n	Read the next row of holes on the input tape, and place the result in storage location n.
O n	Print the character now set up on the teleprinter, and set up on the teleprinter the character represented by the five most significant digits in storage location n.

* ' $C(x)$ ' means ' the contents of storage location x '.
† ' $C(Acc)$ ' means ' the contents of the accumulator '. The accumulator is a special storage location in the arithmetic unit.

In table 1, as on the programmer's worksheet, an order is represented by a function letter which specifies the function of the order, and by a number n, or *address*, which identifies the storage location holding the information to be operated on. From the programmer's worksheet orders are transcribed on to tape in a suitably coded form, and hence into the store, where they are held in the same way as other information. Normally the control unit selects orders from the store in the proper sequence, and supervises the performance of the corresponding operations. The orders are transferred from the store to the control unit by a special channel. However, when desirable, it is possible to treat an order as if it were a number. An example of the numerical interpretation of orders is given in table 2, where C (201) represents

Table 2. An Example of the Transformation of Orders

Location	Content
100	*A* 201
101	*A* 200
102	*T* 201
200	1
201	*A* 25

the order *A* 25. When *C* (100) is interpreted as an order by the control unit and is obeyed, *C* (201), interpreted as a number, is added into the accumulator, presumed to have been previously cleared. After *C* (101) has been obeyed, *C* (*Acc*)=*C* (201)+*C* (200)=the number representing the order *A* 26. *C* (*Acc*) is finally transferred to 201. Hence when *C* (201) is selected by the control unit as an order, it will be interpreted as *A* 26. Only the address was modified in this example, but the same principles apply to the modification of function letters, since these can also be interpreted as numbers.

In normal operation all the information held in the machine, other than orders, is interpreted as numerical information, but this need not always be the case. The validity of the result of any of the non-arithmetic operations *C*, *I*, *O*, *T* and *U* evidently does not depend on a numerical interpretation of the operand. With some restrictions this is true also of arithmetic operations such as *A* and *S*. Hence a non-numerical problem can be treated by numerical means whenever it is possible to establish a correspondence between propositions of the language in which the problem is formulated, and propositions in numerical language, in a manner such that the manipulation of numerical expressions yields expressions corresponding to those which would result if the whole process had been carried out in the original language. For example, in the 'shopping' programme described further on, a system of 'shops' is represented by a matrix. In the 'response-learning' programme, stimuli of varying intensity correspond to numbers of similarly varying magnitude.

In normal operation the control unit selects orders serially; i.e., after using the order *C* (*n*), it selects *C* (*n*+1), and so on. The insertion of an *E* order into a programme radically alters this procedure. It is the function of an *E* order to decide whether operation should proceed serially, or whether an order held in another storage location, *m*, should be obeyed instead. In the latter case serial operation is resumed in a new sequence. The great importance of the *E* order arises from the fact that the choice between these alternatives is based on the results of earlier operations. Hence, while the programmer must essentially foresee the need for a choice and provide *E* orders to meet this need, the actual decision is made by the machine itself on the basis of information obtained in the course of operation either from its own store or, by means of the *I* order, from the outside world.

Since a computing machine like the Edsac is equipped with an information store, it is trivial to programme it to absorb information from the outside world and to reproduce this information verbatim when required. For example, to make the Edsac first 'memorize' the English alphabet and then 'recite' it, by printing it on the teleprinter, only a series of *I* and *O* orders and an input tape holding the alphabet in coded form would be required. More interesting types of learning behaviour can be obtained by giving the machine a programme which

provides for the transformation of its own orders in the fashion described above. By the liberal provision of E orders in the programme the machine is enabled to organize new information meaningfully and to select alternative modes of behaviour on the basis of this organization. Two programmes in which these techniques are applied will now be discussed.

§ 2. Programming the Edsac to go Shopping

The properties of the shopping programme are summarized in the following illustration. The shopping programme may be imagined to define a small child sent on a shopping tour. If this child were asked by its mother to buy different articles in various shops, it would not know at first where to find these articles, and would hunt for them by going from shop to shop in a random fashion until it came to the desired one. Having found an article once, it would remember in what shop, and would go directly to this shop the next time the same article were requested. In addition, as its curiosity would prompt it to note the whereabouts of articles for which it had not had a specific request, when such a request did come, it would often be able to go directly to the right shop.

Before giving the abstract specification of the shopping programme it is helpful to digress for a moment to define the boundary between the 'child machine', defined by the shopping programme, and the outside world. Obviously the simplest definition would be to consider the whole of the Edsac as the machine, and to represent the outside world by a suitably coded input tape. Unfortunately, tape reading is the slowest operation of the Edsac. It is therefore convenient to make a conceptual division of the Edsac into two parts, one to play the role of the experimental subject and designated s-part or s-machine, the remainder to serve as an extension of the outside world. By means of this expedient it becomes possible to conduct experiments at the highest possible machine speed, since less frequent use of the input mechanism need be made.

Provision is made to enter a description of the shops into the part of the Edsac store belonging to the outside world as an $m \times n$ matrix. This matrix has elements a_{ij} such that $a_{ij}=1$ if shop i has article j, and $a_{ij}=0$ otherwise.* The matrix will be called the stock matrix S. The ith row of S may be regarded as a row vector whose components define the stock of shop i, and will be called a shop vector. The ith shop vector is held in storage location $m+i$, where m is a reference address. Similarly, the jth column has components representing the shops where article j may be found, and it will be called an article vector. The stock matrix shown in table 3 has eight rows (shops) and

* A representation of this type was used by N. G. Parke (1949) to specify the membership of a set of committees.

seven columns (kinds of articles). A shopping order for article j is given to the s-machine by a row vector (order vector) consisting of zeros everywhere except in column j, where there is a 1. The top line of column 1 (table 3) shows an order vector for article no. 6. The s-machine proceeds to select a shop number i_k at random,* and to form the address $m+i_k$ of the corresponding shop vector. A C order

Table 3. A Typical Stock Matrix and the Corresponding Shopping Tours

	Shopping Tours		
	1	2	3
(1)	0000010 0000080	13465728	8
(2)	0000010 0000080		8
(3)	0000100 0000480	1234	4
(4)	0000100 0000480		4
(5)	0000001 0000480	62413875	0
(6)	0100000 0550480	45	5
(7)	0010000 0555480		5
(8)	1000000 1555480	3541	1
(9)	0100000 1555480		5
(10)	0010000 1555480		5
(11)	0001000 1555480		5
(12)	0000100 1555480		4
(13)	0000010 1555480		8

Stock Matrix

Articles →

Shops ↓	
	1001000
	1010000
	0110000
	0000100
	0111000
	0001000
	0111100
	0000010

* ' Pseudo-random ' numbers good enough for these experiments are generated by squaring a certain constant and by selecting a number of digits from the result. The middle digits of the square then serve as a new constant.

(table 1), $Cm+i_k$, is constructed with this address and, when obeyed, collates the shop vector with the given order vector. After the C order has been obeyed the content of the accumulator is different from 0 if, and only if, shop i_k has article j in stock, that is if $a_{i_n j}=1$. If this is not the case, another shop number i_l is selected, and so on with i_m, i_n, . . . until either the article is found or all the shops have been scanned. In the first shopping tour of the example given in table 3 the shops were scanned in the order indicated in column 2 ; column 3 shows that article no. 6 was found in shop no. 8. When an article is unavailable, as is the case with no. 7 in the fifth shopping tour, the s-machine tries all shops—the order of search being indicated in column 2—then prints zero in column 3 to indicate the absence of the article. Once an article has been found, the number of the shop in which it was first discovered is recorded in the appropriate column of the s-memory, as shown in the case of the first shopping tour by the second line of column 1. Before attempting a search for an article the s-machine examines its memory to determine whether or not the location of this article is already known to it. If so, it proceeds directly to the shop where the article was found on the earlier trial. The second shopping tour provides an illustration of this mode of behaviour. When an article j is found in shop i a second collation with the shop vector is made, using an inspection vector, a row with zeros everywhere except in the two columns adjacent to column j. In this fashion the presence of the articles $j+1$ and $j-1$ in shop i can be detected, and recorded in the memory. In the sixth tour, for example, article no. 3 was found to be in shop no. 5 while shopping for article no. 2. In the seventh tour the request for article no. 3 was met without search, as a result of the discovery made during the sixth tour.

If the s-machine memory were cleared and a new arbitrary $m' \times n'$ ($m' \leqslant m$, $n' \leqslant n$) matrix S' substituted for the matrix of table 3, then, proceeding as above, the s-machine would soon discover the location of any article requested. Most observers would hesitate to attribute this ability to intelligent thought on the part of the machine, and in the absence of agreement about the meaning of the word ' thought ' it is difficult to decide whether or not a machine can be said to think. Turing (1950) rightly regards as inappropriate attempts to find the meaning of ' thought ' by an examination of the common usage of the word. Instead, he suggests that the question ' Can Machines Think ? ' be replaced by a related but less ambiguous one in terms of what he calls the ' imitation game '. He postulates a game played by a man A, a woman B, and an interrogator C. C knows the man and the woman only by the labels X and Y, and the object of the game is for C to make the correct identification, that is to match X and Y correctly with A and B. A, B, and C are in separate rooms, and communicate only by means of teleprinters. If, when A is replaced by a machine, C is wrong in his identifications as often as when A was a man, the man and the

machine become indistinguishable to C. The question ' Can Machines Think ? ' may therefore be replaced by the question ' Are there imaginable digital computers which would do well in the imitation game ? '.

The imitation game can be played with the shopping s-machine taking the part of A, if A and B are both given the same stock matrix, and if the questions are restricted to shopping orders of the form ' In what shop may article j be found ? ' coded as order vectors. The answer expected from X or Y would be the appropriate shop number, together with a list of the shops that were tried, i.e., the data given in column 2 and column 3 of table 3. Under these conditions the interrogator C would find it difficult to make the correct identification. Potentially, of course, the man could answer a far wider range of questions than the machine, but it is clearly possible, within limits, to find that a man thinking and a computing machine obeying a learning programme are behaving identically as far as an observer is concerned. Hence, by Turing's criterion, a denial of a machine's ability to think which hinges on a question of the sort ' Yes, this machine certainly gives satisfactory answers to questions of such and such a category, but what can it do if I ask it about something else ? ' appears to be not so much a denial of machine intelligence as an admission that this intelligence exists, although in a very limited form.

The shopping programme has some severe limitations. The size of the stock matrix has an upper limit and its position in the store is fixed, and the method by which the stock matrix and the s-memory are scanned is explicitly prescribed. Unless a technical fault develops in the machine in the course of operation, the programme does precisely what it was designed to do, and information presented to the machine is interpreted either as a shopping order, in which case the machine proceeds normally, or as nonsense, in which case the machine soon stops. There is, thus, only an extremely small chance that the s-machine could understand and sensibly answer any request other than a shopping order, and an even smaller chance that such a happy accident would be repeated. While the shopping machine appears to learn, it certainly cannot be taught any subject the experimenter chooses.

Several improvements suggest themselves. Some, as the introduction of memory decay or forgetfulness, would give the learning process a greater degree of verisimilitude, that is a greater resemblance to the mental operations to which we are accustomed. Others would increase the learning capacity of the s-machine. For example, a more general programme could be designed so as to make it possible to teach the s-machine a method of scanning the shop matrix and the s-memory. In the programme described above this scanning method was explicitly prescribed by a fixed sub-programme. The more general programme would allow the s-machine to construct a scanning sub-programme, by trial and error, subject to indications of progress by an external ' teacher '. The method of trial and error itself would now have to be

specified, and hence the set of sub-programmes which could be tried by the s-machine, as well as the order of trial, would essentially be defined implicitly by the initial programme. What would remain for the s-machine to do would be to operate until it obtained explicitly the particular scanning method which met with the approval of the ' teacher '. Once the scanning method had been learned this machine would proceed as before. If the approved sub-programme were not contained in the trial set there would be no way of teaching the s-machine the corresponding scanning method. An s-machine capable of being taught a scanning method would be capable of competing successfully in a less restricted form of imitation game, a form in which the simpler s-machine would fail ; but it is more powerful than the simpler machine only in the sense that its limitations are shifted to a higher level of abstraction. Making it possible to teach the shopping machine the scanning method which it must use in turn to learn the contents of the shops is only one of many imaginable generalizations of the shopping programme. Additional generalizations, and generalizations of these generalizations, could broaden the range of subjects which can be taught to the s-machine, but in every case the method of operation of the machine at the highest level of generalization would have to be prescribed, and the range of operation consequently limited.

§ 3. A Response-Learning S-Machine

The shopping programme defines an s-machine capable of performing functions which, in living organisms, are considered to be the result of intelligent behaviour. The response-learning programme, on the other hand, defines an s-machine operating at a level roughly corresponding to that of conditioned reflexes.

The response-learning s-machine will be described in two stages, with reference to one specific example. The first stage of the description is given in § 4, from the point of view of an experimenter who can control the input to the machine and observe the output, but for whom the machine is essentially a closed ' black-box '. This point of view is analogous to that of an experimenter who is attempting to deduce the structure and the internal mode of operation of an organism from controlled observations of its functions. In the second stage (§ 5), the factors determining the behaviour of the s-machine are revealed, and analysed from the privileged point of view of the designer of the learning programme.

§ 4. The Functions of the Response-Learning S-Machine

This s-machine is provided with a sensory device capable of detecting a stimulus of varying intensity represented by a number whose magnitude corresponds to the intensity. Having defined this representation, it simplifies further descriptions to refer to ' the number corresponding

to a stimulus ' simply as ' the stimulus '. The same applies to the notions of response and of approval introduced below. When the s-machine begins to operate, a stimulus $s_t > 0$, applied at a time t, initiates at random one of a set of possible responses R_i, $i=1, 2, \ldots, 5$. The machine signals the occurrence of the response R_i by printing the number i, after which the operator may express his approval or disapproval. In the example of table 4, s_t is displayed in column 1,

Table 4. A Typical Response-Learning Experiment

	1	2	3	4	5	6	7	8
t	s_t	R_{it}	a_t	S_{1t}	S_{2t}	S_{3t}	S_{4t}	S_{5t}
	02	X		03	03	03	03	03
	02	X		04	03	03	03	03
	02	2	00	03	07	03	03	03
	02	X		03	04	03	01	03
5	02	3	00	03	04	07	03	03
	02	1	00	06	03	03	02	02
	02	X		03	03	02	02	02
	02	X		02	03	03	02	02
	02	3	00	03	03	08	02	02
10	02	X		03	04	04	02	02
	02	X		02	02	03	01	01
	02	X		02	02	02	01	01
	03	2	00	02	05	03	01	01
	03	5	00	02	03	03	01	05
15	03	3	00	02	03	08	01	02
	03	1	01	06	02	03	01	01
	04	3	00	03	02	03	01	01
	03	3	00	03	02	04	01	02
	03	5	00	03	02	05	01	06
20	03	3	00	03	02	05	01	−02
	01	X		02	01	05	01	01
	03	3	−01	01	01	05	01	01
	03	X		02	01	03	01	01
	03	3	−02	02	01	05	01	01
25	03	3	−03	02	01	04	01	01
	03	X		01	01	01	01	01
	03	1	02	06	01	01	01	01
	03	3	−01	04	01	05	01	01
	03	1	02	04	01	01	01	01
30	02	1	01	07	01	02	01	01
	02	1	00	08	01	01	05	01
	02	1	00	11	01	01	01	01
	01	1	00	10	04	01	01	01
	01	1	−03	11	01	05	01	01
35	01	1	−03	09	01	01	01	01

Table 4 (*cont.*)

	1	2	3	4	5	6	7	8
t	s_t	R_{it}	a_t	S_{1t}	S_{2t}	S_{3t}	S_{4t}	S_{5t}
	01	1	−04	06	01	01	01	01
	01	X		04	01	01	01	01
	02	X		04	01	01	01	02
	03	1	−04	04	01	01	01	00
40	03	4	02	01	01	01	04	01
	03	4	01	01	01	02	04	01
	02	X		01	01	01	04	01
	03	4	02	01	01	02	06	01
	03	4	01	00	01	01	09	01
45	02	4	01	01	01	02	11	01
	01	4	−01	01	01	01	10	01
	01	4	−01	00	01	01	13	01
	01	4	00	−01	01	01	13	01
	01	4	−02	01	01	−03	14	01
50	01	4	−02	06	01	01	13	01
	01	4	−04	01	01	01	12	05
	01	4	−04	00	01	01	09	01
	01	4	−04	01	01	01	06	01
	01	X		01	01	01	03	01
55	02	X		01	01	−04	03	01
	03	X		02	01	01	02	01
	03	X		00	01	01	02	01
	03	X		01	01	01	02	03
	03	X		01	02	01	02	01
60	03	2	00	01	06	01	02	01

the resulting R_i at time t, R_{it}, appears in column 2, and the intensity, a_t, of approval or disapproval is given in column 3. At $t=3$, $s_t=2$ initiated the response R_2, and at $t=17$, $s_t=4$ initiated R_3. An X in column 2 at time t indicates that s_t was too weak to initiate any response whatsoever at that time. In the interval $1 \leqslant t \leqslant 12$, $s_t=2$ is frequently too weak to elicit any response, and those responses that are made occur at random. It is possible for the experimenter to train this s-machine to give one particular response only, by expressing his approval ($a_t > 0$) when this response occurs, and his unconcern ($a_t=0$) or his disapproval ($a_t < 0$) otherwise. Conversely, a response can be discouraged by repeated disapproval. Table 4 shows that the approval signals $a_t=2$ given to R_1 at $t=27$ and $t=29$, and $a_t=1$ given at $t=30$ were sufficient to train the machine to respond to every stimulus with R_1, except at $t=28$, when, at an early stage of training, R_3 occurred. An earlier attempt, made at $t=16$, to teach the s-machine to make the response R_1 failed for reasons whose explanation will be given later.

As the training proceeds, errors become less frequent, and the learned response may be initiated by a progressively weaker stimulus. The

attempt to teach the s-machine to give the response R_1 begins at $t=27$ with the stimulus 3 ; at $t=30$ the stimulus 2 was tried and found to be sufficient, and at $t=33$ R_1 occurred when the smallest stimulus, 1, was used. At the same time the need for approval diminishes. At $t=27$ and $t=29$ $a_t=2$, but $a_t=0$ at $t=31$ and at $t=32$, and R_1 nevertheless is still initiated by the small stimulus 1 at $t=33$. From $t=34$ onwards R_1 is discouraged, until it disappears for the stimulus 1 at $t=37$. At $t=38$ even the stimulus 2 will not initiate it, but at $t=39$ the stimulus 3 brings it back. One last sharp disapproval (-4) finally inhibits it. From $t=40$ onwards the same procedure is repeated with R_4. Note how, at $t=42$, a premature attempt to reduce the stimulus from 3 to 2 produced no response at all.

It has already been mentioned that a response may be learned by the s-machine if encouraged by the experimenter, but if the experimenter is neutral and expresses unconcern ($a_t=0$) for every response, it is nevertheless still possible for some particular response to occur more and more frequently. Eventually, occurring to the exclusion of all others, this response becomes a habit. The high frequency of R_3 from $t=15$ onwards is due to this effect. To train the machine to give R_1 it was first necessary actively to discourage R_3, which showed promise of becoming a habit. At $t=21$ the stimulus was reduced to 1 to test how strong a habit R_3 had become by that time. As the stimulus 1 produced no response, $s_t=3$ was used again at $t=22$. The reappearance of R_3 then indicated the necessity for disapproval. It is also possible, under similar conditions, for the s-machine to decay into a lethargic state, making increasingly infrequent responses. In table 5, columns 1, 2, and 3 for $1 \leqslant t \leqslant 15$ are identical with the corresponding columns of table 4. However, at $t=17$ and thereafter s_t (table 5) was reduced to 1, and the frequency of responses dropped sharply. An interaction of the habit-forming effect with that of decay and of the stimulus strength takes place throughout the operations of the s-machine. Examples of this interaction will be given, but first the response-learning programme itself will be described.

§ 5. The Response-Learning Programme

To control the occurrence of responses, a threshold state number S_i, $S_i \gtrless 0$ is associated with each response R_i. Columns 4 through 8 of table 4 display the threshold state numbers at time t, S_{it}, for every i. The set of threshold state numbers is held in the s-machine store in consecutive storage locations. When a stimulus is introduced at time t by suitable use of I orders these storage locations are scanned serially and cyclically, and their contents are compared with a scanning constant which is decreased by unity at every cycle. When the first largest S_{it}, say S_{jt}, is found the scanning stops. S_{jt} found, the s-machine forms $S_{jt}+s_t$, and tests for the condition $S_{jt}+s_t \geqslant T$ by means of an

E-order. T is a fixed number, 7 in the present experiments, called the triggering threshold. A response can occur at time t only if the relation $S_{jt}+s_t \geqslant T$ is satisfied. When this is not the case X is printed in column 2, and the machine prepares to receive the next stimulus, s_{t+1}. When $S_{jt}+s_t \geqslant T$ the scanning proceeds, to find and count those S_{kt} satisfying the relation $S_{kt}=S_{jt}$, $k\neq j$. When no such S_{kt} exists, response R_j occurs, and the number j is printed in column 2. When two or more responses compete with each other, the winning response is selected at random.

After a response R_i has occurred, the machine signals to the experimenter with a buzz of its tape reader, and asks for approval. The experimenter then introduces a number a_t of appropriate magnitude and sign into the s-machine. Given a_t, the machine proceeds to form $S_{i,\,t+1}$ from S_{it} for all i. When R_i has occurred at time t, $S_{i,\,t+1}=S_{it}+a_t+1+N_{it}-N_{i,\,t-1}-d\,(S_{it},\,t)$; the terms of this expression will be described in turn.

By increasing, decreasing, or leaving S_{it} constant, the addition of the factor a_t correspondingly modifies the probability that $S_{i,\,t+1} > S_{j,\,t+1}$, $i\neq j$, and hence the probability that the scanning process will stop at the storage location holding $S_{i,\,t+1}$. Adding unity to the threshold state of the response which has been initiated at time t increases the probability that this response will occur again at time $t' > t$. This device accounts for the habit-forming effect described earlier. It is this effect which, together with the chance selection of R_3 at $t=17$, accounts for the s-machine's delayed learning of the response R_1. Attempts to teach this response were begun at $t=16$, but were unsuccessful until $t=29$, after R_3 had been effectively discouraged.

N_{it} and $N_{i,\,t-1}$ are both pseudo-random numbers. In each interval $(t,\ t+1)$ a pseudo-random number N_t, $-5 \leqslant N_t \leqslant 5$, is added to one S_{jt} selected at random, and N_{t-1} is subtracted from the S_{kt} ($k\neq j$, or $k=j$) to which it had been added in the interval $(t-1,\ t)$. In this fashion random fluctuations are superimposed on the average level of the threshold states. Because of these fluctuations the machine can make mistakes, that is, it can occasionally make a response other than the one it has been taught to make. More important, provided that no S_i is excessively large, each S_i has a reasonable probability of being greater than the others at some time. This makes possible the teaching of a new response, or, when no response is favoured over the others, produces an interesting variety of responses.

The last factor, $d(S_{it},\ t)$, produces a decay trend of all threshold states toward 1. d is different from zero only in the intervals between $t=5n$ and $t=5n+1$, where $n=0,\ 1,\ 2,\ \ldots$ In these intervals $d=+1$ when $S_{it}>1$, $d=-1$ when $S_{it}\leqslant 0$, and $d=0$ when $S_{it}=1$. The effect of $d>0$ is self-explanatory. The negative decay is provided when $S_{it}\leqslant 0$ for the purely practical purpose of preventing the ' death ' of the s-machine. As illustrated in table 5, the decay introduces some lethargy into the behaviour of the machine, by causing all S_i to drop, hence requiring ever increasing

stimuli to produce a response. Were all the S_i to become so strongly negative that $S_{it}+s_t<T$ for all i, given the most favourable random effect and stimulus, no further response could be elicited from the machine. The use of negative decay effectively makes 1 the average minimum level of the S_i. The effect of decay and of the random variations on the threshold states can be observed most clearly in table 5, when $t>15$.

Table 5. The Effect of Decay and Random Fluctuations on the Threshold State Numbers

	1	2	3	4	5	6	7	8
t	s_t	R_{it}	a_t	S_{1t}	S_{2t}	S_{3t}	S_{4t}	S_{5t}
	02	X		03	03	03	03	03
	02	X		04	03	03	03	03
	02	2	00	03	07	03	03	03
	02	X		03	04	03	01	03
5	02	3	00	03	04	07	03	03
	02	1	00	06	03	03	00	02
	02	X		03	03	02	02	02
	02	X		02	03	03	02	02
	02	3	00	03	03	08	02	02
10	02	X		03	04	04	02	02
	02	X		02	02	03	01	01
	02	X		02	02	02	01	01
	03	2	00	02	05	03	01	01
	03	5	00	02	03	03	00	05
15	03	3	00	02	03	08	01	02
	03	1	00	06	02	03	01	01
	01	X		02	02	03	01	01
	01	X		02	02	03	01	01
	01	X		02	02	03	01	02
20	01	5	00	02	02	03	01	06
	01	X		01	01	02	01	—02
	01	X		01	01	02	01	02
	01	X		00	01	02	01	02
	01	X		01	01	00	01	02
25	01	X		01	01	02	01	02
	01	X		01	01	01	01	01
	01	X		01	01	01	01	01
	01	1	00	06	01	01	01	01
	01	X		02	01	05	01	01

For all those R_j which did not occur at time t

$$S_{j,\,t+1}=S_{jt}+N_{jt}-N_{j,\,t-1}+d(S_{it},\,t).$$

In this expression a_t and the habit-forming term 1 do not appear. The essential features of the preceding description are thus summarized by

the three relations which govern the operation of the response-learning s-machine :

1. To initiate a response at time t :

$$S_{jt}+s_t \geqslant T \text{ for some } j ;$$

2. When R_i has occurred at time t :

$$S_{i,t+1}=S_{it}+a_t+1+N_{it}-N_{i,t-1}-d(S_{it}, t) ;$$

3. When R_i has not occurred at time t :

$$S_{i,t+1}=S_{it}+N_{it}-N_{i,t-1}-d(S_{it}, t).$$

The interaction of habit forming, decay and stimulus strength has already been mentioned at the end of § 4, and the promised examples will now be given. The three experiments recorded in table 6 were performed with identical initial threshold states ($S_{i1}=1$, all i) and approval ($a_t=0$, all R_i), but with a variable stimulus.

For A, $s_t=1$, for B, $s_t=3$, and for C, $s_t=4$, at all times. In A the decay effect predominates and responses are rare. In B the increased stimulus stength elicits more frequent responses, while in C R_3 soon becomes a habit. A and B were, in fact, continued to $t=81$, and table 7 shows the response frequencies obtained. Hence for a given distribution of the random numbers N_t, it is possible to vary the stimulus so as to obtain either one of two unstable states, decay or habit formation, or the steady state of frequent and varied responses. It is clearly in the latter state that the s-machine exhibits the most varied behaviour, and is most receptive to training.

The reader may find it interesting now to follow once more the description of teaching processes given with reference to the first three columns of table 4 in § 4, but this time using the threshold states given in columns 4 through 8, and fig. 1, where some of the data of table 4 have been plotted. Graph A of fig. 1 displays S_{1t}, S_{2t}, and S_{4t}, and the triggering threshold T. In graph B, s_t and a_t are plotted against the same time scale as the S_{it}. $a_t=0$ is represented by a dot on the t-axis and $a_t \neq 0$ by a vertical line of appropriate magnitude and direction. The number of the response to which each approval was given is written directly beneath the t-axis of graph B. It must be remembered that, while he is training the s-machine, the experimenter does not know the threshold states, and must rely on his recollection of his own past actions and of the responses the machine made to them. This is the data given in the first three columns of table 4. With this limited insight, training the s-machine is an interesting occupation for which, however, no less patience is required than for work with animal subjects. It was fortunately possible to mechanize the experiments of table 6 and to carry them out at machine speed, since the stimulus and approval were fixed.

The behaviour pattern of the response-learning s-machine is sufficiently complex to provide a difficult task for an observer required to discover the mechanism by which the behaviour of the s-machine is determined. By

Table 6. The Interaction of Habit Forming, Decay and Stimulus Strength

A

	1	2	3	4	5	6	7	8
t	s_t	R_{it}	a_t	S_{1t}	S_{2t}	S_{3t}	S_{4t}	S_{5t}
	01	X		01	01	01	01	01
	01	X		02	01	01	01	01
	01	X		01	05	01	01	01
	01	X		01	01	01	—01	01
5	01	X		01	01	05	01	01
	01	X		05	01	01	01	01
	01	X		01	01	00	01	01
	01	X		00	01	01	01	01
	01	3	00	01	01	06	01	01
10	01	X		01	02	02	01	01
	01	X		01	01	01	01	01
	01	X		01	01	00	01	01
	01	X		01	04	01	01	01
	01	X		01	01	01	01	05
15	01	3	00	01	01	06	01	01
	01	1	00	06	01	02	01	01
	01	X		02	01	02	01	01
	01	X		02	01	02	01	01
	01	X		02	01	02	01	02
20	01	5	00	02	01	02	01	06
	01	X		01	01	01	01	—02
	01	X		01	01	01	01	02
	01	X		00	01	01	01	02
	01	X		01	01	—01	01	02
25	01	X		01	01	01	01	02
	01	X		01	01	01	01	01
	01	X		01	01	01	01	01
	01	1	00	06	01	01	01	01
	01	X		02	01	05	01	01

B

	1	2	3	4	5	6	7	8
t	s_t	R_{it}	a_t	S_{1t}	S_{2t}	S_{3t}	S_{4t}	S_{5t}
	03	X		01	01	01	01	01
	03	X		02	01	01	01	01
	03	2	00	01	05	01	01	01
	03	X		01	02	01	—01	01
5	03	3	00	01	02	05	01	01
	03	1	00	05	01	02	01	01
	03	X		02	01	01	01	01
	03	X		01	01	02	01	01
	03	3	00	02	01	07	01	01
10	03	X		02	02	03	01	01

Table 6 (*cont.*)

	1	2	3	4	5	6	7	8
t	s_t	R_{it}	a_t	S_{1t}	S_{2t}	S_{3t}	S_{4t}	S_{5t}
	03	X		01	01	02	01	01
	03	X		01	01	01	01	01
	03	2	00	01	04	02	01	01
	03	5	00	01	02	02	01	05
15	03	3	00	01	02	07	01	02
	03	1	00	06	01	02	01	01
	03	X		02	01	02	01	01
	03	X		02	01	02	01	01
	03	X		02	01	02	01	02
20	03	5	00	02	01	02	01	06
	03	X		01	01	01	01	−02
	03	X		01	01	01	01	02
	03	X		00	01	01	01	02
	03	X		01	01	−01	01	02
25	03	X		01	01	01	01	02
	03	X		01	01	01	01	01
	03	X		01	01	01	01	01
	03	1	00	06	01	01	01	01
	03	3	00	02	01	05	01	01

C

	1	2	3	4	5	6	7	8
t	s_t	R_{it}	a_t	S_{1t}	S_{2t}	S_{3t}	S_{4t}	S_{5t}
	04	X		01	01	01	01	01
	04	X		02	01	01	01	01
	04	2	00	01	05	01	01	01
	04	X		01	02	01	−01	01
5	04	3	00	01	02	05	01	01
	04	1	00	05	01	02	01	01
	04	X		02	01	01	01	01
	04	X		01	01	02	01	01
	04	3	00	02	01	07	01	01
10	04	3	00	02	02	03	01	01
	04	3	00	01	01	03	01	01
	04	3	00	01	01	03	01	01
	04	3	00	01	04	05	01	01
	04	3	00	01	01	06	01	05
15	04	3	00	01	01	12	01	01
	04	3	00	06	01	07	01	01
	04	3	00	01	01	08	01	01
	04	3	00	01	01	09	01	01
	04	3	00	01	01	10	01	02

examining the data of the first three columns of table 4 such an observer could easily find regularities in the response pattern, and might even develop empirical rules for predicting responses with tolerable accuracy.

Table 7

R	A freq	B freq
X	74	57
1	3	6
2	1	5
3	2	7
4	0	2
5	1	4

Total trials : 81

He would find it very difficult by this means to obtain a good approximation to the description of the response-learning programme given above. Switching the machine off to dissect it would be of limited value only, since this action would make the programme vanish from the store.

Fig. 1

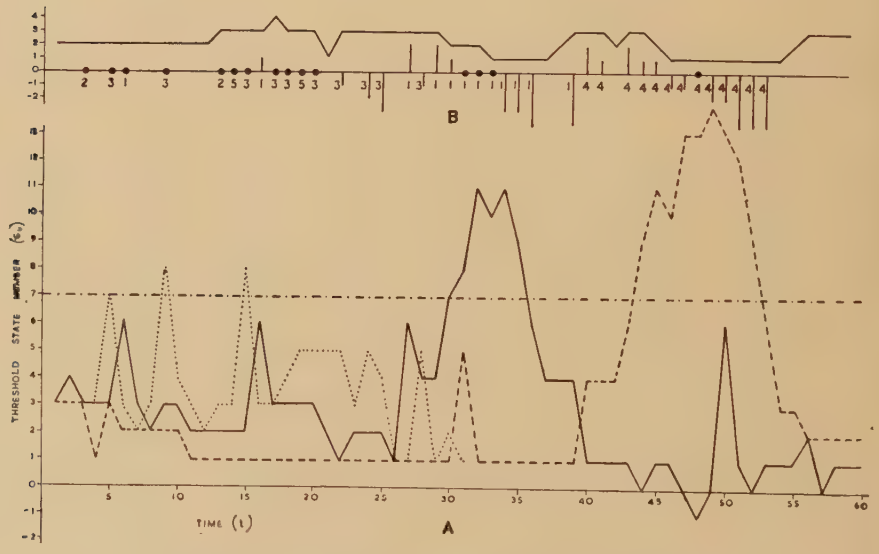

Learning curves of the response-learning s-machine

Graph A : S_1 ———
S_3 . . . . . .
S_4 – – – –
T – . – . –

Graph B : s_t ———
a ● or |

The response-learning s-machine could, as the shopping machine does, hold its own in a restricted version of the imitation game, and, like the shopping machine, it suggests generalizations. It is interesting to envisage the use of the response-learning programme as an elementary building block of a wide variety of more sophisticated systems, including, for example, the shopping programme. In the response-learning s-machine as described the stimulus and the response are external. However, it is possible to form a set of s-machines in which the responses of some serve as stimuli for others. The threshold T of any unit could be allowed to vary under control of some response or conjunction of responses, thus varying the sensitivity to stimulation of this unit. Or again, a response or conjunction of responses could provide approval or disapproval for a member of the system. Such a chain of controls might be open, or it might be closed and regeneration be introduced into the system. No system of this type was actually put into operation, but not, as might have been expected, because of storage capacity limitations. Before this study was begun it was believed that information storage facilities would be the major limiting factor in the design of learning programmes of increasing complexity, but in fact neither the shopping programme nor the response-learning programme require the full Edsac store, and it would be possible to programme the Edsac to act as a system of two, and perhaps of three, response-learning s-machines. However, it was felt that a generalization of the response-learning programme in this way would illustrate no new principles and would be subject to all the limitations already described in connection with the shopping programme. Once a learning programme has been designed, and the s-machine is operating properly, this s-machine is of little further interest to the experimenter unless the functions it performs are of interest in their own right, or unless it can serve as a model of value in the investigation of parallel problems of animal behaviour.

§ 6. Universal Digital Computers as Models

It is important to distinguish carefully between machines intended to be models of the physical structure of animal nervous systems and machines designed to perform specific functions of animal nervous systems. The fact that the s-machines which have been described can play restricted versions of the imitation game implies a correspondence between their functions and some functions of the human nervous system. But as there are usually many means of synthesizing a given pattern of functions it is dangerous to reason from functional to structural correspondence. A special machine could be built, for example, to do only the job of the shopping s-machine. The physical structure and the internal mode of operation of this machine would need to bear no relation to the Edsac and, in turn, to the human brain, other than that of superficial correspondence of certain functions of input and output.

The readiness with which the Edsac, and other universal digital computers, can play different roles at a moment's notice is one of their important properties. When the role a universal digital computer is called upon to play is markedly different from those its designers had in mind, a necessarily large proportion of the orders in a programme must be devoted to specifying this role. In the response-learning programme an aggregate of elementary Edsac orders is required, for example, to imitate the firing of a response, since this is an operation which does not correspond to any single order. This drawback is balanced by some important advantages. Given the Edsac, the only additional equipment required to turn it into a learning machine is a length of teleprinter tape, and changes in s-machine design and the rectification of errors require at most the punching of a new tape. Only a few seconds of input time are required to convert the Edsac from an orthodox computing machine into an experimental learning device, and deconversion is equally rapid. For these reasons a flexible universal digital computer can serve with advantage as a proving ground for a wide variety of models.

Acknowledgments

The author wishes to thank Dr. M. V. Wilkes for suggesting this study. He is indebted to Dr. M. V. Wilkes, Mr. J. W. S. Pringle, Mr. S. Gill and Mr. M. F. C. Woollett for many valuable suggestions, and to Dr. J. C. P. Miller for helpful advice. This study was carried out while the author was the holder of a Henry Fellowship.

References

*Adkins, B. M., 1951, *Brit. J. for the Phil. of Sci.*, II, 248.

Ashby, W. R., 1940, " Adaptiveness and Equilibrium ", *J. Mental Sci.*, **86**, 478–483; 1948, " Design for a Brain ", *Electronic Eng.*, **20**, 379–383.

Berkeley, E. C., 1949, *Giant Brains* (New York : John Wiley).

Craik, K. J. W., 1943, *The Nature of Explanation* (Cambridge University Press).

Crozier, W. J., 1951, " Physiology and Computation Devices ", *Proceedings of a Second Symposium on Large-Scale Digital Calculating Machinery* (Harvard University Press).

Ferranti Ltd., *The Ferranti Nimrod Digital Computer.*

Gill, S., 1951 (manuscript) *Non-numerical Applications of Calculating Machines.*

Grey Walter, W., 1950 " Possible Features of Brain Function and their Imitation ", *Symposium on Information Theory* (see Jackson, W.).

Hadamard, J., 1949, *The Psychology of Invention in the Mathematical Field* (Princeton : University Press).

Hull, C. L., 1937 " Mind, Mechanism, and Adaptive Behaviour ", *Psych. Rev.*, **44**, 1–32.

Jackson, W. (Ed.), 1950, *Proceedings of a Symposium on Information Theory* (London : Ministry of Supply).

Jeffress, L. A. (Ed.), 1951, " Cerebral Mechanisms in Behavior ", *The Hixon Symposium* (New York : John Wiley).

Laslett, P. (Ed.), 1950, *The Physical Basis of Mind* (Oxford : Basil Blackwell).

* Discussions of papers elsewhere in the same journal.

MacKay, D. M., 1951, " Mindlike Behaviour in Artefacts ", *Brit. J. for the Phil. of Sci.*, II, 105–121.
*Mays, W., 1951, *Brit. J. for the Phil. of Sci.*, II, 249–250.
McCulloch, W. S., 1949, " The Brain as a Computing Machine ", *Elect. Eng.*, **68**, 492–497.
McCulloch, W. S., and Pitts, W., 1943, " A Logical Calculus of the Ideas Immanent in Nervous Activity ", *Bull. Math. Biophysics*, **5**, 115–133 ; 1947, " How we know Universals ", *Ibid.*, **9**, 127–147.
Parke, N. G., 1949, *Matrix Methods for the Solution of Scheduling Problems* (Cambridge, Mass., Field Station, U.S.A.F.).
*Pirenne, M. H., 1952, *Brit. J. for the Phil. of Sci.*, II, 315–317.
*Polanyi, M., 1952, *Brit. J. for the Phil. of Sci.*, II, 312–315.
Polya, G., 1948, *How to Solve it* (Princeton : University Press).
Popper, K. R., 1950, " Indeterminism in Quantum Physics and in Classical Physics ", *Brit. J. for the Phil. of Sci.*, I, 117–133, 173–195.
Pringle, J. W. S., 1951, " On the Parallel between Learning and Evolution ", *Behaviour*, III, 174–215.
Prinz, D. G., 1952, " Robot Chess ", *Research*, **5**, 261–266.
Rosenblueth, A., Wiener, N., and Bigelow, J., 1943, " Behavior, purpose and Teleology ", *Phil. of Sci.*, **10**, 18–24.
Ryle, G., 1949, *The Concept of Mind* (London : Hutchinson House).
Shannon, C. E., 1950, " Programming a Computer for Playing Chess ", *Phil. Mag.*, [7] **41**, 256–275.
Turing, A. M., 1936, " On Computable Numbers, with an Application to the Entscheidungsproblem ", *Proc. Lond. Math. Soc.*, **42**, 230–265 ; 1950, " Computing Machinery and Intelligence ", *Mind*, **59**, 433–460.
von Neumann, J., 1951, " The General and Logical Theory of Automata " *Hixon Symposium* (see Jeffress, L. A.).
*Walshe, F. M. R., 1951, *Brit. J. for the Phil. of Sci.*, II, 161–163.
Wiener, N., 1948, *Cybernetics* (New York : John Wiley).
Wilkes, M. V., 1951 a, " Can Machines Think ? ", *Spectator*, No. 6424, 177–178 ; 1951 b, " Automatic Calculating Machines ", *J. Roy. Soc. Arts*, **100**, 56–90.
Wilkes, M. V., Wheeler, D. J., and Gill, S., 1951, *The Preparation of Programs for an Electronic Digital Computer* (Cambridge, Mass. : Addison-Wesley).
Wisdom, J. O., 1951, " The Hypothesis of Cybernetics ", *Brit. J. for the Phil. of Sci.*, II, 1–23.

* Discussions of papers elsewhere in the same journal.

CXXV. *On the Destruction of Superconductivity by Large Currents*

By C. G. Kuper*
Royal Society Mond Laboratory, Cambridge †

[Received August 14, 1952]

Abstract

A theoretical study is made of the restoration of resistance in superconducting wires by large currents. The experiments of Shubnikov and Alexeevsky and of Scott show a marked deviation from the theory of F. London. The present theory uses the same geometrical model of the structure as London, i.e. a string of superconducting conical domains along the axis of the wire. But it takes account of the effect on the resistance of the scattering of electrons at successive normal-superconducting interfaces, when their separation is comparable to the mean free path of the electrons in the normal phase. The scale of the structure is determined by minimizing the 'Magnetic Gibbs' Function'. It is shown that the interfacial surface energy may be neglected. The theory is in fair agreement with the rather scanty experimental data. The only parameter of the theory is the mean free path of electrons, and the value assigned is consistent with that obtained from other phenomena.

§1. Introduction

In the macroscopic theory of the intermediate state of superconductors (London, e.g. 1948) it is assumed that the intermediate state is homogeneous, with $|\mathbf{H}|=H_c$, while $|\mathbf{B}|$ has some value between 0 and H_c. Various bulk properties can then be predicted. However, when observations of such properties are made on small specimens (the meaning of 'small' in the present context will be discussed in § 4), deviations from London's theory are observed. In the case of a specimen under the influence of an external magnetic field, these small deviations are fairly well understood and arise from the surface energy, which will be written as $\Delta H_c^2/8\pi$ per unit area, associated with normal-superconducting interfaces (see e.g. Landau 1937 and 1943, Andrew 1948, Kuper 1951, Lifshitz and Sharvin 1951). But when the intermediate state is set up by currents, the deviations are so large that this explanation is inadequate. After a brief discussion of the discrepancies, we will develop a model which will account for the experimental facts.

We will use the following notation: $\mathbf{H}$=magnetic field, $\mathbf{B}$=magnetic induction, H_c=critical field, I=electric current, $I_c=\frac{1}{2}H_c\rho_0$=critical current (see next paragraph), R=resistance of wire per unit length,

* Now at Department of Theoretical Physics, University of Liverpool.
† Communicated by the Author.

R_n=normal resistance per unit length, ρ_0=radius of wire, ρ=radius of 'core' in the intermediate state (see fig. 1). Instead of taking explicit account of all the supercurrents, we will use the picture of a superconductor in which the permeability $\mu=0$. We will assume that $\rho=\rho_0$ when $I=I_c$.

In London's theory of the destruction of superconductivity by currents in cylindrical wires (London 1948, p. 120) the model assumed is as shown in fig. 1. The field in the core is everywhere critical ($|\mathbf{H}|=H_c$), and outside the core, $|\mathbf{H}|>H_c$. Thus the outer sheath is normal, and the core is in the intermediate state. Silsbee's (1918) suggestion that $I_c=\frac{1}{2}H_c\rho_0$ (introduced to explain the original observation of Kamerlingh Onnes (1911) that superconductivity is destroyed by large currents) is confirmed, and it is predicted that the resistance changes discontinuously, at Silsbee's critical current, from zero to half the normal value. The relation London obtains between resistance and current is (cf. fig. 2)

$$R=\tfrac{1}{2}R_n[1+\sqrt{(1-I_c^2/I^2)}] \qquad (I>I_c). \quad . \quad . \quad . \quad . \quad . \quad (1)$$

Fig. 1

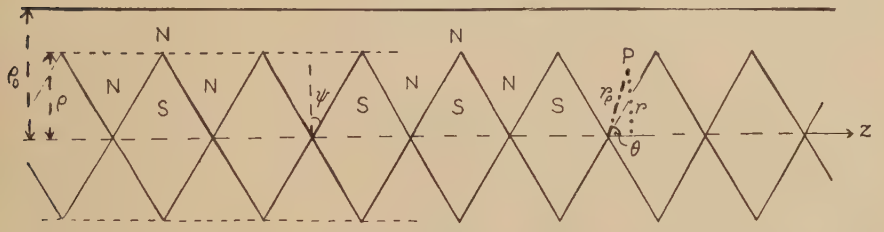

The structure of the wire in the intermediate state. The coordinate systems to be used are indicated.

(A result equivalent to this one was given in a private communication by Langevin to Silsbee, but London's was the first published derivation.) The angle ψ (see fig. 1) between a domain wall and a cross-section of the wire is undetermined, but provided it is small it will not affect the resistance curve.

In marked contrast, experiments (Shubnikov and Alexeevsky 1936, Alexeevsky 1938, Scott 1948) while further confirming Silsbee's hypothesis, show a larger discontinuity than is predicted by London. Thus when I increases through the value I_c, R rises discontinuously from zero to about $0{\cdot}8R_n$. At $I=I_c$, the right-hand derivative of R with respect to I is finite, while according to eqn. (1) it should be infinite. Also for decreasing currents, some hysteresis is observed (see fig. 2).

Three effects capable of influencing the configuration are left out of consideration in London's treatment. These are: (i) the geometrical spreading of the lines of current flow, (ii) the fact that the current is flowing in regions small compared with the mean free path of the electrons in the normal metal, and (iii) the surface energy associated with the interfaces between normal (N-) and superconducting (S) phases.

(ii) will be referred to as the 'size effect'. Scott tentatively suggests that the deviations from London's theory may be due to effect (iii), but it will be shown to be unimportant compared with spreading and the size effect.

§ 2. Outline of the Theory

We will assume the same model as London (fig. 1), but will attempt to take account of the increase of resistance resulting from the size effect (i). It then appears that the discontinuity in the resistance is not independent of the angle ψ; the value that this angle takes will be discussed in §§4 and 5. The value of ψ should be determined by the condition

Fig. 2

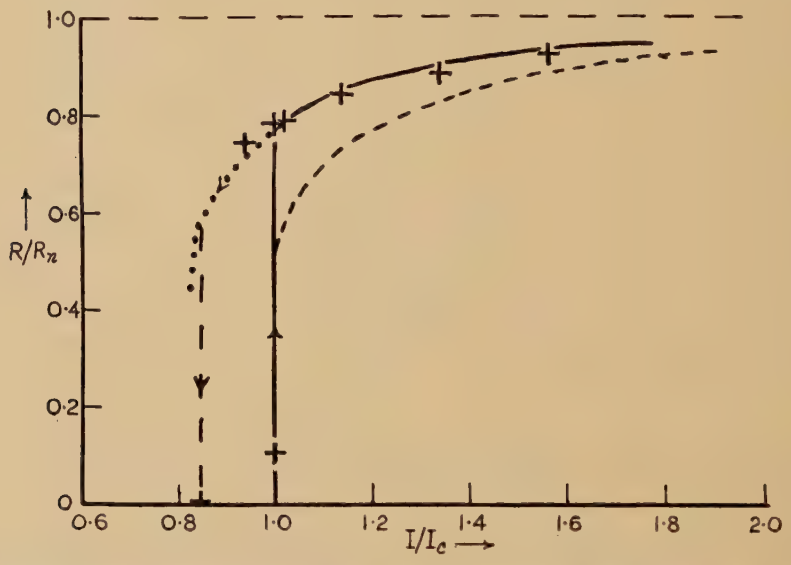

The resistance-current curves. The broken curve is that given by London, the full curve that predicted by the present theory, using the value $l=2{\cdot}8\times10^{-3}$ cm. The points are those found experimentally by Scott for his specimen 3, of radius $17{\cdot}8\times10^{-3}$ cm. The dotted curve is the extrapolation of the theoretical curve into the hysteresis region.

that the 'Magnetic Gibbs' Function' $G=\int(U-TS-\mathbf{B}\,.\,\mathbf{H}/4\pi)\,d\tau$ is a minimum (§ 4). It is difficult to calculate the effect of the spreading (ii) of the current stream lines on G when ψ is large, but an approximate calculation valid for small ψ will be performed. This will lead to ψ-values around $\pi/6$, unfortunately *not* small, which will be seen to vary only slowly with the radius of the core. (The error in G results from neglect of terms in ψ^3, and is likely to be about 10 to 20%.) To a first approximation, we shall thus take $\psi=\pi/6$, independent of ρ. It will be shown in § 5, that effect (iii) leads to only a small change in G.

An exact calculation of the increase of resistance caused by the size effect is also impracticable. But by the use of an approximate interpolation formula (3), we are able to derive an expression for the resistance.

The shape of the observed resistance curves is well reproduced (see fig. 2), and the variation of $R(I_c)/R_n$ with the wire radius ρ_0 is in fair agreement with Scott's data (fig. 3). The hysteresis shown by some of Scott's specimens will be discussed in § 5.

§ 3. The Size and Spreading Effects

(*a*) *The Size Effect*

It will be assumed that electrons are diffusely scattered when they impinge on an N–S interface. This assumption receives some support from the experiments of Pippard (1950), which suggest a ' range of order ' of electrons in the S-phase, of the order of 10^{-4} cm, which is small compared with the mean free path in the N-phase. The existence of this order suggests that an electron impinging on the interface, from the N-phase, will be scattered in a distance comparable with the range of order. The analysis in the present paper would not be modified in substance by assuming instead that a large fraction p was scattered, and the remainder transmitted. This would merely introduce p as another parameter, and in view of the paucity of experimental data, would add little to the physical content of the theory.

We will take a system of cylindrical polar coordinates (r, ϕ, z), with z as the axis of the wire, and the origin at the point of contact of two S-domains, or where it is more convenient for certain approximations, spherical polar coordinates (r_P, θ, ϕ), (see fig. 1). In conformity with the usual notation, we shall use n for the number of conduction electrons per unit volume, e and m for the electronic charge and mass, v for the velocity of an electron at the Fermi surface, and l for the mean free path of an electron in the N-phase.

Owing to the geometry of the configuration, it appears that an exact calculation by Fuchs' (1938) method of the ' size effect ' contribution to the resistance is impracticable. The following rather crude approximation will be used instead (Thomson 1901, Lovell 1936). The conductivity σ is assumed to be a point function. Let σ be written $\sigma_0 \Lambda/l$, where $\sigma_0 = ne^2 l/mv$ is the bulk conductivity. Then Λ at a point P is to be evaluated as follows: Construct a sphere of radius l about the point P. Draw a cone of small solid angle $d\omega$, with P as vertex. Let λ be the distance from P to the surface of the sphere or the bounding surface of the domain, whichever is the less. Then

$$\Lambda = \int \lambda \, d\omega / 4\pi. \quad . \quad . \quad . \quad . \quad . \quad . \quad . \quad . \quad (2)$$

Even this approximation is intractable except in two special cases. One occurs when P is the origin of coordinates. Here $\Lambda = l \sin \psi$. The other is where the sphere does not intersect the domain boundaries, i.e. far from the axis of the wire. Here $\Lambda = l$. A convenient interpolation formula for intermediate points is

$$\sigma/\sigma_0 = \Lambda/l = 1 - (1-s) \exp(-rs/l), \quad . \quad . \quad . \quad . \quad . \quad (3)$$

where $s=\sin\psi$. This yields $\Lambda/l=\sin\psi$ for $r=0$, and has risen to near unity when the path length $2rs \gg l$. Equation (3) assumes σ to be constant along a line of constant r. This is not true, for when P is near a domain boundary σ/σ_0 is appreciably less than when $z=0$. We can interpret eqn. (3) as giving an average of σ along a stream line. In view of this, we are able to fix the coefficient of $-rs/l$ in the exponent as unity, since by eqn. (2) when $rs \sim l$, $\sigma(z=0) \sim \sigma_0$ but $\sigma(z=l) \sim \frac{1}{2}\sigma_0$, so that σ/σ_0 should be, say, 0·8. Taking $s \sim \frac{1}{2}$, eqn. (3) gives $\sigma/\sigma_0 \sim 0{\cdot}75$. The detailed choice of the form of the interpolation formula has little influence on the final result.

(*b*) *Spreading Effects*

We shall make two assumptions, true only in the limiting case of ψ small. These are that σ is a function of r_P only and not of θ, and that Λ is constant along a stream line. With the latter assumption the electrostatic potential V satisfies Laplace's equation. For* if $\mathbf{j}$ is the current density, the equation of continuity gives

$$\frac{\partial}{\partial r}(rj_r)+r\frac{\partial}{\partial z}j_z=0.$$

Defining a stream function Ψ, such that

$$rj_r=\partial\Psi/\partial z\,; \qquad rj_z=-\partial\Psi/\partial r,$$

we have

$$0=\frac{\partial\Psi}{\partial a}=\frac{j_r}{|\mathbf{j}|}\frac{\partial\Psi}{\partial r}+\frac{j_z}{|\mathbf{j}|}\cdot\frac{\partial\Psi}{\partial z},$$

where $\partial/\partial a$ means differentiation along a stream line. Also by Ohm's Law,

$$j_r=\sigma E_r\,; \qquad j_z=\sigma E_z.$$

Hence

$$\partial\Psi/\partial z=\sigma r E_r\,; \qquad \partial\Psi/\partial r=-\sigma r E_z.$$

As we have assumed $\sigma=ne^2\Lambda/mv$ is constant along a stream line, we may define $\chi=\int\sigma^{-1}\,d\Psi$ and then

$$\frac{\partial\chi}{\partial z}=r\frac{\partial V}{\partial r}\,; \qquad \frac{\partial\chi}{\partial r}=-r\frac{\partial V}{\partial z},$$

whence $\nabla^2 V=0$, as stated above.

If we assume that when the current is greater than I_c (and the core radius correspondingly less than ρ_0), the current in the core still remains strictly confined to the radius of the core, then we may apply the boundary condition $\partial V/\partial r=0$ to the surface of the core. The other boundary conditions may be chosen as $V=0$ on the normal cross-section through the vertex of the cone (fig. 1); $V=\epsilon$ on the conical domain surface. In order to solve the Laplace equation we will simplify the conditions by replacing the cylindrical boundary $r=\rho$ by the spherical one $r_P=\rho$. Then the solution is such that the lines of current flow are arcs of circles, whose centre is the origin. Then by the axial symmetry, the magnetic field lines are circles about the axis, and the field at the point (r_P, θ, ϕ) is

$$H=\frac{2}{r}\int_0^{r_P}2\pi r_P j(r_P)dr_P=\frac{2}{r_P\sin\theta}\int_0^{r_P}2\pi r_P j(r_P)dr_P=\frac{\cos\psi}{\sin\theta}H_1, \quad . \quad (4)$$

* I am indebted to Professor D. R. Hartree for this proof.

where H_1 is the field for $\theta=\pi/2-\psi$. Thus the only effect of spreading, in this approximation, is to introduce the factor $\cos\psi/\sin\theta$ in H. Thus the spread of current does not alter the resistance, but it will affect the magnetic Gibbs' function considerably (§ 4). In a better approximation, we should expect spreading to produce a slight modification of the resistance as well.

§ 4. The Magnetic Gibbs' Function

Owing to the presence of irreversible effects (Joule heating and heat conduction) it is not immediately obvious that the usual thermodynamic methods are applicable, and that the equilibrium configuration may be got from the condition that the magnetic Gibbs' function

$$G=\int (U-TS-BH/4\pi)\, d\tau$$

is minimal. While it should be possible to justify it by the methods of irreversible thermodynamics, we may do so more simply by appealing to experiment. For Scott (1948) has shown that the form of the resistance curve (fig. 2) is nearly independent of the temperature, though the actual value of the critical current varies through a wide range. Since the Joule heating and thermal conduction are both proportional to $\mathbf{j}^2$, this invariance of the curve of fig. 2 with the value of I_c shows that conditions in the wires and their heat-baths are nearly isothermal. By performing the experiments close enough to the normal transition temperature T_0, we can make the irreversible effects as small as we choose, and hence we can apply the usual thermodynamic formulae. The invariance of the shape of the curve then confirms the continued validity of this procedure, even at temperatures well below T_0.

The only terms in G which depend on the configurational parameter ψ are (where $\Delta H_c^2/8\pi$ is the surface energy)

$$-\frac{1}{8\pi}\int_{N\text{–regions}} H^2\, d\tau+\frac{1}{8\pi}\int_{N\text{–}S\ \text{interfaces}} \Delta H_c^2\, dS,$$

of which the surface energy term will be shown to be unimportant. To evaluate $\mathcal{G}_N=-\int_{N\text{–regions}} H^2\, d\tau/8\pi$, we require an expression for H. The current density is

$$j=\sigma\epsilon/r\psi, \qquad (5)$$

and thus

$$H_1=\frac{2}{r}\int_0^r 2\pi r\, j(r)\, dr, \qquad (6)$$

where H_1 is the value of H at $\theta=\pi/2-\psi$ (see eqn. (4)), i.e.,

$$H_1=\frac{4\pi\sigma_0\epsilon}{r\psi}\int_0^r \frac{\sigma}{\sigma_0}\, dr=\frac{4\pi\sigma_0\epsilon}{r\psi}\int_0^r [1-(1-s)\exp(-rs/l)]\, dr$$
$$=\frac{4\pi\sigma_0\epsilon}{\psi}\left[1-\frac{1-s}{sx}\{1-\exp(-sx)\}\right],$$

where $x=r/l$; $s=\sin\psi$. Hence

$$H=\frac{\cos\psi}{\sin\theta}\cdot\frac{4\pi\sigma_0\epsilon}{\psi}\left[1-\frac{1-s}{sx}\{1-\exp(-sx)\}\right].$$

Now the potential difference ϵ across half a domain is related to the mean electric field by the equation $E=\epsilon/\rho\psi$ and therefore

$$H=\frac{\cos\psi}{\sin\theta}\cdot 4\pi\sigma_0 E\rho\left[1-\frac{1-s}{sx}\{1-\exp(-sx)\}\right]. \quad . \quad . \quad . \quad (7)$$

At large distances from the axis of the wire, we assume that $H_1=H_c$ so that we find for ρ the equation

$$H_c=4\pi\sigma_0 E\rho. \quad . \quad . \quad . \quad . \quad . \quad . \quad . \quad . \quad . \quad (8)$$

Thus

$$-8\pi\mathscr{G}_N=2\pi\int_{N\text{-domains}}H^2r^2\,dr\sin\theta\,d\theta=2\pi\int_0^{\pi/2-\psi}\frac{\cos^2\psi}{\sin\theta}d\theta\int_0^{\varrho}H_1^2r^2\,dr$$

or

$$-\mathscr{G}_N=\tfrac{1}{4}\rho^3(1-s^2)\log\sqrt{\left(\frac{1+s}{1-s}\right)}\cdot(4\pi\sigma_0E\rho)^2$$
$$\times\int_0^{\varrho/l}\left[1-\frac{1-s}{sx}(1-e^{-sx})\right]^2l^3x^2dx \quad \text{per half-domain,}$$

or from eqn. (8), if $y=\rho/l$,

$$-\mathscr{G}_N=\tfrac{1}{4}H_c^2\rho^3(1-s^2)\log\sqrt{\left(\frac{1+s}{1-s}\right)}\frac{1}{y^3}\int_0^y\left[1-\frac{1-s}{sx}(1-e^{-sx})\right]^2x^2dx$$

per half-domain

$$=\tfrac{1}{4}H_c^2\rho^2(1-s^2)^{3/2}s^{-1}\log\sqrt{\left(\frac{1+s}{1-s}\right)}\cdot\left\{\frac{1}{3}-\frac{1-s}{sy}\left[1-\frac{1-s}{sy}-\frac{1+3s}{2s^2y^2}\right]\right.$$
$$\left.-2\frac{(1-s)}{s^2y^2}\cdot\frac{1+y}{y}\cdot e^{-sy}-\frac{(1-s)^2}{2s^3y^3}\cdot e^{-2sy}\right\} \text{ per unit length}$$

$$. \quad . \quad . \quad . \quad . \quad . \quad . \quad . \quad . \quad (9)$$

(since the length of a half-domain is $\rho\tan\psi=\rho s/\sqrt{(1-s^2)}$).

Table 1. $-4\mathscr{G}_N/H_c^2\rho^2$

y \ s	0·2	0·3	0·4	0·5	0·6	0·7	0·8
1	0·021	0·043	0·062	0·0808	0·0894	0·0880	0·071
5	0·061	0·100	0·1276	0·1410	0·1481	0·119	

In table 1, the values of $-4\mathscr{G}_N/H_c^2\,\rho^2$ are tabulated for varying s, for $y=1$ and $y=5$. The maximum is seen to occur at $s=0{\cdot}64$ for $y=1$, and at $s=0{\cdot}57$ for $y=5$. Thus the approximation of small ψ cannot be valid, and little reliance should be placed on the exact numerical equilibrium s-values. On the other hand since the error in $\mathscr{G}_N$ due to the approximation in (4) is $O(\psi^3)$, we should not expect the values to be in error by more than about 20%, and we can have rather more confidence in the qualitative assertion that s_{equil} varies very slowly with ρ. In comparing the theory

with experiment, we shall thus (as an adequate approximation) take $s_{equil}=\frac{1}{2}$, independent of the radius $\rho=yl$ of the core. We shall see, in § 5, that this value of s leads to a perfectly sharp transition for wires of vanishingly small radius, as we should expect.

We have not yet taken account of the surface energy, $\Delta H_c^2/8\pi$ per unit area, associated with the N–S interfaces. The contribution to the free energy is

$$\mathscr{G}_{surf}=\frac{\Delta H_c^2}{8\pi}\int_{N-S\ interfaces} ds=\tfrac{1}{4}\Delta H_c^2\rho L\sin\psi$$

per half-domain, where $L=\rho\tan\psi$=the half-domain length; or per unit length,

$$\mathscr{G}_{surf}=\tfrac{1}{4}H_c^2\rho^2\frac{\Delta}{\rho}\cdot\frac{1}{2s}. \quad . \quad . \quad . \quad . \quad . \quad . \quad . \quad (10)$$

$H_c^2\rho^2/8s$ is comparable in order of magnitude to $\mathscr{G}_N$, but the factor Δ/ρ is of order 10^{-3} (see, e.g. Kuper 1951, for a discussion of the value of Δ). Thus the contribution of the surface energy to the Gibbs' function is not significant; the minimum of $\mathscr{G}$ will not be shifted far in consequence.

The meaning of a 'small' specimen in § 1 is now clear—in those intermediate state phenomena where surface energy is important 'small' means of the order of magnitude of Δ, while where mean free path effects dominate, as in the present situation, 'small' means of the order of l—about 100 times larger than Δ.

§ 5. The Resistance–Current Curve

The current is made up of two parts, that in the core, I_1, and that outside the core, I_2. The expressions for I_1 and I_2 are

$$I_1=\rho H(\rho)/2\,;\quad I_2=\pi\sigma_0 E\,(\rho_0^2-\rho^2). \quad . \quad . \quad . \quad . \quad . \quad . \quad (11)$$

From eqns. (7) and (8), the sum $I=I_1+I_2$ may be written

$$I=I_1+I_2=\pi\sigma_0 E\rho_0^2+H_c^2\left[1-2\frac{1-s}{sy}(1-e^{-sy})\right]/16\pi\sigma_0 E,$$

or with the notation $f^2=1-2\xi=1-2\dfrac{1-s}{sy}(1-e^{-sy})$, ... (12)

$$I=\pi\sigma_0 E\rho_0^2+H_c^2 f^2/16\pi\sigma_0 E. \quad . \quad . \quad . \quad . \quad . \quad . \quad . \quad (13)$$

(Compare London 1948, p. 122, eqns. (3) to (5).) Following London, we can solve (13) to give the resistance, R per unit length,

$$R=E/I=\frac{1}{2\pi\sigma_0\rho_0^2}[1+\sqrt{(1-I_c^2f^2/I^2)}]=\tfrac{1}{2}R_n[1+\sqrt{(1-I_c^2f^2/I^2)}]\ (I>I_c)\,.$$
$$. \quad . \quad . \quad (14)$$

We can now account for the observed features of the resistance curves which are not reproduced by London's theory. For while the current I is increased from zero to I_c, the resistance remains zero, but as soon as it

passes I_c, the resistance rises abruptly, on to the curve of (14), approximately of the form of London's curve, but with a ' critical current ' less than the true critical current. This will therefore account both for the restored resistance in excess of $\frac{1}{2}R_n$, and for the finiteness of the right-hand derivative of the resistance at $I=I_c$. With increasing current, the core will contract, and f^2 will consequently approach zero. This will result in a rather more rapid approach of the resistance to R_n than would be the case if f^2 were constant, but it will not affect the general features of the curves. To derive an expression for f^2 in terms of I, we insert in (12) for $y=\rho/l$ its value from (8), $y=H_c/4\pi\sigma_0 El=H_c/4\pi\sigma_0 RIl=(I_c/I)(R_n/R)y_0$ where $y_0=\rho_0/l$. This leads to

$$R=\tfrac{1}{2}R_n\left(1+\sqrt{\left[1-\frac{I_c^2}{I^2}\left\{1-2\frac{(1-s)IR}{s\,I_cR_ny_0}\,(1-\exp[-sI_cR_ny_0/IR])\right\}\right]}\right).$$

To solve this implicit equation for R, we approximate, inserting $R=R_n$ on the r.h.s. to give (putting $s=\frac{1}{2}$; see below),

$$R=\tfrac{1}{2}R_n\left(1+\sqrt{\left[1-\frac{I_c^2}{I^2}\left(1-2\frac{I}{I_cy_0}\{1-e^{-y_0I_c/2I}\}\right)\right]}\right) \quad . \quad . \quad . \quad . \quad . \quad (15)$$

We can see that using the value $s_{equil}=\frac{1}{2}$ leads, for very small wires, to the result that $\xi\to\frac{1}{2}$, or $f^2\to 0$. Thus, in the limit as $\rho_0\to 0$, we find the *whole* resistance restored at $I=I_c$. This is in accord with an extrapolation from the existing experimental data. The retention of $s_{equil}=\frac{1}{2}$ for such small wires is partially justified by the following considerations: Although eqn. (9) would give $s_{equil}\to 1$ as $\rho\to 0$ this is just the condition for the approximations made in deriving (9) to have *no* validity at all. On the other hand in the region $y\sim 1$ to $y\sim 10$, s_{equil} as derived from (9), $s_{(9)}$ for brevity, is not very different from $\frac{1}{2}$, and the errors in $\mathscr{G}_N$ are of order ψ^3, or about 20%, say. Thus throughout the region of ρ-values where the approximations made in deriving $\mathscr{G}_N$ are at all tolerable, $s_{(9)}\simeq\frac{1}{2}$. Further, though these approximations break down in the limit $\rho\to 0$ there is no apparent reason why the model itself should do so. Finally, the result that the N–S transition should be quite sharp for small enough specimens is to be expected, by analogy with a similar extrapolation in other intermediate state phenomena (e.g. Andrew 1948).

The form of (14) or (15) suggests the occurrence of hysteresis, for when I decreases through the value I_c, the curve can formally be extrapolated to where it has a vertical tangent. In the present model, it is true, this extrapolation has no physical meaning, for it would imply $\rho>\rho_0$, which is absurd. But if the S-domains have slightly rounded edges at the boundary of the core, and consequently do not quite touch the surface of the wire when $I=I_c$ (this is a small modification of the model, to be expected when the surface energy is taken into account) then the extrapolation, for some distance at least, will be physically significant. (The greatest possible range of currents between which hysteresis can occur is roughly from $I=fI_c$ to $I=I_c$.)

§ 6. Comparison with Experiment

The only experiments in which the variation of the form of the resistance curves with the radius of the wire has been investigated are those of Scott (1948). Three indium wires of differing radius were investigated. The mean free path of electrons in indium is unfortunately not known with any precision, but has to be determined from the observations as a parameter. The continuous curves in fig. 3 are the graphs of $R(I_c)/R_n$ and $f^2(I_c)$ as functions of y_0 (from eqn. (12)). The first three rows of table 2 indicate Scott's experimental values of $R(I_c)/R_n$ and the values of $f^2(I_c)$ deduced from them, for varying ρ_0. The value of l for best fit is $l=2{\cdot}4\times10^{-3}$ cm. If we express the values of ρ_0 in terms of y_0 using this l then the experimental points lie as indicated in relation to the curves in fig. 3.

Fig. 3

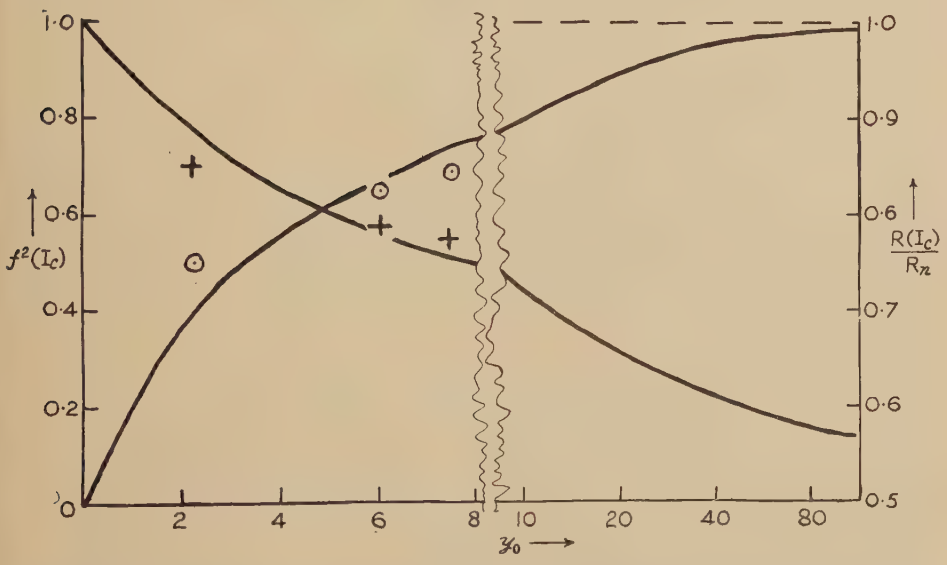

Graphs of $R(I_c)/R_n$ and $f^2(I_c)$ against y_0. The experimental points of Scott are shown, taking $l=2{\cdot}4\times10^{-3}$ cm. After the break, a logarithmic scale is used. $+$ $R(I_c)/R_n$; $\odot$ $f^2(I_c)$. The rising curve is of $f^2(I_c)$.

Table 2

Specimen	Substance	Radius (ρ_0)	$R(I_c)/R_n$	$f^2(I_c)$
Scott, 1, 1a	In	$5{\cdot}3\times10^{-3}$ cm	0·854	0·498
Scott, 2	In	$14{\cdot}3\times10^{-3}$ cm	0·795	0·651
Scott, 3	In	$17{\cdot}8\times10^{-3}$ cm	0·778	0·689
Alexeevsky I, II	Sn	$5{\cdot}6\times10^{-3}$ cm	0·80	0·64

In fig. 2, we have drawn the curve of eqn. (15) for the value $l=2{\cdot}8\times10^{-3}$ cm, and indicate Scott's experimental points for his specimen 3, of radius $\rho_0=17{\cdot}8\times10^{-3}$ cm. (This value of l is chosen as the best for this particular specimen, rather than the mean value, $2{\cdot}4\times10^{-3}$ cm, for all the specimens.)

Although Alexeevsky has not studied the variation of the resistance curves with ρ_0 in detail, but has only given adequate data for one specimen radius, he has fortunately worked on tin, where a good estimate of l may be found from the experiments of Chambers (1950) on the anomalous skin effect. For this specimen (see the last row of table 2), $f^2=0{\cdot}64$ corresponding to $y_0=5$, or since $\rho_0=5{\cdot}6\times10^{-3}$ cm, to $l=1{\cdot}1\times10^{-3}$ cm. This is to be compared with the value of l found from Chambers' result that $\sigma_0/l=\text{constant}=9{\cdot}5\times10^{-10}$ mho/cm^2 for Sn. For this specimen we estimate $\sigma_0^{-1}=2{\cdot}4$ to $3{\cdot}6\times10^{-8}$ ohm–cm, whence $l=0{\cdot}35$ to $0{\cdot}6\times10^{-3}$ cm. The agreement is satisfactory, in view of the approximations we have made.

§ 7. Discussion

There are several difficulties in the present treatment. Thus, as in London's theory, we are still left with a singularity of the magnetic field on the axis of the wire (as a consequence of the infinite current density at the point of contact of two S-domains). But when the surface energy is taken into account, we should expect the domain boundaries to become rounded, so that instead of touching, they have a separation of order Δ. The phenomenon of hysteresis observed by Scott has already been interpreted in terms of the rounding of the domain boundaries at the core surface.

The effect of spreading is interesting. Even in the absence of size effects, spreading will reduce the magnetic field *inside* the N-domains, though not on the domain boundaries. If the field is H_c on the boundary, it is $H_c\cos\psi/\sin\theta$, less than H_c, inside the N-metal, which is therefore not in true thermodynamic equilibrium. A similar difficulty occurs in Landau's (1937) theory of the intermediate state under external fields, and has not really been satisfactorily resolved. Either the intermediate state is not in true thermodynamic equilibrium, as seems likely, (though the departure from equilibrium is small) or the model is inadequate to deal with this difficulty. The ratio H/H_c inside the S-metal is, in any case, never less than $\cos\psi$, or about 0·9. In fact the approximations used in § 3 (*b*) overestimate the effectiveness of spreading, and H/H_c is really still closer to unity.

The ' tails ' in the resistance curves of both Alexeevsky and Scott are not accounted for by the present theory. The fact that not all of Scott's specimens showed this behaviour suggests that this behaviour represents a departure from ideal conditions—perhaps a consequence of strains or impurities. The smallness of the electronic mean free path ($l<10^{-3}$ cm) in Alexeevsky's specimens confirms the impression that the specimens were strained or contained impurities, since in very carefully prepared tin

specimens l can become about 10^{-2} cm. Experiments on such specimens (and also on specimens in which l had been deliberately reduced by addition of impurities) would be of great interest.

Acknowledgments

I wish to thank Mr. H. N. V. Temperley, Dr. D. Shoenberg, Dr. A. B. Pippard, Dr. R. G. Chambers, Mr. A. Klug, and other members of the Mond Laboratory for much helpful discussion and criticism. I am indebted to Cambridge University for a Research Maintenance Grant.

References

Alexeevsky, N. E., 1938, *Zh. Eksp. Teor. Fiz.*, **3,** 342.
Andrew, E. R., 1948, *Proc. Roy. Soc.* A, **194,** 98.
Chambers, R. G., 1950, *Nature, Lond.*, **165,** 239.
Fuchs, K., 1938, *Proc. Camb. Phil. Soc.*, **34,** 100.
Kamerlingh Onnes, H., 1911, *Commun. Phys. Lab. Univ. Leiden*, **13,** No. 133 a.
Kuper, C. G., 1951, *Phil. Mag.*, **42,** 961.
Landau, L., 1937, *Phys. Zeit. Sowjet.*, **11,** 129 ; 1943, *J. Phys. U.S.S.R.*, **7,** 99.
Lifshitz, E. M., and Sharvin, Yu. V., 1951, *Dokl. Akad. Nauk. S.S.S.R.*, **79,** 783.
London, F., 1948, *Superfluids, Vol. I.* (New York: Wiley).
Lovell, A. C. B., 1936, *Proc. Roy. Soc.* A, **157,** 311.
Pippard, A. B., 1950, *Proc. Roy. Soc.* A, **203,** 210.
Scott, R. B., 1948, *Bur. Stand. J. Res.*, **41,** 581.
Shubnikov, L. W., and Alexeevsky, N. E., 1936, *Nature, Lond.*, **138,** 804.
Silsbee, F. B., 1918, *Bull. U.S. Bur. Stand.*, **14,** 301.
Thomson, Sir J. J., 1901, *Proc. Camb. Phil. Soc.*, **11,** 120.

CXXVI. *On the Born–Green Theory of Binary Mixtures*

By G. S. Rushbrooke
King's College, Newcastle, University of Durham*

[Received September 10, 1952]

Summary

The Born–Green equations for binary mixtures are related to certain approximations to the integrals occurring in Mayer–Montroll expansions of radial distribution functions in powers of density and composition. The significance of the vanishing of the denominator in the resulting formulae is discussed.

§1. Introduction

The statistical theory of classical fluids, formulated in terms of the radial distribution function and based on the superposition approximation of Kirkwood and Boggs (1942), was recently discussed by Rushbrooke and Scoins (1951)† who showed, in particular, that the resulting equations for the three distribution functions, $g_{AA}(r)$, $g_{AB}(r)$ and $g_{BB}(r)$, appropriate to a binary mixture (N_A A-systems, N_B B-systems in a volume V at temperature T, pressure p, etc.) are mutually consistent only if these equations are first linearized in the way that Born and Green (1949) and Rodriguez (1949) have linearized the corresponding equation for a pure, one component, fluid. This linearization involves writing

$$g_{ij}(r)=\exp\left[-\phi_{ij}(r)/kT\right]\exp\left[f_{ij}(r)\right]=\exp\left[-\phi_{ij}(r)/kT\right](1+f_{ij}(r)), \quad . \quad (1)$$

i=A, B ; j=A, B ; where ϕ is the interatomic potential function and $f(r)\to 0$ as $r\to\infty$. With this normalization $g_{AB}(r)=g_{BA}(r)$. And the two forms of (1) are effectively equivalent since only terms linear in $f_{ij}(r)$ are retained in the linear equations concerned.

These equations, satisfied by $f_{ij}(r)$, are (eqn. (34) of I)

$$rf_{ij}(r)=2\pi\rho_A\int_0^\infty\int_{-s}^{s}(t+r)[f_{iA}(t+r)+\epsilon_{iA}\alpha_{iA}(t+r)]\,dt\,\epsilon_{jA}s\alpha_{jA}(s)\,ds$$
$$+2\pi\rho_B\int_0^\infty\int_{-s}^{s}(t+r)[f_{iB}(t+r)+\epsilon_{iB}\alpha_{iB}(t+r)]\,dt\,\epsilon_{jB}s\alpha_{jB}(s)\,ds, \quad . \quad (2)$$

i=A, B ; j=A, B ; where

$$\alpha(r)=\exp[-\phi(r)/kT]-1,\ \rho_A=N_A/V,\ \rho_B=N_B/V$$

and the ϵ's are parameters which will be discussed more fully below.

In I we did not give explicitly the solutions of these equations, which are easily found by the method of Fourier transforms, for their

* Communicated by the Author.
† Referred to hereafter as I.

interpretation was felt to be obscure. They have, however, been published independently by Fournet (1951). In our notation, these solutions are

$$f_{AA}(r)=\frac{1}{\sqrt{(2\pi)}}\int_{-\infty}^{\infty}\frac{\rho_A a^2(s)+\rho_B c^2(s)-\rho_A\rho_B a(s)[a(s)b(s)-c^2(s)]}{(1-\rho_A a(s))(1-\rho_B b(s))-\rho_A\rho_B c^2(s)}\,s\,\frac{\sin rs}{r}\,ds,$$

$f_{AB}(r)=$ . . . (3)

$$\frac{1}{\sqrt{(2\pi)}}\int_{-\infty}^{\infty}\frac{\rho_A a(s)c(s)+\rho_B b(s)c(s)-\rho_A\rho_B c(s)[a(s)b(s)-c^2(s)]}{(1-\rho_A a(s))(1-\rho_B b(s))-\rho_A\rho_B c^2(s)}\,s\,\frac{\sin rs}{r}\,ds, \quad (4)$$

and similarly for $f_{BB}(r)$. Here $\rho_A=(2\pi)^{3/2}\rho_A$, $\rho_B=(2\pi)^{3/2}\rho_B$ and

$$a(s)=\epsilon_{AA}\beta_{AA}(s),\ b(s)=\epsilon_{BB}\beta_{BB}(s),\ c(s)=\epsilon_{AB}\beta_{AB}(s) \quad . \ . \ . \quad (5)$$

with

$$\beta_{ij}(s)=\frac{1}{\sqrt{(2\pi)}}\int_{-\infty}^{\infty}\alpha_{ij}(r)r\,\frac{\sin rs}{s}\,dr.$$

It is the purpose of the present paper both to throw some light on the interpretation of these equations and to relate them to the cluster-integral theory of Mayer and Montroll (1941), as has been done recently for a pure, one component, fluid by Rushbrooke and Scoins (1952).* In particular, we are interested in the significance of the vanishing of the denominator in (3) or (4). For a one component fluid, when the corresponding denominator is $1-\rho\epsilon\beta(s)$, it is supposed that condensation, from gas to liquid at a given temperature, occurs at that value of ρ for which $1-\rho\epsilon\beta(0)=0$; i.e. that the significant root of the denominator is at $s=0$. Support is certainly lent to this assumption by the work of II, and we shall assume that here too, in the case of a binary mixture, we are concerned only with the roots of

$$(1-\rho_A\epsilon_{AA}\beta_{AA}(s))\,(1-\rho_B\epsilon_{BB}\beta_{BB}(s))=\rho_A\rho_B\epsilon_{AB}{}^2\beta_{AB}{}^2(s) \quad . \quad (6)$$

at the point $s=0$.

§ 2. Connection with the Theory of Mayer and Montroll

Analogously with the expansion of $g(r)$ in powers of ρ given by Mayer and Montroll (1941) we have, for a binary mixture, the three expansions

$$g_{ij}(r)=\exp[-\phi_{ij}(r)/kT]\left[1+\sum_{m+n\geqslant 1}\rho_A{}^m\rho_B{}^n g_{mn}^{ij}(r)\right] \quad . \ . \ . \quad (7)$$

where (ij) stands for (AA), (AB) or (BB) and m and n are positive integers. The functions $g_{mn}^{ij}(r)$ are related to the irreducible cluster integrals familiar in the virial coefficient theory of imperfect gases: and it is appropriate to refer to them as open cluster integrals. Graphically, an open cluster integral involved in $g_{mn}^{ij}(r)$ has two fixed major points, distance r apart, occupied by species A or B according to the upper specification (ij), and $m+n$ other points, over which spatial integrations are performed, of which m are occupied by A-species and n by B-species.

* Referred to hereafter as II.

$g^{ij}_{mn}(r)$ is the sum of all distinguishable such open cluster integrals, the integrand in each case being a product of the appropriate $\alpha(r)$ factors between pairs of the $m+n+2$ points (excluding any direct link between the two major points). In each case there must be sufficient linkages for the corresponding cluster diagram to form an irreducible cluster diagram of the type familiar in virial coefficient theory were a link to be included between the two major points.

Fig. 1

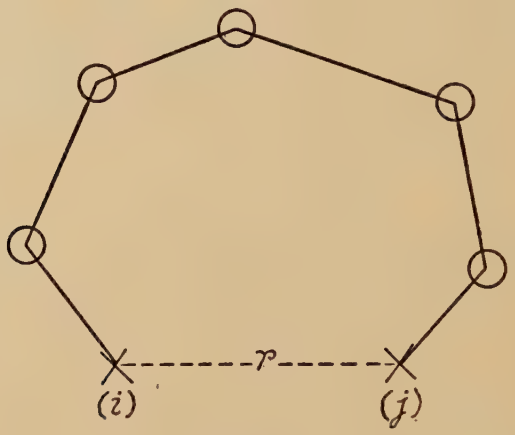

Fig. 2

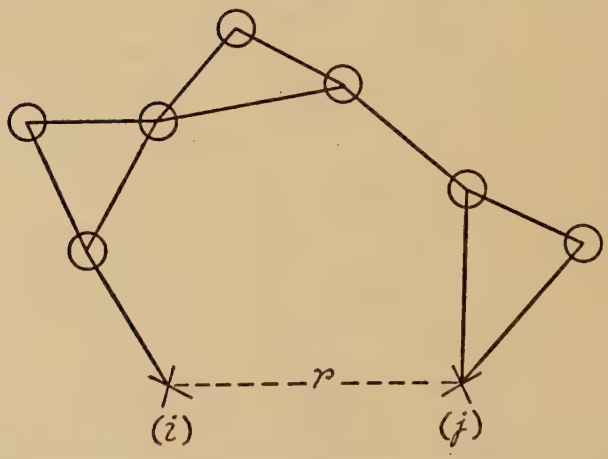

In each case there are $m+n$ ○'s of which m are occupied by A's and n by B's.

Now it is quite impracticable, on this basis, to derive a closed expression for the right-hand side of (7); but there are two simple approximations to the functions $g^{ij}_{mn}(r)$ which enable us so to do. They consist in replacing $g^{ij}_{mn}(r)$ by either $c^{ij}_{mn}(r)$ or $d^{ij}_{mn}(r)$ (the latter approximation being the better, but more elaborate) where the integrals involved in $c^{ij}_{mn}(r)$ are simple chain integrals, fig. 1, while those involved in $d^{ij}_{mn}(r)$ correspond to netted chains, fig. 2. In neither case, of course, is full

justice done to $g^{ij}_{mn}(r)$ except when $m+n=1$; but we have shown in II that for an imperfect gas either approximation gives the second and third virial coefficients, B and C, correctly, while the netted chain approximation takes very satisfactory account of the fourth virial coefficient, D. The analysis for mixtures is a little more difficult, in that linear Ising lattice problems are involved, but equally practicable: it is hoped that the following rather condensed account will sufficiently indicate the method of derivation of the final formulae.

(i) *The Simple Chain Approximation*

According to Lemma I of I, the chain integral involving p A-A links, q B-B links and X A-B links is simply

$$\frac{1}{\sqrt{(2\pi)}}(2\pi)^{3(m+n)/2}\int_{-\infty}^{\infty} s\beta^{p}_{\mathrm{AA}}(s)\beta^{q}_{\mathrm{BB}}(s)\beta^{X}_{\mathrm{AB}}(s)\frac{\sin rs}{r}ds. \quad . \quad . \quad (8)$$

In evaluating $\sum_{m+n\geqslant 1}\rho_{\mathrm{A}}{}^{m}\rho_{\mathrm{B}}{}^{n}c^{ij}_{mn}(r)$, therefore, we require to find

$$\Sigma\rho_{\mathrm{A}}{}^{m}\rho_{\mathrm{B}}{}^{n}\beta^{p}_{\mathrm{AA}}(s)\beta^{q}_{\mathrm{BB}}(s)\beta^{X}_{\mathrm{AB}}(s), \quad . \quad . \quad . \quad . \quad . \quad . \quad . \quad (9)$$

where the sum is over all appropriate values of m, n, p, q and X.

Consider, for definiteness, the approximation to $g_{\mathrm{AB}}(r)$. Then we are concerned with linear arrangements of the type, fig. 3, in which

Fig. 3

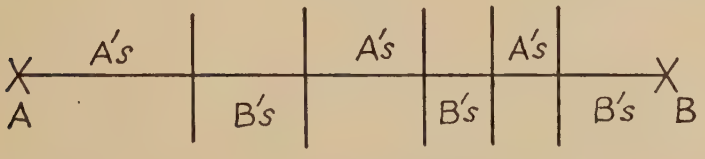

$X=2Y+1$ and, apart from the terminal blocks, there are Y blocks of A's and Y blocks of B's, each containing one or more systems. Thus for given Y, >0, the contribution to (9) is

$$\frac{1}{(1-\rho_{\mathrm{A}}\beta_{\mathrm{AA}})}\left(\frac{\rho_{\mathrm{A}}}{1-\rho_{\mathrm{A}}\beta_{\mathrm{AA}}}\right)^{Y}\left(\frac{\rho_{\mathrm{B}}}{1-\rho_{\mathrm{B}}\beta_{\mathrm{BB}}}\right)^{Y}\beta^{2Y+1}_{\mathrm{AB}}\frac{1}{(1-\rho_{\mathrm{B}}\beta_{\mathrm{BB}})}. \quad . \quad (10)$$

In the particular case $Y=0$, however, when we have terminal blocks only, the contribution is

$$\frac{\beta_{\mathrm{AB}}}{(1-\rho_{\mathrm{A}}\beta_{\mathrm{AA}})(1-\rho_{\mathrm{B}}\beta_{\mathrm{BB}})}-\beta_{\mathrm{AB}}, \quad . \quad . \quad . \quad . \quad . \quad (11)$$

it being necessary to remove the contribution, β_{AB}, corresponding to $m+n=0$. Summing (10) and (11), $Y\geqslant 1$, we find that (9) reduces to

$$\frac{\beta_{\mathrm{AB}}}{(1-\rho_{\mathrm{A}}\beta_{\mathrm{AA}})(1-\rho_{\mathrm{B}}\beta_{\mathrm{BB}})-\rho_{\mathrm{A}}\rho_{\mathrm{B}}\beta^{2}_{\mathrm{AB}}}-\beta_{\mathrm{AB}}. \quad . \quad . \quad . \quad (12)$$

Consequently, on this simple chain approximation, we find (combining (7), (8), (12) and (1))

$$f_{AB}(r)=\frac{1}{\sqrt{(2\pi)}}\int_{-\infty}^{\infty}\left[\frac{\beta_{AB}(s)}{(1-\rho_A\beta_{AA}(s))(1-\rho_B\beta_{BB}(s))-\rho_A\rho_B\beta_{AB}^2(s)}-\beta_{AB}(s)\right]\times s\frac{\sin rs}{r}\,ds, \quad . \quad . \quad . \quad . \quad . \quad . \quad . \quad . \quad . \quad . \quad (13)$$

which is exactly equivalent to eqn. (4) if in (4) we put $\epsilon_{AA}=\epsilon_{BB}=\epsilon_{AB}=1$. In the same way, the present approximation to $f_{AA}(r)$ yields eqn. (3) with $\epsilon_{AA}=\epsilon_{BB}=\epsilon_{AB}=1$. In other words, if in the Born–Green theory we put all the parameters ϵ equal to unity the ensuing equations are just those which result from replacing, in the Mayer–Montroll expansion formulae, every $g_{mn}^{ij}(r)$ by the simple chain approximation $c_{mn}^{ij}(r)$.

(ii) *The Netted Chain Approximation*

The corresponding formulae based on the netted chain approximation are derived by essentially the same argument. We require the generating function which replaces the expression (12). Along the length of the principal (shortest) chain joining the major points, themselves occupied by A and B systems respectively, we have a sequence of A's and B's falling, as before, into blocks, fig. 3. Let there be $X=2Y+1$ divisions between these blocks. Now consider one of the Y central blocks with A's along the main chain: this can comprise as many

units as we like in any order, which entails a generating factor

$$\frac{\rho_A}{1-\rho_A\beta_{AA}-\rho_A^2\gamma_{AAA}-\rho_A\rho_B\gamma_{ABA}} \quad . \quad . \quad . \quad . \quad (14)$$

the first term corresponding to a single A (we have still to introduce the appropriate factor for all the A–B links in the main chain). Here γ_{ABA}, for example, is defined by

$$\gamma_{ABA}=\gamma_{ABA}(s)=\frac{1}{2\pi}\int_{-\infty}^{\infty}\int_{-\infty}^{\infty}\alpha_{AA}(t)u\beta_{AB}^2(u)\frac{\sin st\sin ut}{s}\,du\,dt, \quad . \quad (15)$$

again using Lemma *I* of paper I.

Similarly, since each A–B link in the main chain can be

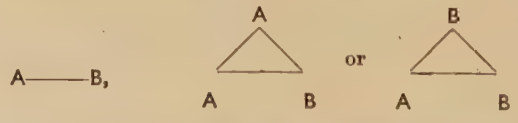

in place of $\beta_{AB}(s)$ in (12) we now have $\beta_{AB}+\rho_A\gamma_{AAB}+\rho_B\gamma_{ABB}$.

In fact, quite generally, changing from simple to netted chains, i.e. from $c_{mn}^{ij}(r)$ to $d_{mn}^{ij}(r)$, alters our previous results to the extent that

$$\left.\begin{aligned}\beta_{AA} \text{ becomes } &\beta_{AA}+\rho_A\gamma_{AAA}+\rho_B\gamma_{ABA},\\ \beta_{BB} \text{ becomes } &\beta_{BB}+\rho_A\gamma_{BAB}+\rho_B\gamma_{BBB},\\ \beta_{AB} \text{ becomes } &\beta_{AB}+\rho_A\gamma_{AAB}+\rho_B\gamma_{ABB}.\end{aligned}\right\} \quad . \quad . \quad . \quad (16)$$

Consequently $f_{AA}(r)$ and $f_{AB}(r)$ are now given by eqns. (3) and (4) with ϵ_{AA}, ϵ_{BB} and ϵ_{AB} replaced by $\epsilon_{AA}(s)$, $\epsilon_{BB}(s)$ and $\epsilon_{AB}(s)$, where

$$\left.\begin{aligned}\epsilon_{AA}(s)\beta_{AA}(s)&=\beta_{AA}(s)+\rho_A\gamma_{AAA}(s)+\rho_B\gamma_{ABA}(s),\\ \epsilon_{BB}(s)\beta_{BB}(s)&=\beta_{BB}(s)+\rho_A\gamma_{BAB}(s)+\rho_B\gamma_{BBB}(s),\\ \epsilon_{AB}(s)\beta_{AB}(s)&=\beta_{AB}(s)+\rho_A\gamma_{AAB}(s)+\rho_B\gamma_{ABB}(s).\end{aligned}\right\} \quad . \quad . \quad . \quad (17)$$

Thus we find that the netted chain approximation, in which $g_{mn}^{ij}(r)$ is replaced by $d_{mn}^{ij}(r)$, is not quite the same as the Born–Green linearized integral equation theory, for there the parameters ϵ are taken to be independent of s. The work of Rushbrooke and Scoins on pure fluids, paper II, shows that the netted chain approximation is in fact better than the Born–Green theory, in that a closer approach is made to the fourth virial coefficient of an imperfect gas. But the *singularities* of the two theories are the same, i.e. at the same values of ρ and T. In the one-component case these conclusions rest on the approximation (see I), $\epsilon=1+(3C/2B)\rho$ which has to be replaced in the present, binary mixture, problem by the equations

$$\left.\begin{aligned}\epsilon_{AA}&=1+(3C_{AAA}\rho_A+3C_{AAB}\rho_B)/2B_{AA},\\ \epsilon_{BB}&=1+(3C_{ABB}\rho_A+3C_{BBB}\rho_B)/2B_{BB},\\ \epsilon_{AB}&=1+(3C_{AAB}\rho_A+3C_{ABB}\rho_B)/2B_{AB}.\end{aligned}\right\} \quad . \quad . \quad . \quad . \quad (18)$$

Here the B's and C's are the coefficients in the virial expansion of the pressure of a binary gas mixture (see § 3 below). Then at $s=0$ eqn. (16) reads

$$\begin{aligned}&(1+2B_{AA}\rho_A+3C_{AAA}\rho_A{}^2+3C_{AAB}\rho_A\rho_B)\\ &\quad(1+2B_{BB}\rho_B+3C_{ABB}\rho_A\rho_B+3C_{BBB}\rho_B{}^2)\\ &\qquad=\rho_A\rho_B(2B_{AB}+3C_{AAB}\rho_A+3C_{ABB}\rho_B)^2, \quad . \quad . \quad (19)\end{aligned}$$

since $(2\pi)^{3/2}\beta_{AA}(0)=-2B_{AA}$, etc. ; and this is also the condition for the vanishing of the denominator in the netted chain theory, provided this also occurs at $s=0$, since

$$(2\pi)^3\gamma_{AAA}(0)=-3C_{AAA},\ (2\pi)^3\gamma_{ABA}(0)=(2\pi)^3\gamma_{AAB}(0)=-3C_{AAB}, \quad . \quad (20)$$

etc., the eqns. (20) following from (15) and Mayer's virial coefficient theory, see I. It remains, therefore, to interpret eqn. (19).

§3. Significance of the Vanishing of the Denominator

We are now in a position to interpret the vanishing of the denominator in eqns. (3) and (4), assumed to occur at $s=0$, for we have seen that this implies eqn. (19) which is evidently related to the equation of state

$$p=kT\left[\frac{N_A+N_B}{V}+\frac{1}{V^2}[N_A{}^2B_{AA}+2N_AN_BB_{AB}+N_B{}^2B_{BB}]\right.$$
$$\left.+\frac{1}{V^3}[N_A{}^3C_{AAA}+3N_A{}^2N_BC_{AAB}+3N_AN_B{}^2C_{ABB}+N_B{}^3C_{BBB}]\right]. \quad (21)$$

Equation (21) is simply the virial expansion for a binary gas mixture including terms up to those in ρ^3, but no further. From this equation we can determine the two chemical potentials, μ_A and μ_B (see Guggenheim 1952), and find

$$\left.\begin{aligned}\mu_A&=kT\ln\frac{N_A}{V\phi_A}+\frac{2kT}{V}[N_AB_{AA}+N_BB_{AB}]\\&\quad+\frac{3kT}{2V^2}[N_A{}^2C_{AAA}+2N_AN_BC_{AAB}+N_B{}^2C_{ABB}],\\\mu_B&=kT\ln\frac{N_B}{V\phi_B}+\frac{2kT}{V}[N_AB_{AB}+N_BB_{BB}]\\&\quad+\frac{3kT}{2V^2}[N_A{}^2C_{AAB}+2N_AN_BC_{ABB}+N_B{}^2C_{BBB}],\end{aligned}\right\} \quad (22)$$

where ϕ_A and ϕ_B depend only on T. It is then easily verified that eqn. (19) simply expresses the condition

$$\frac{\partial(\mu_A,\mu_B)}{\partial(N_A,N_B)}=0 \text{ or } \frac{\partial(\mu_A,\mu_B)}{\partial(\rho,x)}=0 \quad (23)$$

where $\rho=(N_A+N_B)/V$ and $x=N_A/(N_A+N_B)$.

For a given temperature, eqns. (22) and (23) together define a curve in the (ρ,x) plane. For values of the density and composition corresponding to points on this curve small isothermal changes, $d\rho$ and dx, of density and composition can be found which leave the chemical potentials, μ_A and μ_B, unchanged. The denominator with which we are concerned in the Born–Green theory, or the netted chain approximation, for a binary mixture vanishes, at a given temperature, for just these values of ρ and x.

It is easy to prove that as $x\to1$ eqn. (23) becomes simply $\partial p/\partial\rho=0$.

References

Born, M., and Green, H. S., 1949, *A General Kinetic Theory of Liquids* (Cambridge : University Press), ch. I and II.

Fournet, G., 1951, *J. Phys. et Rad.*, **12**, 292.

Guggenheim, E. A., 1952, *Mixtures* (Oxford : Clarendon Press), ch. VIII.

Kirkwood, J. G., and Boggs, E. M., 1942, *J. Chem. Phys.*, **10**, 394.

Mayer, J. E., and Montroll, E. W., 1941, *J. Chem. Phys.*, **9**, 2.

Rodriguez, A. E., 1949, *Proc. Roy. Soc.* A, **196**, 73.

Rushbrooke, G. S., and Scoins, H. I., 1951, *Phil. Mag.*, **42**, 582 ; 1952, in course of publication.

CXXVII. *On the Decay of Charged V-particles*

By J. P. Astbury, P. Chippindale, D. D. Millar, J. A. Newth, D. I. Page, A. Rytz and A. B. Sahiar

The Physical Laboratories, University of Manchester*

[Received September 18, 1952]

Abstract

Among 18 000 photographs taken during an experiment with a large cloud chamber at the Jungfraujoch (3 580 m) 13 examples of the decay of charged V-particles have been observed. A summary of the measurements of the 13 particles is given. Two of them are produced in nuclear interactions of remarkably low energy.

The average time that the particles would have taken to cross the chamber, if they had not decayed in flight, is $\sim 10^{-9}$ sec, and the distribution of the decay events does not differ significantly from that which would be expected for particles with a mean life greater than 10^{-9} sec.

§1. Introduction

In the course of a cloud chamber experiment carried out at the Jungfraujoch, 13 photographs have been obtained which show the decay of charged V-particles. We have found no evidence which conflicts with the assumption that charged V-particles are identical with the χ- and κ-mesons found in the photographic emulsions.

The first part of this paper is devoted to the interpretation and discussion of the 13 decay events. In § 5, the mean life of V-particles is considered.

§2. Apparatus and Results

The apparatus used in this work is a large cloud chamber, situated in a magnetic field of 5 800 gauss ; the illuminated volume of the chamber is $54 \times 54 \times 9$ cm^3. The equipment is installed on the Jungfraujoch (3 580 m) where the mean atmospheric pressure is 49 cm mercury.

The photographs discussed here were obtained in about a year of effective operation. Three different arrangements of Geiger counters have been used to control the chamber expansions. Figures 1 (*a*) and (*b*) show the disposition of the counters and absorbers for selection systems A and B respectively. Selection system C is a modification of system B ; the absorber inside the chamber has been removed ; each of the counters in the middle tray has been shielded from its neighbours by $\frac{1}{4}$ in. of lead ; and expansions are controlled by five-fold coincidences comprising two counters from the top tray, two from the middle tray and one from the bottom tray.

* Communicated by Professor P. M. S. Blackett, F.R.S.

The absorber above the chamber with system C has been either 12 cm of copper or 30 cm of lead. We have observed no outstanding difference between the results with the different absorbers, but no detailed analysis has yet been made.

The results obtained with the different selection systems are summarized in table 1.

Fig. 1

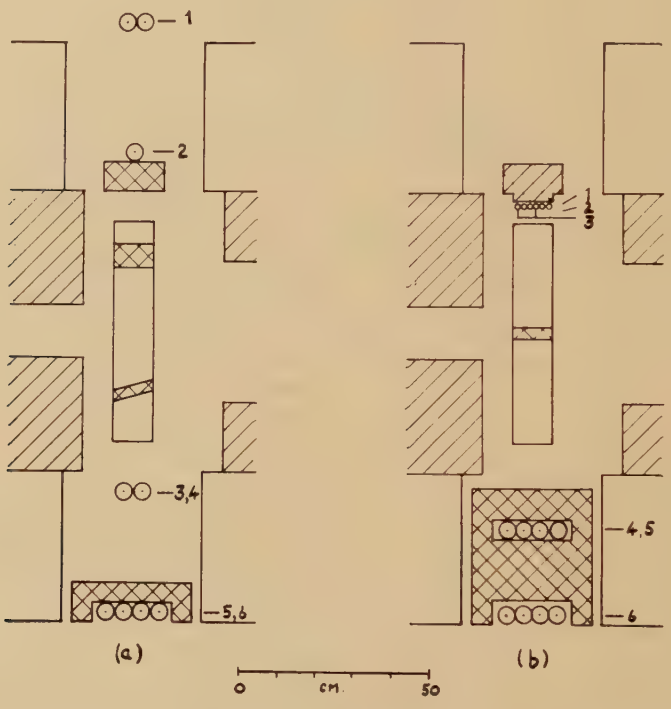

(*a*) Selection system A. The counter immediately above the cloud chamber is 50 cm×4 cm. All other counters are 65 cm×4 cm. A six-fold coincidence is required to expand the cloud chamber.

(*b*) Selection system B. The counter tray above the chamber contains 6 counters 40 cm×1·5 cm. The remaining counters are 65 cm×4 cm. Six-fold coincidence is required.

Table 1. Statistical Analysis of Results from Three Selection Systems

Selection	Running Time (wks)	No. of Photographs	Penetrating Showers	Probable Penetrating Showers	Neutral *V*-decays	Charged *V*-decays
A	14	5814	502	249	10	1
B	14	5881	783	1229	29	4
C	12	6631	1318	1807	40	8

For systems A and B a shower was classified as penetrating if at least two of the secondary particles penetrated the 3 cm lead plate in the chamber without producing an electron cascade. This stringent condition is not satisfied by many high energy nuclear interactions above the cloud chamber. Table 1 gives, in column 5, the number of photographs which show convincing evidence for such interactions yet do not satisfy the penetrating shower criterion. For selection system C, with no lead plate in the chamber, the allocation of any event to column 4 or column 5 has inevitably to be left to the discretion of the observer; it is possible, therefore, that the number of events given for system C in column 4 has been over-estimated.

We have observed 40 examples of tracks undergoing sudden deflections in the gas through angles greater than 3°. An analysis of these kinks is given in table 2.

Table 2. Interpretation of 40 Sudden Deflections of Tracks in the Gas

$V^{\pm}$-decays	13
π–μ decays	13
μ–ϵ-decays	1
Elastic scattering	3
Indeterminate	10

§ 3. Measurements and Interpretation of Charged V-decays

The measurements made on the photographs of the 13 events classified as charged V-decays are given in table 3. Photographs of events 3, 4, 6 and 11 are reproduced in Plates 1 and 2.

Table 3. Measurements Made on Charged V-Particle Tracks

Event	Sign	Primary			Angle of Decay (Degrees)	Secondary		
		Momentum (10^8 ev/c)	Ionization (I/I_0)	Mass (m_e)		Momentum (10^8 ev/c)	Ionization (I/I_0)	Mass (m_e)
(1)	+	>8	<2·5	—	15±2	7 to 10	<2·5	—
(2)	−	2·3±15%	2·5 to 5	630 to 1420	95±7	—	—	—
(3)	+	1·5 to 7	3 to 6	550 to 4200	80±7	—	—	—
(4)	+	>5	<2·5	—	90±5	0·47±8%	4 to 7	200 to 330
(5)	−	4·2±10%	<2·5	<1490	75±5	>1	<2·5	—
(6)	−	3·0±15%	2–4	690 to 1570	53±2	2·8±18%	<2·5	—
(7)	?	>10	<2·5	—	35±2	—	—	—
(8)	?	>4	<2·5	—	57±2	—	<2·5	—
(9)	?	>4	<2·5	—	5±1	>10	<2·5	—
(10)	−	>10	<2·5	—	11±1	5±40%	<2·5	—
(11)	+	>4	<2·5	—	28±2	4·9±10%	<2·5	—
(12)	+	>3	<2·5	—	18±2	5·2±10%	<2·5	—
(13)	?	>8	<2·5	—	45±5	—	—	—

The errors in the momenta given in table 3 are probable errors resulting from gas motion in the cloud chamber, uncertainty in the magnetic field strength, spurious curvature due to multiple scattering of the particles in the gas and errors in measuring the track curvature. The ionization values are the limits of the visual estimates made by three observers. In some cases the momentum and ionization values enable the masses of the particles to be deduced. The mass limits given in table 3 have been obtained by combining first the minimum values of momentum and ionization and then the maximum values. The secondary particles in events 2, 3 and 13 are travelling almost directly away from or towards the camera, and nothing more than their direction of travel can be determined. In event 3 a convection current in the cloud chamber distorted all the tracks immediately below the lead plate. Measurement shows that the distortion increased the apparent momentum of the primary particles, and the measured curvature is assumed to give the upper limit to the momentum. The lower limit has been found by estimating the effect of the convection current on neighbouring tracks and assuming similar distortion of the V-track.

Ionization estimates have been made by comparison with neighbouring tracks produced by energetic particles. The work of Ghosh, Jones and Wilson (1952) shows that the reference tracks may have an ionization density as much as 30% above minimum. Bearing in mind the errors of our visual estimates we do not consider that we can distinguish with certainty tracks for which $I/I_0 < 2{\cdot}5$ from tracks of minimum ionization.

Interpretation

In interpreting the 13 events as decays of charged V-particles we have followed closely the arguments used by Armenteros *et al.* (1952). In all cases interpretation in terms of a large angle scattering in the gas can be excluded by the absence of a recoil track. Events 2, 3 and 6 cannot be decays of light mesons because the masses of the primary particles are far too large. In the remaining events the momenta of the particles and the angles of decay are incompatible with the known dynamics of π and μ decays. In most cases P_t, the component of the secondary momentum transverse to the line of flight of the primary, is much greater than the maximum possible in a π or μ decay (for π, $P_{t\,\max} = 29$ MeV/c; for μ, $P_{t\,\max} = 55$ MeV/c). In event 13 the angle between the tracks is much greater than that possible in the decay of a π or μ meson with such a high primary momentum. Whichever particle is regarded as the primary of event 4 (Plate LXXVIII) interpretation in terms of π or μ decay can be excluded by one or the other of the foregoing arguments. This event can however be interpreted as the decay of an upward moving $V_2{}^0$-particle. No case has so far been reported of a V^0-particle producing a slow positive light meson ; and V^0-particles moving upwards are rarely found. In view of the high momentum of the lightly ionizing particle, and in the absence of any obvious origin for a V^0-particle, we consider that it is more reasonable to

interpret the photograph as representing the decay into a light meson of a charged particle travelling downwards in the chamber. The primary particle is inclined at 35° to the plane of the cloud chamber and we presume that it comes from a secondary nuclear interaction in the magnetic pole.

§ 4. Discussion of the Decay Events

The average energy of the penetrating showers causing the expansion of our cloud chamber is estimated at 1 to 5×10^{10} ev. The 13 events discussed here were not in general associated with penetrating showers noticeably different from the average. However, three of the charged V-particles were produced in secondary nuclear interactions of the particles in the main shower. Two of these (events 2 and 3) took place inside the cloud chamber and in these two cases the total energy of the secondary interactions appear to have been very low ($\lesssim5\times10^{9}$ ev). In these two events heavily ionizing V-particles were produced. The third example of the decay of a heavily ionizing particle occurred in a shower which does not appear to be exceptionally energetic (event 6, Plate LXXIX(a)).

These observations may be important for the design of experiments to study charged V-particles, but it must be remembered that there is a strong instrumental bias against observing the decay of very energetic V-particles. The more energetic the particle, the less likely it is to decay in the chamber ; if it does decay, the smaller will be the angle between the two tracks and therefore the more difficult it will be to recognize and interpret the event.

In two of our events (1 and 5) the geometry of the decay was such that the γ-rays produced by a secondary π^0-meson might be expected to enter the 3 cm lead plate in the chamber. In neither case is there any indication of an electron cascade from this cause. However the probability of such a cascade being observed is rather low owing to the wide angular divergence of the photons from the decay of a low momentum π^0-meson. If π^0-mesons were produced in these two events we estimate the probability of our observing evidence for them as $\sim30\%$ for each event.

§ 5. The Mean Life of V-particles

In accordance with the recommendation of Butler and Wilson (1952) we present the measurements relevant to mean life determination. In table 4 we list the visible path lengths of the particles before decay (l), their possible path lengths in the cloud chamber had they not decayed (L) and the corresponding times measured in the rest systems of the particles (t and T).

The relation between t and l is

$$l=(P/M)\,ct\,,$$

where P and M are the momentum and rest mass of the particle, measured in energy units.

Estimated values of P/M are given in table 4, column 4. For events 2, 3 and 6 they are made by taking the mean of the ionization estimates. For the remaining events they are obtained from the measured momentum associated with a value for the mass assumed to be 1 200 m_e. For all but four of the events only lower limits can be given.

Table 4

Event	l (cm)	L (cm)	P/M	t (10^{-10} sec)	T (10^{-10} sec)	t/T
1	6·5	21·0	>1·3*	<1·7	<5·4	0·31
2	13·0	33·0	0·47	9·2	23·4	0·39
3	10·0	22·0	0·40	8·3	18·3	0·45
4	8·0	16·5	>0·8*	<3·3	<6·8	0·48
5	13·0	19·0	0·7*	6·2	9·0	0·69
6	38·3	60·5	0·53	24·1	38·0	0·63
7	11·1	15·0	>1·6*	<2·3	<3·1	0·74
8	20·2	41·0	>0·7*	<10·4	<21·2	0·49
9	9·6	30·0	>0·7*	<4·9	<15·3	0·32
10	33·7	44·5	>1·6*	<6·9	<9·1	0·76
11	8·0	18·5	>0·7*	<4·1	<9·5	0·43
12	6·6	26·0	>0·5*	<4·5	<17·7	0·25
13	22·2	43·5	>1·3*	<5·7	<11·2	0·51

* Assuming mass of $V^{\pm}=1\,200\,m_e$.

The quoted ratios t/T are, however, independent of the measured momenta. They are listed in table 4, column 7. All the distances have been measured to the surface of the illuminated volume. The correction suggested by Butler and Wilson has not been applied. The mean value of t/T for the group is about 0·5, and no reasonable ajustment of a ' fiducial surface ' would make the mean value of t/T differ significantly from 0·5.

The expected value of $1/n\,\Sigma\,(t/T)$, for particles with a mean life much greater than their average time of flight across the chamber, is 0·5 ; our result therefore indicates that there may be present in our data some particles at least whose mean life is long compared with $\overline{T}$, the average value of T. The value of $\overline{T}$ depends on the uncertainty in the estimates of P/M, and for 9 events we have only been able to obtain estimates of an upper limit of their T-values. We can, however, get a rough indication of the value of the average $\overline{T}$ by assuming (i) that in every indeterminate case the T-value is zero ; and then, (ii) that in every indeterminate case the T-value is given by the upper limit. We thus obtain

$$(7<\overline{T}<14)\times 10^{-10}\text{ sec.}$$

It should be emphasized that, in spite of the extreme assumptions, the above values of the limits for $\overline{T}$ are themselves subject to error.

Some of the estimates of P/M, although given as definite values in table 4, are nevertheless only known very roughly. But the main contribution to the average value of T comes from the three heavily ionizing particles, for which the value of P/M has been estimated most directly.

The mean value of t/T is also affected by errors in measurement. The length l can usually be obtained relatively accurately, but the values of L given in table 4 may in a few cases differ from the true value by about a centimetre. The effect of this error is, however, small compared to the statistical uncertainty in the mean value, due to the paucity of the data.

We do not attempt here to assess any quantitative confidence limits ; but we consider that the most reasonable interpretation of our data is that the particles represented by our observed tracks have a mean life $\gtrsim 10^{-9}$ sec. An investigation of the mean life by a more powerful method will be described in a later paper.

§ 6. Conclusions

Our apparatus is sensitive to penetrating showers with average energy between 1 and 5×10^{10} ev. The decay events considered as a group come from showers not noticeably different from the average ; but we have found two examples which show that $V^{\pm}$-particles can be produced in very low energy secondary interactions.

In two events where evidence for π^0-mesons among the decay products might have been observed it has not been found. This fact has little significance until combined with further evidence, as the probability of detection of π^0-mesons was only $\sim 30\%$ for each event.

The distribution of the decay events even in our large chamber does not differ significantly from that which would be expected for particles with a mean life greater than 10^{-9} sec. This result is consistent with those obtained in other cloud chamber experiments (Annis *et al.* 1952, Barker *et al.* 1952).

Acknowledgments

This work has been financed largely by grants from the Nuffield Foundation and the Department of Scientific and Industrial Research. The magnet and cloud chamber used in the experiment were made by Metropolitan-Vickers Electrical Company of Manchester, and financial support was received from the D.S.I.R. A grant from U.N.E.S.C.O. covered a part of the cost of the installation and part of the running expenses.

A. B. Sahiar has been on leave from the Tata Institute of Fundamental Research and was financed by the Indian Atomic Energy Commission. A. Rytz has received a fellowship from the Jungfraujoch Research Station Foundation. P. Chippindale and D. I. Page have received maintenance grants from the D.S.I.R. during their work.

Professor von Muralt and the officers of the Jungfraujoch Research Station have provided us with every facility, and we are particularly indebted to Dr. R. Stämpfli for his constant help and co-operation. To

Herr H. Wiederkehr, the curator of the station, we owe much, and we should like to record our thanks for the many things which he has done to make our work at the station both profitable and agreeable.

We have received great assistance from discussions with the Manchester team working at the Pic-du-Midi and are indebted to them for communicating their results before publication.

Our research was directed by Professor J. G. Wilson and owes much to discussions with him. Professor P. M. S. Blackett has made generous provision for our work and we have profited immensely from his guidance and stimulus.

References

Annis, M., Bridge, H. S., Courant, S., Olbert, S., and Rossi, B. (Private communication.)

Armenteros, R., Barker, K. H., Butler, C. C., Cachon, A., and York, C. M., 1952, *Phil. Mag.*, **43,** 597.

Barker, K. H., Butler, C. C., Sowerby, M. G., and York, C. M., 1952, *Phil. Mag.*, **43,** 1201.

Butler, C. C., and Wilson, J. G., 1952, *Phil. Mag.*, **43,** 993.

Ghosh, S. K., Jones, G. M. D. B., and Wilson, J. G., 1952, *Proc. Phys. Soc.* A, **65,** 68.

CXXVIII. *Investigations on Positron–Electron Scattering*

By R. R. Roy and L. Groven
Université Libre de Bruxelles, Laboratoire de Physique, Bruxelles*

[Received September 2, 1952]

Abstract

The scattering of positrons by electrons has been studied in nitrogen by a cloud-chamber method. In 6000 photographs 5600 positrons were measured, giving a total track length of 792 metres between the energies 0·5 Mev and 1·1 Mev. The experimental results, when compared with the exchange theory of Bhabha, show satisfactory agreement.

§ 1. Introduction

The theory of electron–electron scattering as formulated by Møller (1931, 1932) is generally accepted for comparison with experimental results. The theory has been developed taking into account the effects of exchange and of retardation in collisions between two free electrons. Because of the fact that sources of fast electrons are easily available, considerable experimental work has been done on this scattering problem by many workers, notably by Champion (1932), Hornbeck and Howell (1941) and Shearing and Pardue (1942). The results of all these workers showed agreement with the theory of Møller. In the case, however, of more recent experiments performed by Groetzinger, Leder, Ribe and Berger (1950), the results agree equally well with the theories of Møller, Mott (1930) and with Rutherford's relativistic formula, having regard to the statistical fluctuation.

The investigation of positron–electron scattering is not so extensive, due, perhaps, to the difficulty in obtaining suitable positron sources, but in some respects it is more interesting than the electron–electron scattering owing to the fact that it is possible to distinguish between the incident positron and the secondary electron in a cloud-chamber by applying a magnetic field.

The effect of exchange phenomena arising out of the interaction of a fast positron with an electron when a positron passes through matter was first pointed out by Bhabha (1936). Due to this exchange, the number of fast secondary electrons ejected in the collision process between the positron and the free electron will be more than would be expected if it were a simple scattering process in which the positron is considered as an independent positively charged particle.

* Communicated by the Author.

The formula of Bhabha, after von Ritter, Lieseberg, Maier–Leibnitz, Papkow, Schweiser and Bothe (1951), can be written as

$$W(\gamma, \epsilon)\, dl\, d\epsilon = (e^2/m_0c^2)^2 \pi N\, dl\, d\epsilon (P_l + P_{ll} + P_i)/\{(\gamma+1)(\gamma-1)\}^2, \quad . \quad . \quad (1)$$

where

$$P_l = 2\gamma^2/\epsilon^2 - 2(\gamma^2-1)/\epsilon + (\gamma-1)^2,$$

$$P_{ll} = \left(\frac{\gamma-1}{\gamma+1}\right)^2 \{\gamma^2+2\gamma+3-2(\gamma-1)^2\epsilon(1-\epsilon)\},$$

$$P_i = -2\left(\frac{\gamma-1}{\gamma+1}\right) \{\gamma(\gamma+2)/\epsilon - 2(\gamma^2-1) + (\gamma-1)^2\epsilon\}.$$

Formula (1) gives the probability, as calculated by Bhabha, that a positron with total energy γm_0c^2 transfers the ratio ϵ to $\epsilon+d\epsilon$ of its energy to an electron, for a track length dl in a gas with N number of electrons per unit volume.

The term P_l corresponds to the ordinary scattering of the positron when considered as an independent positively charged particle, according to the Dirac hole theory, while the effects of exchange are taken into account in the terms P_{ll} and P_i. The physical significance of P_{ll} is that the positron in interaction with the atomic electron annihilates only to create a new pair of electrons of opposite charge. P_i gives the interference between the ordinary scattering term, P_l, and the pair-production term, P_{ll}.

The aim of the present experiment is to study the scattering of positrons by electrons and to compare the results with the exchange theory of Bhabha.

§ 2. Experimental Arrangements

A fully automatic cloud-chamber was employed in this investigation. The positron source ^{102}Rh was kept inside a curved container to allow only high energy positrons to appear in the chamber, which was filled with nitrogen at near-atmospheric pressure, and to this a mixture of water and alcohol was added for the formation of good tracks. A pair of coils supplied the magnetic field used to determine the energy of the tracks. The strength of the field was 739·6 gauss and was uniform within 0·4% across the 24 cm of the diameter of the chamber. About 6000 photographs were taken, out of which, 5 600 tracks, between the energies 0·5 Mev and 1·1 Mev, were selected for measurement. The number of tracks per expansion was kept to a minimum in order to ensure that the error due to spurious effects remained negligible. These effects, which may give the impression of secondary electrons originating from primary positron tracks, may arise from the crossing of the track after reflection from the wall of the chamber or from the appearance of a δ-track near the primary positron caused by annihilation radiation from the source container.

§ 3. Measurements and Calculations

To determine the energies of the interacting particles the tracks were first reprojected to their original size. The measurements were then taken of the curvatures before collision, and of either the ranges and curvatures, or the curvatures and angles, depending on the type of energy-transfer, after the collision. The curvatures were measured by fitting circles of known radius through the beginning and end of the track so that there was a minimum mean square difference between the two. The maximum error involved in this method was estimated to be 5%. When the energy-transfer was very great or very small the energy of the positrons or electrons after impact had to be ascertained from their range, the minimum value of which taken into account was 15 mm. This lower limit was decided having regard to three considerations: (*a*) that, according to the theory of Bhabha, the electrons are free; consequently the binding energy of the electron must be negligible compared with the energy-transfer; (*b*) that the determination of the energy will be inaccurate by a higher percentage as the range is diminished; and (*c*) that in fixing the lower limit at a comparatively high range it is sometimes possible to make a counter-check on the energy-transfer by measuring the change of curvature. The estimated error involved in the range measurement is about 9%.

Accurate determination of the energy of the primary positron and of the positron and electron after collision indicated, within experimental error, that the energy was conserved between the interacting particles.

Since the photographs were taken by one vertical camera, some of the scattering events may be altogether missed from the measurements. It is, however, possible to correct the observed number in the following way. Let θ be the angle of scattering in the laboratory system, λ its projection on the horizontal plane, and ϕ the angle made by the horizontal plane and the plane of scattering. We then obtain

$$\cos\phi = \tan\lambda/\tan\theta.$$

By limiting the observation to $\lambda \geqslant \lambda_0$ ϕ is also limited to

$$\phi \leqslant \text{arc cos } (\tan\lambda_0/\tan\theta) = \phi_0.$$

Therefore the probability of not observing a scattering is

$$1 - 2\phi_0/\pi.$$

For this reason it is necessary to multiply the number of events measured at angle θ by

$$C(\theta) = \frac{\pi}{2\phi_0} = \pi/\{2 \text{ arc cos } (\tan\lambda_0/\tan\theta)\}.$$

Again (see Bhabha 1936, pages 198 and 203),

$$\tan\theta = \left\{\frac{2\epsilon}{(1+\gamma)(1-\epsilon)}\right\}^{1/2}.$$

Therefore

$$C(\theta)=\pi \Big/ \left\{2 \arccos\left[\left\{\frac{(1+\gamma)(1-\epsilon)}{2\epsilon}\right\}^{1/2} \tan \lambda_0\right]\right\},$$

where $\gamma=E/m_0c^2$ and ϵ is the ratio of the energy transfer.

§4. Results and Discussion

From eqn. (1) probabilities were calculated for the energy transfer to lie in the regions 0·03–0·1, 0·1–0·2 . . . . etc., with γ in the intervals 2·0–2·4, 2·4–2·8, 2·8–3·0.

Three histograms, figs. 1 (*a*), (*b*) and (*c*), have been plotted with the number of collisions as ordinate and ϵ as abscissa. 312 metres of track were measured between the interval 0·5 MeV and 0·7 MeV, 270 metres between 0·7 MeV and 0·9 MeV and 210 metres between 0·9 MeV and 1·1 MeV. The experimental results, given by the thick line, and the theoretical results, the dotted line, show satisfactory agreement. Calculation made from the formula with the term P_l only gave results which did not accord with those of the experiment, hence confirming that, in addition to the ordinary scattering of positron and electron given by the term P_l, the exchange effect plays a part in the collision process.

Fig. 1

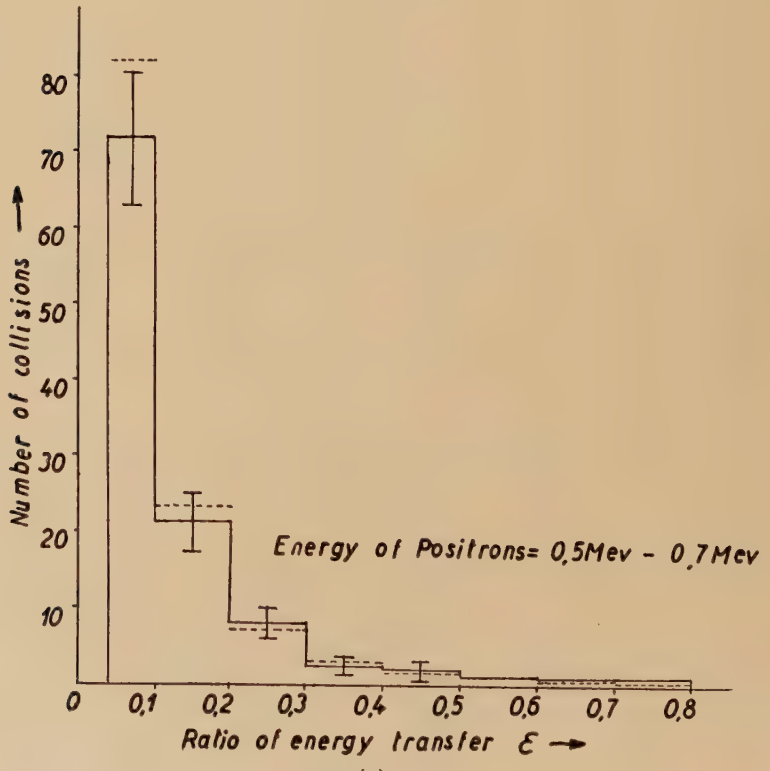

(*a*)

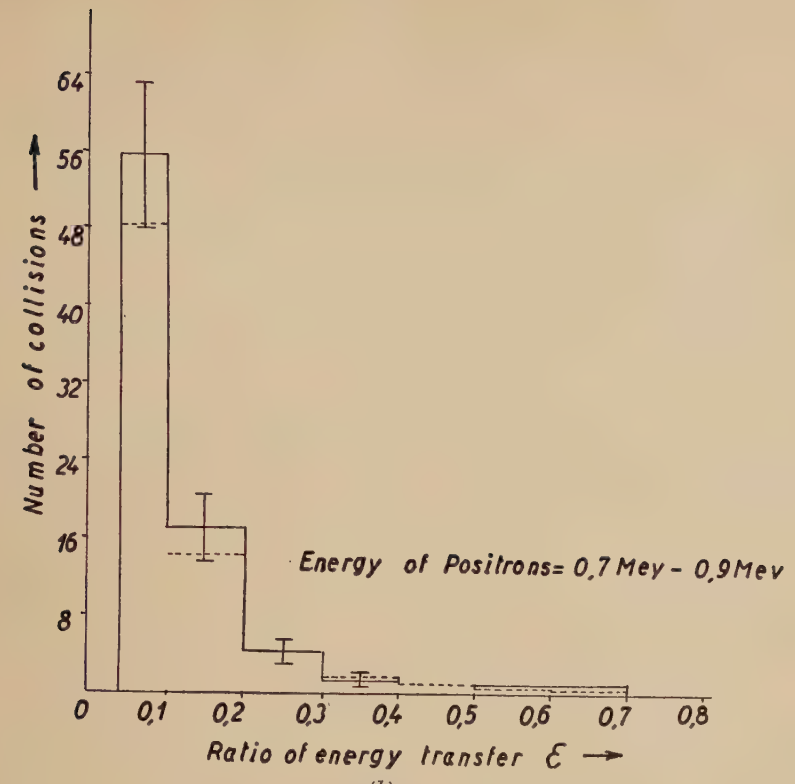

(*b*)

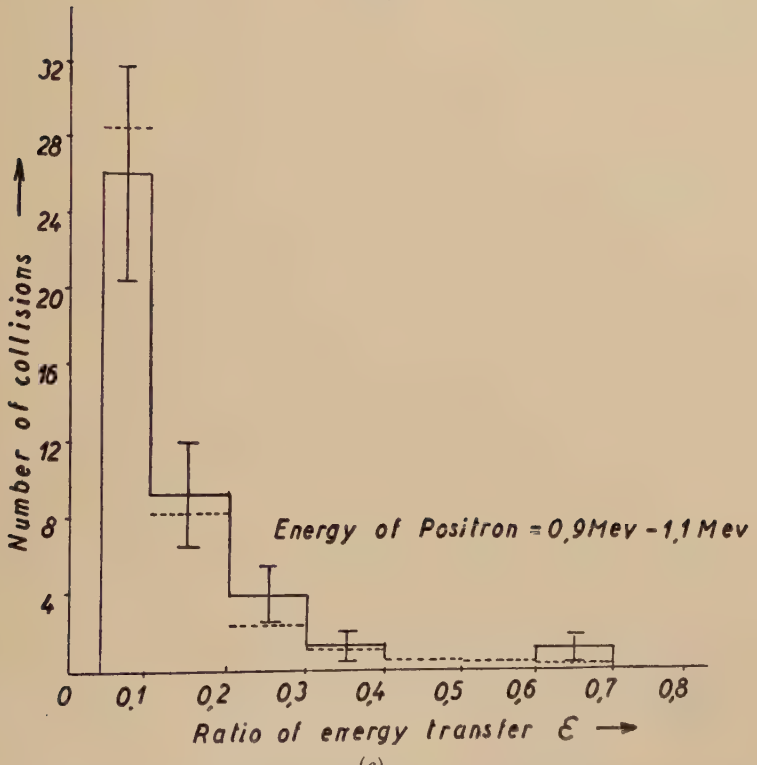

(*c*)

Experimental results of the positron–electron scattering are given by the thick line, whereas the dotted line shows the values as calculated from Bhabha's theory.

The first experiment to investigate the Bhabha exchange was performed by Ho ZaH-Wei (1946) with energies of positron varying from 0·025 MeV to 0·8 MeV and a total track length of 170 metres. She observed discrepancies between the value, as calculated from the theory, and the experimental value in the region $\epsilon \geqslant 0{\cdot}5$.

Results published recently by von Ritter, Lieseberg, Maier-Leibnitz, Papkow, Schweiser, Bothe (1951) on positron–electron collisions where positrons of low energies—from 0·1 MeV to 0·4 MeV—were used do not, however, confirm these discrepancies.

Similarly, in the present experiment, in which the positrons were of high energies, where the Bhabha exchange is important, we noted no disagreement with the theory.

References

Bhabha, H. J., 1936, *Proc. Roy. Soc.* A, **154,** 195.

Champion, F. C., 1932, *Proc. Roy. Soc.* A, **137,** 688.

Groetzinger, G., Leder, L. B., Ribe, F. L., and Berger, M. J., 1950, *Phys. Rev.*, **79,** 454.

Hornbeck, G., and Howell, I., 1941, *Proc. Amer. Phil. Soc.*, **84,** 33.

Ho ZaH-Wei, 1946, *Comptes Rendus*, **222,** 1168.

Møller, C., 1931, *Zeits. f. Physik*, **70,** 786 ; 1932, *Ann. d. Physik*, **14,** 531.

Mott, N. F., 1930, *Proc. Roy. Soc.* A, **126,** 259.

Ritter, O. von, Lieseberg, C., Maier-Leibnitz, H., Papkow, A., Schweiser, K., Bothe, W., 1951, *Z. f. Naturforschung*, **6a,** 243.

Shearin, P. E., and Pardue, T. E., 1942, *Proc. Amer. Phil. Soc.*, **85,** 243.

CXXIX. *The Alignment of Cobalt* 58

By J. M. Daniels, M. A. Grace, H. Halban, N. Kurti and F. N. H. Robinson
Clarendon Laboratory, Oxford*

[Received September 29, 1952]

Abstract

The technique for obtaining aligned Cobalt nuclei has been applied to the isotope Cobalt 58. An examination of the angular distribution of the 0·805 mev γ-ray shows that this transition cannot be dipole but is probably quadrupole. The temperature dependence of this angular distribution gives for the nuclear magnetic moment a value of $3{\cdot}5 \pm 0{\cdot}3$ nuclear magnetons. This result is discussed in relation to the nuclear shell-model.

The technique for the alignment of Cobalt nuclei has now been established (Daniels *et al.* 1951, Gorter *et al.* 1951) and demonstrated for the radioactive isotope Cobalt 60. We have used the same technique to align the isotope Cobalt 58 in its ground state. The disintegration scheme of this nucleus has been investigated by Deutsch and Elliott (1944) and by Strauch (1950) (see fig. 1). They showed that decay was by K electron capture ($\sim 85\%$) and by positron emission ($\sim 15\%$) to an excited state of Fe 58, and thence by a single 0·805 mev γ-ray to the ground state. Strauch concluded from measurement of the internal conversion coefficient α_K that this γ-ray was $M1$: however, it seems unlikely that this measurement could exclude $E2$ which is more probable on the basis of existing knowledge of the first excited states of even–even nuclei. Since there is only one γ-ray and the positron spectrum has allowed form, no further information can be expected from angular correlation measurements. However, a measurement of the angular distribution of γ-rays from aligned nuclei can certainly distinguish dipole from other multipole transitions (Steenberg 1951). Hence this is a case where nuclear alignment offers special advantages.

The experimental technique was the same as that employed for Cobalt 60 except that scintillation counters fitted with 1 in. cube NaI(Tl) crystals were used to discriminate against annihilation radiation, scattered 0·805 mev radiation, and low energy γ-rays from Cobalt 57 which was present as weak contamination.

The fact which was immediately observed, that the γ-rays are emitted preferentially at the nuclear equator, shows that the γ-ray transitions cannot be dipole. From the presence of coincidences between x-rays

---

* Communicated by the Authors.

and γ-rays (Deutsch *et al.* 1944) and from Strauch's value for α_K we conclude that the radiation is quadrupole. It follows from the allowed form of the positron spectrum that the angular momentum carried away in the β transition, $i_\beta \geqslant 1$. This allows the spin assignments to the levels to be made in three possible ways :—

(A) $I_\beta=2$, $I_1=2$, $i_\beta=0$,
(B) $I_\beta=3$, $I_1=2$, $i_\beta=1$,
(C) $I_\beta=2$, $I_1=2$, $i_\beta=1$,

where I_β, I_1 are the spins of the nuclear levels before and after the K-capture process.

Fig. 1

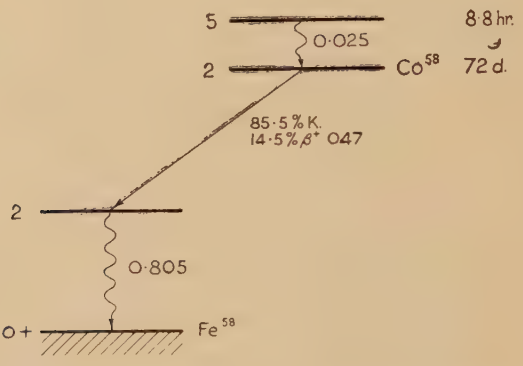

Measurements of γ-ray intensity (W) were made along the K_1-axis ($W(0°)$), the K_2-axis ($W(90°)$) and along the bisector of these ($W(45°)$). (The K_1 and K_2 axes are the axes of maximum and minimum magnetic susceptibility of the Co^{++} ions in the salt used.) For quadrupole radiation the polar diagram at any temperature (Spiers 1948) T is known to be of the form

$$W(\theta)=1-A(T)\cos^2\theta-B(T)\cos^4\theta$$

and three different expressions for the functions A and B can be obtained theoretically for the three different spin assignments given above.

The magnitude of the anisotropy

$$\epsilon \equiv A(T)+B(T)=\frac{W(90°)-W(0°)}{W(90°)}$$

was obtained from measurements of the γ-ray intensity, and the results are shown in fig. 2, where $\sqrt{\epsilon}$ is plotted against $1/T$. On the same diagram the three theoretical curves are plotted, fitted at the point $1/T=52$. The $1/T$ scale of these curves is arbitrary by a factor proportional to the magnetic moment of the parent nucleus ; this factor is chosen so that the curves fit the experimental results at the point $1/T=52$. It is seen that the best fit over the whole range is obtained from Curve C. Further confirmation of the correctness of this spin-assignment is obtained by determining experimentally values of the function

$$B(T)=\{4W(45°)-2W(0°)-2W(90°)\}/W(90°).$$

These are shown in fig. 3, along with the three theoretical curves, and it is seen that the experimental results again favour curve C. Assuming the decay scheme C to be correct, we find, from the fit of the theoretical curve to the experimental points, that the magnetic moment of Co 58 is $3{\cdot}5 \pm 0{\cdot}3$ nuclear magnetons assuming that no reorientation of the nucleus occurs following the K-capture process.

Fig. 2

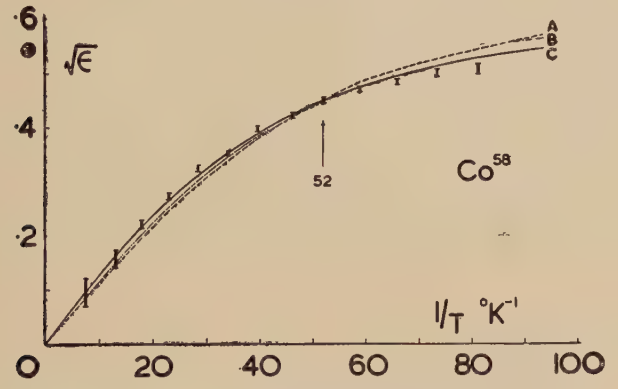

ANISOTROPY OF γ-RADIATION FROM $Co^{58}Rb_2(SO_4)_2 . 6H_2O$

Fig. 3

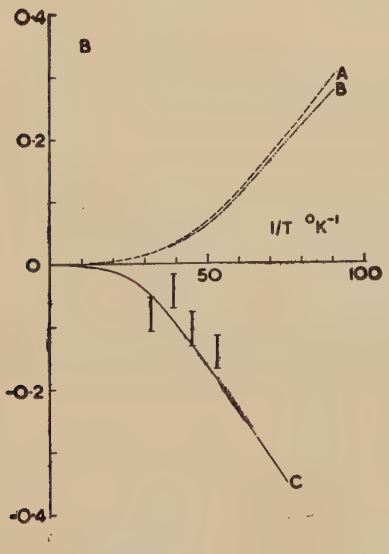

The nuclear shell model (Mayer 1950) suggests that in the ground state of both Co 58 and Co 60, the odd proton and odd neutron are in f7/2 and p3/2 states respectively. Pryce (1952) has shown that the coupling energy is greatest, and nearly equal, for the parallel and antiparallel configurations. These give states of 5+ and 2+ respectively.

This model satisfactorily accounts for the established features of Cobalt 60, namely the isomeric transition with $\Delta I=3$, the ground state spin of 5 deduced from the decay scheme, and the magnetic moment (Bleaney *et al.* 1952) of the ground state, 3·5 nuclear magnetons, which is close to the Schmidt limit of 3·8. In our previous paper (Bleaney *et al.* 1952), owing to an error, the magnetic moment was given as $3{\cdot}0\pm0{\cdot}5$ instead of $3{\cdot}5\pm0{\cdot}5$ nuclear magnetons.

In Cobalt 58 also, the ground state is fed by an isomeric transition with $\Delta I=3$, and our assignment of spin 2 to the ground state is in keeping with one of the alternatives offered by the shell model. However, the Schmidt limit for the magnetic moment of this state is 6·2 nuclear magnetons, which is considerably larger than our experimental value of 3·5. It has been suggested (Grace and Halban 1952) that some reorientation of the nucleus may take place after the K-capture process due to the large field of the odd K electron. A detailed examination (to be published) of this effect shows that it is unlikely to account for this difference.

We wish to thank Professor Lord Cherwell for his continued interest and encouragement. We are grateful to Professor F. E. Simon for many helpful and stimulating discussions. We are indebted to Dr. W. I. B. Smith and the Nuffield Cyclotron Group at Birmingham for their cooperation in the irradiation of the source, and to Dr. P. F. D. Shaw of this laboratory for the chemical separation of the Cobalt 58.

References

Bleaney, B., Daniels, J. M., Grace, M. A., Halban, H., Kurti, N., and Robinson, F. N. H., 1952, *Phys. Rev.*, **85,** 688.

Daniels, J. M., Grace, M. A., and Robinson, F. N. H., 1951, *Nature, Lond.*, **168,** 780.

Deutsch, M., and Elliott, L. G., 1944, *Phys. Rev.*, **65,** 211.

Gorter, C. J., Poppema, O. J., Steenland, M. J., and Beun, J. A., 1951, *Physica*, **17,** 1050.

Grace, M. A., and Halban, H., 1952, *Conference on β and γ Radioactivity* (Amsterdam).

Mayer, M. G., 1950, *Phys. Rev.*, **78,** 16.

Pryce, M. H. L., 1952, *Proc. Phys. Soc.* A, **65,** 773.

Spiers, J. A., 1948, *Nature, Lond.*, **161,** 807; Directional Effects in Radioactivity, *N.R.C.C. pub. No. 1925.*

Steenberg, N. R., 1951, *Phys. Rev.*, **84,** 1051.

Strauch, K., 1950, *Phys. Rev.*, **79,** 487.

CXXX. *The Effect of Mechanical Deformation on the Growth of Cadmium Iodide Crystals from Solution*

By A. Korndorffer, H. Rahbek and F. S. A. Sultan
Royal Holloway College, Egham, Surrey*

[Received September 12, 1952]

Abstract

CdI_2 crystals growing in thin plates, have been subjected to mechanical deformation, by an indentation process. As a result of this deformation, the growth properties of the crystals are altered, and several other striking effects take place, which have not previously been observed. It is concluded from the experiments that the mechanical deformation is the vital factor for these growth effects to occur. Variation in concentration by disturbing the mother liquor has no effect. Slip processes, leading to the creation of dislocation or increase of dislocations already present in the crystal, may account for the spiral nature of the growth sometimes observed.

§ 1. Introduction

CdI_2 crystals growing from aqueous solution have been studied by Forty (1951, 1952) and the spiral features as well as the step heights are in support of Frank's hypothesis of growth by a dislocation mechanism. When CdI_2 grows from solution one may also observe thin crystal plates of an extremely uniform thickness growing in extension to about $\frac{1}{2}$ mm with little or no observable change in thickness. Buckley (1952) has drawn attention to these plates and raised the question of how this correlates with the spiral growth.

It was thought that these plates may have nearly perfect (0001) planes and if exposed ledges were produced on these planes they might grow faster in the [0001] direction.

Experiments were performed to see whether an external force could deform the crystal in such a way that exposed ledges were formed and rapid growth started. Although the method of deformation used has not been developed to give controlled stresses, the results obtained are very informative.

The experimental technique will be briefly described and the results discussed.

§2. Experimental Technique

The crystals were grown in a drop of solution placed on a microscope cover slip. This was placed on the moveable stage of a Cooke-Troughton-Simms microscope, so that it could be observed in transmission and reflexion.

* Communicated by Professor S. Tolansky, F.R.S.

An indenter was made by drawing out a glass rod to a fine point. This was adjusted above the cover slip in the centre of the field of view. It could be raised or lowered by a vertical screw motion. In this way the transmitted light was not affected by the presence of the indenter when the latter was not in contact with the crystal. As the indenter was lowered it came into the field of view as a shadow, so that the position of contact of the indenter could be controlled, and the complete behaviour of the crystal before, during and after indentation could be observed.

A Leica adaptor was used in place of the eyepiece with a 35 mm Leica camera body, so that the process of growth could be observed simultaneously while photographing.

In general a crystal growing as a flat plate was selected and a photograph taken. The indenter was very carefully lowered until slight contact was made and then carefully raised out of the field of view. Often no growth was observed at the point of contact for a few seconds and this emphasizes the slight amount of deformation caused. Precaution was also taken to see that the indenter was clean. As growth proceeded a series of photographs was taken at intervals.

§3. Results

Several of the crystals were observed over a long period of time and they remained as flat plates increasing in size laterally. Buckley (1952) has observed this for several hours. The neighbouring liquid was disturbed but this had no effect on the crystals, as will be seen later. Only a few seconds after the indenter had touched the crystal more rapid growth in the [0001] direction was observed. The growth features will be classified into three groups :

(*a*) growth originating from the indent and along visible cracks which may develop during the indentation ;

(*b*) growth originating at points far from the position of the indent and with no visible markings connecting it with the indent ;

(*c*) development of the $(11\bar{2}0)$ faces of an incomplete crystal to the first order $(10\bar{1}0)$ close packed faces forming the stable hexagon.

The growth features of groups (*a*) and (*b*) were very similar to the features found on the thicker crystals growing in the solution and very often spirals were clearly seen. One striking difference is that an intermediate state exists, where the growth initiated at certain points has covered part of the original crystal with a rather thick layer of new material, but has left other parts of it unthickened. This point will be discussed again later.

The observations belonging to group (*c*) are very numerous, but no information about the mechanism leading to this growth phenomenon has been obtained from them.

The photographs given here show some of the interesting features, and we shall describe these in some detail. The first series, figs. 1–8 (Plate LXXX, figs. 1–4 ; Plate LXXXI, figs. 5–8), gives an example of a hexagonal plate, which before the indentation, fig. 1, showed no features on the

basal plane. The kink in one edge is merely a growth irregularity and nothing exceptional happens at this place. Figure 2 is a photograph in reflexion of the crystal only a few seconds after indentation. Small hexagonal layers are formed at the point of indentation, with the same symmetry as the large crystal. The crystal shows uniform tint over the whole area except where the hexagonal layers are forming.

In the next photograph, fig. 3, a spiral is seen originating at the point where the indentation was made, and a thick hexagonal plate of the same symmetry as the main crystal is seen to have developed on the opposite side.

Figure 4 is a reflexion picture in which the spiral is visible, and more complex growth features. The interference fringes show how the thickness of the crystal is varying, though away from the indent it is still of the same initial uniform tint.

More complex growth patterns with a number of growth hills at the crystal edges are seen in fig. 5. Also it may be observed how the kinks at the edges appearing in the earlier pictures have moved, tending to complete the sides.

Figure 6 shows in transmission that the plate formed is now very thick, but there is no sign of any growth features belonging to the exposed basal plane of this plate.

The reflexion picture, fig. 7, shows how the spiral mechanism is working at two of the corners of the hexagon. The part where broad fringes still occur must be growing slowly upwards and a filling-in of these areas from the edges is now taking place.

In the last picture of this series, fig. 8, the growth pattern has become very complex. The spiral is still visible, and the hexagon plate has increased considerably in thickness.

The next series is an example of the observations on an incomplete hexagon. Figure 9 (Plate LXXXII, figs. 9–14) shows the crystal plate before indentation. Crystals of this type occur frequently and maintain this shape during growth. The long curved edge is unstable on indentation, however, and growth phenomena have been observed on this edge, which have not been seen on any crystal which was left untouched.

In the following figure (fig. 10) indentation has been made near to the edge. Growth has taken place round the indent and there is a thickening of the edge of the crystal at this point.

Figure 11. A second indentation has now been made in the centre of the same crystal. A crack, which appears to be discontinuous, extends downwards towards the long edge. The growth by the first indent has proceeded, but the thickened edge has begun to dissociate. Further along the edge there is a kink, and crack from which a layer has started to form.

These features have become more marked in fig. 12. The crack from the second indentation has formed a layer one edge of which has taken up the crystal symmetry. The small facet where the curved edge meets

the $(10\bar{1}0)$ face started to increase after the second indentation. It has now become a definite face, so tending to form a complete hexagon. The original thickened edge has thinned and dissociated. At the kink the edge is also tending to form the edge of a complete hexagon, and the layer growing here has taken the symmetry of the crystal.

In fig. 13 the above features have continued to develop, and the layer coming from the edge due to the first indentation has met the visible end of the crack. At this point a very rapid growth is initiated, and as can be seen in the next figure (fig. 14), this seems to have a spiral nature.

In this picture, under higher magnification ($\times 300$) than the others ($\times 150$), the crystal on the right is the one previously indented. The growth at the crack may be noted to have occurred at a far greater rate than any other feature on the crystal. The crystal on the left may be seen in all the previous pictures to have been unaffected by the disturbances around it. The little facet at the right point has increased slightly during the growth.

This crystal was now indented and the facet may be seen to have grown remarkably in size, and new growth has been started by the indentation process. The crystal has taken the normal hexagon shape. A kink similar to the one formed in the other crystal has occurred on the lower side of this one, though in this case it is seen to be joined to the main indentation by some crack or flaw. It is worth noticing that although this connecting disturbed region in the crystal is visible, there is no growth taking place along it.

The remaining pictures are individual ones taken out of a series. In each case the crystal before indentation was a flat plate showing no layer growth.

Figures 15 and 16 (Plate LXXXIII, figs. 15–20). This crystal was initially as in fig. 15 and on indentation the long unstable edge changed to the shape as in fig. 16, where all the edges are of the stable hexagonal type.

Figure 17. The photograph shows the thinning effect of the unstable edge and building up of the hexagon edges very beautifully. The edges completed themselves later and layer growth started at the re-entrant point.

Figure 18 shows the growth at the boundary of a hexagonal crystal plate away from the indentation, which can be seen at the top in the photograph. Growth around the indentation has hardly started.

Figure 19 shows the initiation of growth on a crystal in contact with the indented crystal. The crystal is of the unstable type, and the unstable edge is in contact with the indented crystal. Growth has started at this point. Hexagonal layers have formed around the indentation. The crystal on the left of the picture has also been indented and this shows features typical of those already described.

Figure 20 shows a crystal where screw dislocations are promoting growth at the point of indentation. It is very significant that the affected area is limited and its boundary crystallographic.

§4. Discussion

The discussion will be confined to growth of the three types mentioned previously. The following points are observed on the hexagonal plate crystal (figs. 1–8). A spiral has formed on one side of the plate and a hexagonal plate on the opposite side. The point of emergence of the spiral is very nearly at the centre of this small plate. If the dislocation group responsible for creating the spiral is extending right through the mother crystal, it may be that no spiral features are seen on the small plate because dissociation into dislocation of lesser strength has taken place. The rate of growth in the [0001] direction on the small plate is relatively greater than that of the face having the spiral.

The great number of irregular lines of discontinuity which are observed in fig. 8 may be seen to develop higher visibility during growth, and their shape is changing only very slightly. A line of discontinuity is most likely marking out a surface of misfit, a fault surface, due to presence of partical (imperfect) dislocations. If so, it means that fault surfaces are created by indenting the crystal. Their visibility is increasing as growth proceeds because they form barriers for the advancing layers.

The existence of fault surfaces extending to the boundary of the crystal provides a possible explanation to the observed growth at the edges separated from the indent by ' unaffected area ' (fig. 18).

The spiral growth caused by the indenter does not spread over the whole crystal face. This effect is pronounced in fig. 20. Any exposed ledge running to the edge of the crystal might be expected to sweep over the whole (0001) face, unless obstacles, lines of discontinuity, or an equal number of positive and negative dislocations are present. Lines of discontinuity are seen in figs. 4–8. In several figures the boundaries of the growing region have crystallographic directions, which indicates that they are not discontinuity lines.

In several cases crystals with a curved edge have been indented. The main behaviour was always the same. The curved edge at once started growing out tending to complete the crystal symmetry. The deformation of the crystal by the indenter has caused slip to occur, which is transmitted to the edge forming steps such that growth in thin sheets parallel to the (0001) plane takes place. Figure 17 shows very strikingly how the crystal is growing out, the original edge being dissociated into very thin layers with almost invisible edges. These layers catch up on each other in the directions of close packing and finally complete the crystal symmetry. This is also seen in fig. 12.

It has been pointed out that in fig. 14 a connecting line between the indent and the edge phenomenon is visible. In other cases the deformation caused by the indentation is transmitted to the edge of the crystal without any observable change of the crystal material in between. Figure 18 illustrates how growth starts at the edge and appears to be promoted by screw dislocations.

Buckley (1952) says that these crystal plates were so thin that they would fold up in the presence of concentration currents, or of other thicker crystals. In order to see whether the observed effects could be due to disturbances transmitted through the mother liquid, the neighbouring crystals were always kept under observation. In the figs. 9–14 one neighbouring thin crystal is seen to be unaffected until this very crystal is indented.

Only when neighbour crystals were actually in contact with the indented crystal as in fig. 19, growth is initiated so that the mechanical deformation seems to be the controlling factor.

It is admitted that very little can be said about the actual deformation process in these experiments, where rather a rough indenter has been used, and it is not possible to say whether Frank's (1951) " buckle, followed by shear mechanism ", is in operation. Simple or complicated slip processes may well account for the observed facts, and uneven slip on a slip plane will provide the screw dislocations for spiral growth.

Further experiments are in progress with other crystals, some of which have not yet been proved to grow by the spiral mechanism.

Acknowledgments

We are much indebted to Professor S. Tolansky in whose laboratory this work has been carried out. A. Korndorffer wishes to acknowledge financial assistance from the Department of Scientific and Industrial Research. H. Rahbek was staying here on a scholarship from the British Council while on study leave from the Technical University of Denmark, and he wishes to thank these two bodies for their generosity. F. S. A. Sultan expresses his thanks to the Egyptian Government for a grant.

References

Buckley, H. E., 1952, *Z. Elektrochem.*, **56**, 275.
Forty, A. J., 1951, *Phil. Mag.*, **42**, 670 ; 1952, *Ibid.*, **43**, 72.
Frank, F. C., 1951, *Phil. Mag.*, **42**, 1014.

CXXXI. *Film Flow and the Behaviour of He Cryostats below the λ-Point**

By E. Ambler and N. Kurti
Clarendon Laboratory, Oxford †

[Received September 8, 1952.]

Abstract

A description is given of experiments which confirm in detail the mechanism proposed by Rollin and Simon concerning the behaviour of the helium film in pumping tubes of low temperature cryostats. In particular the temperature distribution along these tubes which, as a result of the film, is of an unusual nature, was determined. Experiments were carried out both on tubes having uniform cross sections and tubes containing a constriction, and it is shown how the above mechanism can be used to measure film transfer rates in each case. The results are finally discussed from the point of view of the design of helium cryostats.

§1. Introduction

The existence of a helium film on surfaces in contact with liquid helium below the lambda-point was first suggested by Rollin and Simon (Rollin 1936, Rollin and Simon 1939) in order to explain the high rate of evaporation from vessels kept at constant temperature by pumping off the helium vapour, and also to account for the abnormally high warming-up rates of such containers when the pump was turned off. They also pointed to a possible connection between this behaviour and the puzzling ' distillation ' phenomenon observed by Kamerlingh Onnes (1922). They proposed the following mechanism. There exists a film of liquid helium on the walls of the pumping tube which evaporates at its warm end and which is being continuously replenished from the bulk liquid by flow in the film. This mechanism could account not only for the high rate of evaporation but also for the high warming-up rates, as, with the pump shut off, the vapour would be forced to condense on the colder bulk liquid and warm it up. The well known fundamental experiments of Daunt and Mendelssohn (1938) proved directly the transfer of liquid helium in a film and fully vindicated the mechanism proposed by Rollin and Simon.

The main purpose of the present experiments was to test in more detail this explanation and some of its consequences. In particular, the question of the actual point where the helium film evaporates in the tube has not hitherto been considered. If the proposed mechanism is the correct

* This work was briefly reported at the Oxford International Conference on Low Temperature Physics in 1951.

† Communicated by the Authors.

one, and if one assumes the pumping tube to be everywhere at the same temperature as the liquid helium film on its inside, then since no appreciable temperature differences can exist in the film (Kikoin and Lasarew 1938), there should be no temperature gradient along the lower part of the pumping tube. The film will exist up to the point where the heat influx, which is mainly due to conduction along the material of the tube, is just sufficient to evaporate the helium creeping up in the film. Taking, for instance, a German silver pumping tube of 0·1 mm wall thickness whose upper end is at 4·2° K, one finds, using Berman's (1951) value for the heat conductivity, that the film should evaporate about 3 mm below the warm end of the tube.

Fig. 1

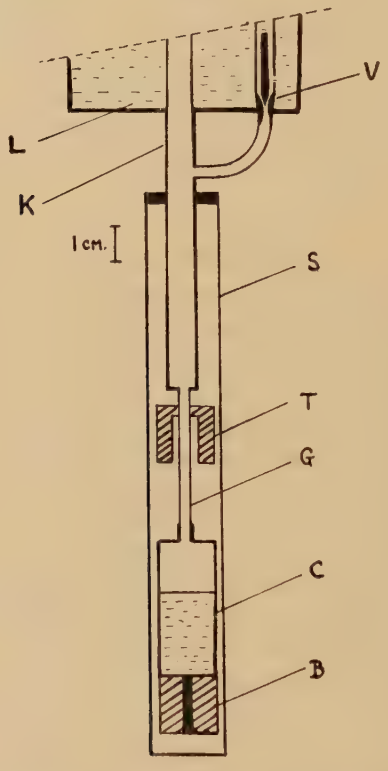

Experimental cryostat : pumping tube of uniform cross section.

Accordingly the experimental arrangement was such that, besides measuring the rate of evaporation and the rate of warming up, it was possible to obtain information on the temperature distribution along the pumping tube.

§ 2. Apparatus and Experimental Method

Figure 1 shows schematically the general arrangement. The experimental cryostat C and the liquid helium container L into which helium was liquefied by a small Linde liquefier was situated in a vacuum case

surrounded by liquid hydrogen. The liquefier and all its auxiliary apparatus, which comprised a small refrigerator compressor for circulating the helium, has been described elsewhere (Ambler 1952).

C could be filled with liquid helium from L through the bellows sealed valve V, a method which has several advantages over condensation. It is more efficient, it is much quicker and the liquid helium introduced into C is clean. This last point is important for these experiments because, as has been shown by Bowers and Mendelssohn (1950), impurities introduced by condensing helium may increase the creep rate considerably. The leakage through valve V with liquid helium at 1 atm pressure in L and vacuum in C was about 0·01 c.c. of gas (N.T.P.) per minute, and this was small compared with the evaporation rate from C of between 0·5 and 3 c.c. per minute. When L was cooled below the λ-point the leak, of course, became prohibitively large and, therefore, L was never allowed to cool below 2·2°.

S is a copper shield attached to the thick-walled copper tube K so that it was always at the temperature of L. Its function, was to reduce heat influx into C through residual gas in the vacuum jacket so that the rate of evaporation from C was entirely determined by the creep phenomenon. This was proved by measurements of the warming-up rate above the λ-point and also by the fact that the rate of evaporation was the same whether S was at 4·2° or 2·3°. B and T are two iron alum crystals used for measuring temperature by the magnetic method; they were so attached to the apparatus that B was always at the cryostat temperature and T at the temperature of the German silver pumping tube G at a point 4 mm from the top.

In order to obtain a reliable calibration curve for T it was essential that during the calibration no temperature gradient existed along G, and to ensure this the following procedure was adopted. After C had been filled with liquid helium V was closed and the temperature brought to the various calibrating points by pumping L instead of pumping C as is usual. By throttling the pump the temperature of L was held constant at each calibrating point and the temperature of T and B quickly reached the same steady value. In every other respect the procedure was the same as that described by Hull (1947).

After the calibration L was allowed to reheat to 4·2° K and C was pumped with a diffusion pump. The final temperatures of T and B and the steady evaporation from C were measured. The pump was then shut off and temperature determinations were made on T and B at regular intervals during the subsequent warming up.

§3. The Experiments

(*a*) *Pumping Tube of Uniform Diameter*

When pumping the cryostat through a 45 mm long German silver tube, of 3 mm diameter and 0·1 mm wall thickness, the temperatures indicated by B and T (see fig. 1) were 0·92° K and 0·93° K respectively. This small apparent temperature difference is, however, within the experimental error,

and the result therefore proves that the conclusion mentioned in the introduction about the temperature distribution along the pumping tube is essentially correct.

The steady evaporation from the cryostat was 3·5 c.c. gas N.T.P./min. which can wholly be accounted for by film flow up the 3 mm diameter pumping tube.

The way in which the temperatures of B and T increased with time after the pump had been shut off is shown in fig. 2. Up to 1·9° K the temperatures of the two were equal and then T rose more quickly. The reason for this is that on approaching the λ-point the rate of film transfer decreases and consequently the heat of evaporation which must be

Fig. 2

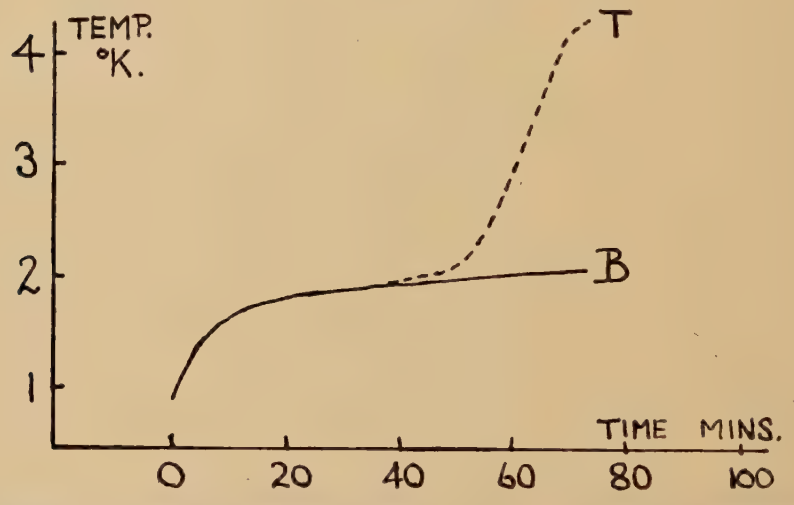

Warming-up curves for cryostat shown in fig. 1. Curve B—temperature of cryostat. Curve T—temperature near top of the pumping tube.

conducted down the pumping tube becomes smaller. Therefore the point where the film evaporates recedes down the tube, and when it falls below the point of attachment of T the temperature of T rises above that of B.

From the rate at which the cryostat temperature increases the rate of film transfer on the walls of the pumping tube can be deduced. According to the mechanism proposed by Rollin and Simon, after the film evaporates part of the helium condenses back into the cryostat (say at a rate dm_2/dt), causing it to heat up, and part fills the dead space (say at a rate dm_1/dt) so that the pressure there remains equal to the vapour pressure of the helium in the cryostat. dm_1/dt is calculable from the volumes and temperature distribution in the dead space and the rate of increase of pressure; dm_2/dt is then obtained from the expression

$$H\frac{dT_c}{dt}=T_c\Delta S\left(\frac{dm_1}{dt}+\frac{dm_2}{dt}\right)+\{L+(T_i-T_c)C_p\}\frac{dm_2}{dt},$$

where H and T_c are the thermal capacity and temperature of the cryostat and its contents respectively, $T_c\Delta S$ is the 'fountain' heat, L the latent heat of vaporization of helium, C_p the specific heat of helium gas and T_i the temperature to which the gas is heated before condensing back. It is not possible to determine T_i, so in using the above formula we have adopted the simple and plausible assumption that $T_i=T_c$.

The transfer rate R is simply given by

$$\frac{dm_1}{dt}+\frac{dm_2}{dt}$$

and its values are shown in table 1 together with the data used in the calculation. The results are plotted against temperature in fig. 3, curve (*b*), which also shows the rate on glass as measured by Daunt and Mendelssohn (curve (*c*)) and the measured rate while pumping (point (*a*)).

Table 1

T_c °K	$\frac{dT_c}{dt}$ °K/min.	$\frac{dm_1}{dt}$ g/min. ($\times10^4$)	$H\frac{dT_c}{dt}$ cal/min. ($\times10^3$)	$\left(H\frac{dT_c}{dt}-T_c\Delta S\frac{dm_1}{dt}\right)$ ($\times10^3$)	$\frac{dm_2}{dt}$ g/min. ($\times10^4$)	Transfer rate R c.c. cm^{-1} sec^{-1} ($\times10^5$)
1·25	0·11	2·60	2·4	2·4	4·35	8·4
1·69	$0·020_5$	2·30	2·4	2·4	$4·2_5$	8·0
1·84	$0·010_0$	1·65	$1·7_5$	$1·7_0$	$2·9_5$	5·6
1·93	0·0068	1·15	$1·5_0$	$1·4_5$	$2·4_5$	4·4
1·98	0·0044	0·85	1·10	1·06	1·78	3·2
2·03	0·0022	0·70	0·61	$0·57_5$	0·95	2·0
2·07	0·0017	0·66	0·53	$0·49_5$	0·82	1·8
2·10	0·0015	0·65	0·50	$0·46_0$	0·76	1·7

Mass of helium in cryostat=0·225 g.

The fair agreement between (*a*), (*b*) and (*c*) provides quantitative confirmation of the interpretation of Rollin and Simon; conversely we may say that, using their interpretation, the warming-up process can be used to measure transfer rates to a reasonable accuracy. It is worth mentioning that, if contrary to our above assumption, $T_i>T_c$, the effect is to bring curve (*b*) into better agreement with (*a*) and (*c*). The discrepancy, anyway, is not significant in view of the higher rates that are frequently observed on metal surfaces (Mendelssohn and White 1950).

Having proved quantitatively the correctness of the Rollin–Simon interpretation, we decided to make similar measurements on pumping tubes containing a constriction.

(*b*) *Pumping Tubes with Constriction*

In general the effect of a constriction is to reduce the rate of evaporation while pumping the cryostat, so that a lower final temperature can be produced (Blaisse, Cooke and Hull 1939).

The arrangement is shown in fig. 4, where P is a 0·5 mm diameter German silver capillary soldered into the top of the cryostat C and then burnished. The pumping tube G had a diameter of 6 mm and wall thickness 0·1 mm and was also made of German silver. In every other respect the arrangement was the same as in the previous experiment.

It was found that the rate of evaporation while pumping was only reduced to two-thirds of the value found in the previous experiment, indicating that the transfer rate per cm perimeter through the capillary

Fig. 3

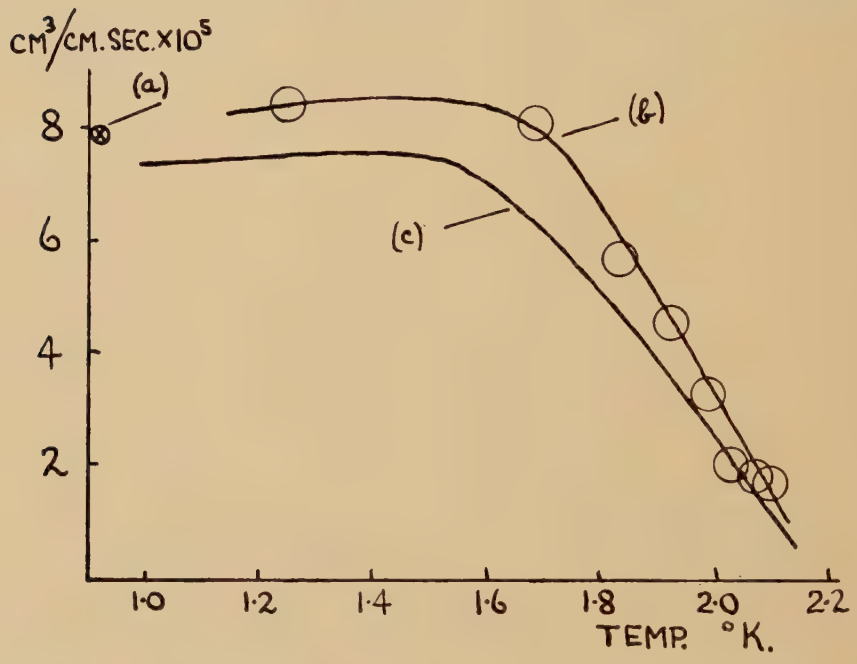

Transfer rates for cryostat shown in fig. 1 : (*a*) steady evaporation rate, (*b*) calculated from warming-up rates (see table 1), (*c*) measurements of Daunt and Mendelssohn (1938).

was about four times that for the 3 mm diameter tube. Such anomalous rates through small apertures have been observed previously by Hudson, Hunt and Kurti (Kurti 1948) and by Brown and Mendelssohn (1950). With this evaporation we should expect the film to evaporate about 1 cm from the top of the tube G, i.e. below the level of T, so that the temperature of T should be higher than B. This was found to be so, the temperatures of T and B being 2·25° K and 0·91° K respectively. The way in which the temperatures of T and B changed when the cryostat was allowed to warm up is shown in fig. 5, and it will be seen that there was an initial fall in the temperature of T. The transfer rate calculated as before is shown in fig. 6 (curve (*b*)) together with the evaporation rate while

pumping (point (*a*)). The explanation for the lack of correlation between those two and for the initial fall in temperature of T is as follows. When the cryostat was being pumped the film flow along G, being limited by that which could creep through P, was fairly small, so that it evaporated below T. When the pump was turned off, however, the helium which condensed back did so as film on top of the cryostat and was available

Fig. 4

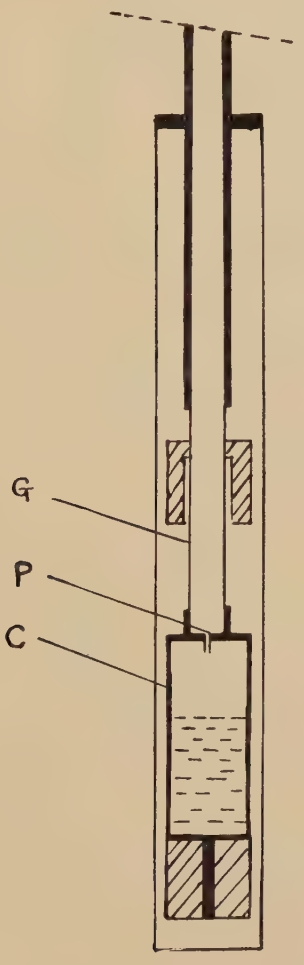

Experimental cryostat : constricted pumping tube.

for further transport along G, where the rate was subcritical. Hence the transfer rate along G got bigger and the film reached a higher point in the tube, thus cooling T. The rate reached a maximum value which was less than the critical value, as can be seen from fig. 6, where we have plotted (curve (*c*)) the transfer rate for a 6 mm diameter clean glass tube.

Fig. 5

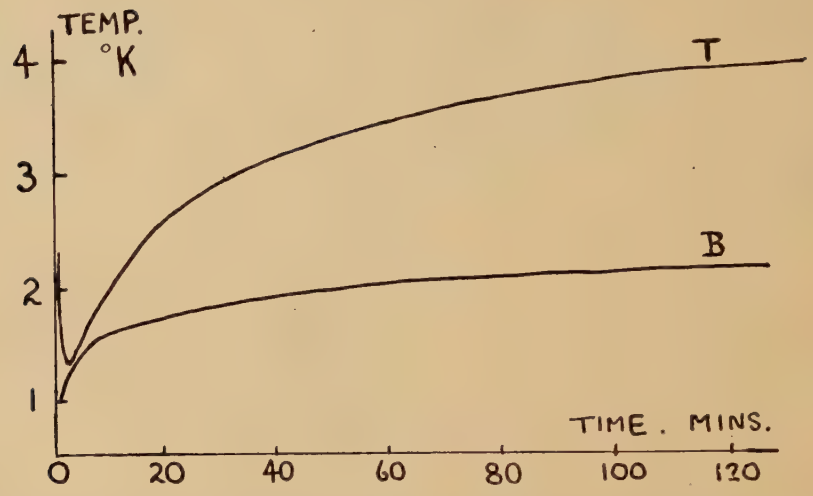

Warming up curves for cryostat shown in fig. 4. Curve B—temperature of cryostat. Curve T—temperature near top of the pumping tube.

Fig. 6

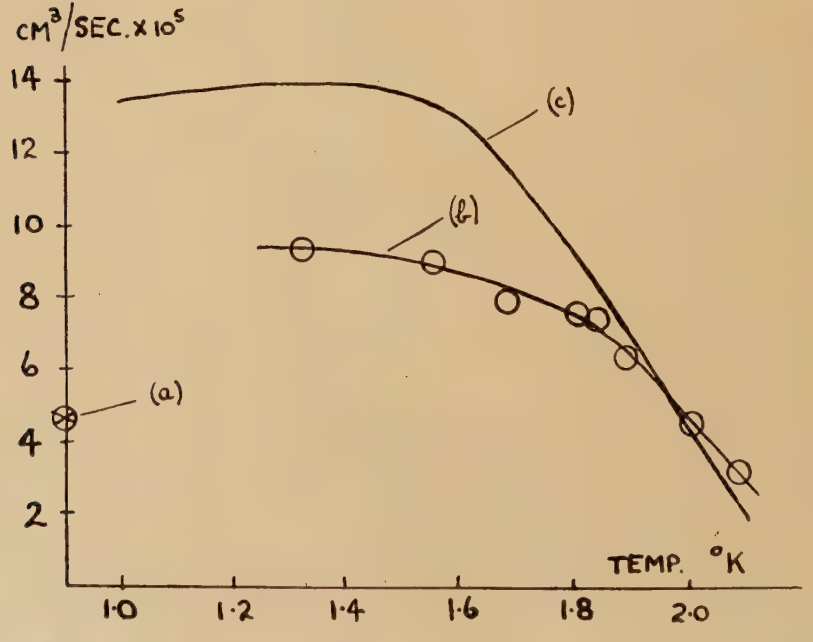

Transfer rates for cryostat shown in fig. 4: (*a*) steady evaporation, (*b*) calculated from warming-up rates, (*c*) measurements of Daunt and Mendelssohn (1938).

The fact that the rate on G was subcritical during the warming-up period is of no fundamental importance. It could be brought up to the critical value either by decreasing the dead-space so that the amount of helium refluxing is bigger or by increasing the transport rate through P. In an experiment where the German silver capillary was replaced by one of the same size made of copper, which happened to give a transport rate about twice as big, it was indeed found that, while pumping, the rate on G was subcritical, but when the pump was turned off the rate quickly built up to the critical value.

The difference between the transfer rates on G with the pump on and off arose because the capillary, being an integral part of the cryostat, was in good thermal contact with the bulk helium inside. We would expect that if this thermal contact were very bad the refluxing helium would condense only inside the cryostat (i.e. below the constriction) and the transport rate along G would be always the same as that through the constriction. This was confirmed by an experiment where the constriction was thermally insulated from the top of the cryostat. The constriction was a glass capillary 4 mm long and 0·5 mm diameter which was attached to the metal parts by means of small Housekeeper seals. The final temperature reached while pumping was 0·8° K, with an evaporation corresponding to a transfer rate through the glass capillary of $7{\cdot}8\times10^{-5}$ c.c./cm sec. The rate calculated from the heating-up process was $8{\cdot}2\times10^{-5}$ c.c./cm sec at about 1° K, in good agreement with both the steady evaporation and the values given by Daunt and Mendelssohn for glass.

§ 4. Discussion

Apart from the conclusions already drawn we may use the results of the above experiments in the design of low temperature cryostats. If, for example, the only connection to the cryostat is the pumping tube, then by making the pumping tube longer than a certain minimum length we secure no reduction of heat influx into the cryostat. It is only necessary to ensure that the film evaporates inside the tube, and with a German silver tube of 0·1 mm wall thickness the minimum length is 3 mm if its upper end is at 4·2° K and 70 mm if its upper end is at 20° K.

In the case of cryostats to which there is an external heat influx (e.g. along additional tubes or through gas conduction) it has been generally assumed that this would produce an evaporation from the bulk liquid which is additional to the film evaporation, the two being independent (Blaisse, Cooke and Hull 1939). It appears to us, however, from a consideration of the temperature and pressure distributions along the pumping tube, that this may not be the complete picture, and that the effect of an external heat influx is rather to evaporate film than bulk liquid, provided of course that it does not exceed the total heat of evaporation of the film.

Even if this were not so (we hope to investigate this question experimentally) an arrangement could be devised which in any case

would ensure that the external heat influx would evaporate film rather than bulk liquid. For example, any additional tubes to the cryostat could be brought into thermal contact (e.g. by a copper link) with the pumping tube at a short distance above the cryostat, and the heat influx along all the tubes will then be used to evaporate the film. Provided the heat influx is not too big the film can reach the level of the link so that at the point of contact all tubes are at the cryostat temperature and there can be no heat flow to the bulk liquid. In the same way heat influxes due to radiation and gas conduction can be minimized by surrounding the cryostat with a copper shield attached to a suitable point on the pumping tube. In brief, the cryostat should be so designed that any external heat influx evaporates the film and not the liquid.

We wish to thank Professor F. E. Simon for his interest in this work and the Department of Scientific and Industrial Research for E. A.'s maintenance grant.

References

Ambler, E., 1952, *Proc. 8th Int. Cong. Refrig.* (In course of publication.)
Berman, R., 1951, *Phil. Mag.*, **42**,, 642.
Blaisse, B. S., Cooke, A. H., and Hull, R. A., 1939, *Physica*, **6**, 231.
Bowers, R., and Mendelssohn, K., 1950, *Proc. Phys. Soc.* A, **63**, 1318.
Brown, J. B., and Mendelssohn, K., 1950, *Proc. Phys. Soc.* A, **63**, 1312.
Daunt, J. G., and Mendelssohn, K., 1938, *Nature, Lond.*, **141**, 911.
Hull, R. A., 1947, *Report of Cambridge Conference on Low Temperatures* (London : Physical Society), p. 74.
Kamerlingh Onnes, H., 1922, *Comm. Phys. Lab. Univ. Leiden*, No. 159.
Kikoin, A. K., and Lasarew, B. G., 1938, *Nature, Lond.*, **141**, 912.
Kurti, N., 1948, *Les Phénomènes Cryomagnétiques*, Cérémonies Langevin-Perrin, Paris, p. 31.
Mendelssohn, K., and White, G. H., 1950, *Proc. Phys. Soc.* A, **63**, 1328.
Rollin, B. V., 1936, *Proc. 7th Int. Cong. Refrig.* **1**, 187.
Rollin, B. V., and Simon, F., 1939, *Physica*, **6**, 219.

CXXXII. *The Thermal Instability of a Fluid Sphere Heated Within*

By S. Chandrasekhar, F.R.S.
Yerkes Observatory, University of Chicago*

[Received September 8, 1952]

Summary

In this paper the problem of the thermal instability of an incompressible fluid sphere heated within and in equilibrium under its own gravitation is considered. A general disturbance is analysed into modes in terms of spherical harmonics of various orders, l, and the criterion for the onset of convection for the first fifteen modes is found both when the bounding surface is free and when it is rigid ; and it is shown that in both cases the mode $l=1$ is the first to be excited.

§ 1. Introduction

The manner of the onset of convection in a horizontal layer of fluid heated below has been the subject of experimental and theoretical investigations since Benárd's (1900) first discoveries on the subject. The related problem of thermal instability of a fluid sphere heated within has not received the same attention though it is of interest in a number of geophysical and astrophysical connections. However, a beginning in the study of this problem was made by Wasiutynski (1946) who derived the basic equations of the theory. More recently, Jeffreys and Bland (1951) have re-examined the same problem along somewhat different lines ; in particular, they have attempted to solve the underlying characteristic value problem by a variational procedure. In this paper we shall show that Jeffreys and Bland have not formulated the variational procedure in its most effective form ; and that when this is done it is capable of solving the mathematical problems of the theory to a high degree of precision. While this paper will be limited to the case of thermal instability in a homogeneous sphere, the methods of this paper can be readily extended to the treatment of convection in spherical shells—a problem of very specific geophysical interest ; it will therefore be developed in that connection in a separate paper.

§ 2. The Equations of the Problem

While the basic equations of the theory have been derived in the papers of Wasiutynski and Jeffreys and Bland, the perturbation in temperature which they use as the dependent variable does not appear to be the most convenient one to use ; the radial component of the

* Communicated by the Author.

velocity u_r (or, rather, ru_r) appears to be a more suitable one and has the additional advantage that the boundary conditions can be more readily expressed in terms of it. For these reasons, it may be useful to develop the equations of the problem *ab initio*.

Consider then a homogeneous sphere of radius R, in equilibrium under its own gravitation and with a uniform distribution of heat sources such that in the absence of conduction the temperature at each point will rise at a rate ϵ. In the steady state the temperature distribution, $T(r)$, inside the sphere will be governed by

$$\kappa\nabla^2 T=\epsilon, \quad . \quad . \quad . \quad . \quad . \quad . \quad . \quad . \quad . \quad (1)$$

where κ is the coefficient of thermometric conductivity. The solution of eqn. (1) appropriate to the problem on hand is

$$T=\beta(R^2-r^2) \qquad \text{where} \qquad \beta=\epsilon/6\kappa. \quad . \quad . \quad . \quad . \quad . \quad (2)$$

In writing the solution in the form (2) we have assumed that $T=0$ at $r=R$; this clearly entails no loss of generality.

Let the temperature distribution in the perturbed state be given by

$$T=\beta(R^2-r^2)+\theta. \quad . \quad . \quad . \quad . \quad . \quad . \quad . \quad . \quad (3)$$

The equation governing θ is

$$\frac{\partial\theta}{\partial t}+u_i\frac{\partial T}{\partial x_i}=\kappa\nabla^2\theta, \quad . \quad . \quad . \quad . \quad . \quad . \quad . \quad . \quad (4)$$

where u_i denotes the component of velocity. Further in eqn. (4) (and in the sequel) summation over repeated indices is to be understood.

The equation of motion is

$$\rho\frac{\partial u_i}{\partial t}+\rho\frac{\partial}{\partial x_j}u_iu_j=-\frac{\partial p}{\partial x_i}+\rho\frac{\partial V}{\partial x_i}+\rho\nu\nabla^2 u_i, \quad . \quad . \quad . \quad (5)$$

where V denotes the gravitational potential and the rest of the symbols have their usual meanings. Following Rayleigh (1916) we shall allow in eqn. (5) for the variation of density only in so far as it modifies the external field. Thus, in eqn. (5) we shall replace ρ which occurs in front of $\partial V/\partial x_i$ by

$$\rho=\rho_0(1-\alpha T), \quad . \quad . \quad . \quad . \quad . \quad . \quad . \quad . \quad (6)$$

where α denotes the coefficient of volume expansion and ρ_0 is the density at $r=R$ (where $T=0$) and regard ρ occurring elsewhere in eqn. (5) as a constant equal to ρ_0. On these assumptions eqn. (5) becomes

$$\frac{\partial u_i}{\partial t}+\frac{\partial}{\partial x_j}u_iu_j=-\frac{\partial}{\partial x_i}\left(\frac{p}{\rho_0}-V\right)-\alpha[\beta(R^2-r^2)+\theta]\frac{\partial V}{\partial x_i}+\nu\nabla^2 u_i, \quad . \quad (7)$$

where we have substituted for T according to eqn. (3). With the variation of density due to thermal expansion allowed for in this manner, we shall from now on treat u_i as a solenoidal vector

$$\frac{\partial u_i}{\partial x_i}=0. \quad . \quad . \quad . \quad . \quad . \quad . \quad . \quad . \quad . \quad (8)$$

When the external field is that due to the action of gravity in a homogeneous sphere,

$$\frac{\partial V}{\partial x_i} = -\frac{4}{3}\pi\bar{\rho}Gx_i, \quad \ldots\ldots\ldots \quad (9)$$

where G denotes the constant of gravitation. With the substitution (9), eqn. (7) may be written in the form

$$\frac{\partial u_i}{\partial t} + \frac{\partial}{\partial x_j}u_iu_j = -\frac{\partial \varpi}{\partial x_i} + \gamma\theta x_i + \nu\nabla^2 u_i, \quad \ldots\ldots \quad (10)$$

where

$$\gamma = \frac{4}{3}\pi\bar{\rho}G\alpha, \quad \ldots\ldots\ldots \quad (11)$$

and

$$\varpi = \frac{p}{\rho_0} - V - \frac{1}{4}\beta\gamma(2R^2r^2 - r^4). \quad \ldots\ldots \quad (12)$$

We shall now suppose that u_i and θ are small quantities of the first order and that we can ignore products and squares of them. On this supposition eqns. (4) and (10) reduce to

$$\frac{\partial\theta}{\partial t} = \kappa\nabla^2\theta + 2\beta u_i x_i, \quad \ldots\ldots\ldots \quad (13)$$

and

$$\frac{\partial u_i}{\partial t} = -\frac{\partial \varpi}{\partial x_i} + \gamma\theta x_i + \nu\nabla^2 u_i. \quad \ldots\ldots \quad (14)$$

Taking the divergence of eqn. (14) and remembering that u_i is solenoidal, we get

$$\nabla^2\varpi = \gamma\left(3\theta + x_j\frac{\partial\theta}{\partial x_j}\right). \quad \ldots\ldots\ldots \quad (15)$$

Equations (13) to (15) are the basic equations of this theory.

§ 3. The Boundary Conditions

The solution of eqns. (13) to (15) must satisfy certain boundary conditions. Some of these conditions will depend on whether the bounding surface considered is rigid or free. But in all cases we must require that

$$\theta = 0 \text{ and } u_ix_i = ru_r = 0 \text{ (on a bounding spherical surface).} \quad (16)$$

Additional boundary conditions needed to make the problem determinate follow from the equation of continuity ; and these depend on the nature of the bounding surface.

Now the equation of continuity in spherical polar coordinates (r, ϑ, φ) is

$$\frac{\partial u_r}{\partial r} + 2\frac{u_r}{r} + \frac{1}{r}\frac{\partial u_\vartheta}{\partial\vartheta} + \frac{u_\vartheta\cot\vartheta}{r} + \frac{1}{r\sin\vartheta}\frac{\partial u_\vartheta}{\partial\varphi} = 0, \quad \ldots \quad (17)$$

where u_r, u_ϑ and u_φ are the components of velocity along the principal elements of arc dr, $r\,d\vartheta$ and $r\sin\vartheta\,d\varphi$, respectively. On a bounding

surface which is rigid and on which no slip occurs, u_r, u_ϑ and u_φ must vanish; and when the bounding surface is spherical, it follows from eqn. (17) that

$$\frac{\partial u_r}{\partial r}=0 \qquad \text{(on a rigid spherical surface)}, \quad . \quad . \quad . \quad (18)$$

or, equivalently (since $u_r=0$)

$$\frac{\partial}{\partial r}(ru_r)=\frac{\partial}{\partial r}(u_i x_i)=0 \qquad \text{(on a rigid spherical surface)}. \quad . \quad (19)$$

On the other hand on a bounding spherical surface which is free, we must require (in addition to $u_r=0$) that the viscous stresses $p_{r\vartheta}$ and $p_{r\varphi}$ also vanish. Now, quite generally, the expression for these stresses are (cf. Ramsey 1949, p. 374)

$$\left.\begin{aligned} p_{r\vartheta}&=\rho\nu\left(\frac{\partial u_r}{r\partial\vartheta}-\frac{u_\vartheta}{r}+\frac{\partial u_\vartheta}{\partial r}\right),\\ p_{r\varphi}&=\rho\nu\left(\frac{\partial u_r}{r\sin\vartheta\partial\varphi}-\frac{u_\varphi}{r}+\frac{\partial u_\varphi}{\partial r}\right).\end{aligned}\right\} \quad . \quad . \quad . \quad . \quad (20)$$

Since u_r vanishes (identically) on a bounding surface (cf. eqn. (16)), the vanishing of $p_{r\vartheta}$ and $p_{r\varphi}$ on such a surface requires that

$$\frac{\partial u_\vartheta}{\partial r}-\frac{u_\vartheta}{r}=\frac{\partial u_\varphi}{\partial r}-\frac{u_\varphi}{r}=0 \qquad \text{(on a free surface)}. \quad . \quad . \quad (21)$$

From the equation of continuity (17) it now follows that

$$\left(\frac{\partial}{\partial r}-\frac{1}{r}\right)\left(r\frac{\partial u_r}{\partial r}+2u_r\right)=0 \qquad \text{(on a free surface)}. \quad . \quad . \quad (22)$$

On expanding the left-hand side of this equation and remembering that $u_r=0$ on a bounding surface, we find

$$r\frac{\partial^2 u_r}{\partial r^2}+2\frac{\partial u_r}{\partial r}=\frac{\partial^2}{\partial r^2}(ru_r)=\frac{\partial^2}{\partial r^2}(u_i x_i)=0 \qquad \text{(on a free surface)}. \quad . \quad (23)$$

The boundary conditions (19) and (23) agree with those derived by Jeffreys and Bland (1951) by a somewhat less direct line of reasoning.

§ 4. The Equations Governing Marginal Stability

In this paper we shall assume that the principle of the exchange of stabilities is valid; its justification for the problem on hand will be given in a later paper. On this principle the equations governing marginal stability are those for which $\partial/\partial t=0$. Hence setting $\partial/\partial t=0$ in eqns. (13) to (15), we have

$$\kappa\nabla^2\theta=-2\beta u_i x_i, \quad . \quad . \quad . \quad . \quad . \quad . \quad . \quad . \quad . \quad (24)$$

$$\nu\nabla^2 u_i=\frac{\partial\varpi}{\partial x_i}-\gamma\theta x_i, \quad . \quad . \quad . \quad . \quad . \quad . \quad . \quad . \quad (25)$$

and

$$\nabla^2\varpi=\gamma\left(3\theta+x_j\frac{\partial\theta}{\partial x_j}\right). \quad . \quad . \quad . \quad . \quad . \quad . \quad (26)$$

We can eliminate ϖ from these equations in the following manner :

$$\nabla^2(\gamma\theta x_i+\nu\nabla^2 u_i)=\nabla^2\frac{\partial\varpi}{\partial x_i}=\frac{\partial}{\partial x_i}\nabla^2\varpi=\gamma\frac{\partial}{\partial x_i}\left(3\theta+x_j\frac{\partial\theta}{\partial x_j}\right). \quad . \quad (27)$$

On simplifying the outer parts of this equality and rearranging, we find

$$\nabla^4 u_i=\frac{\gamma}{\nu}\left(\frac{\partial}{\partial x_i}+\frac{\partial}{\partial x_i}x_j\frac{\partial}{\partial x_j}-x_i\nabla^2\right)\theta. \quad . \quad . \quad . \quad . \quad (28)$$

On operating this last equation once more by ∇^2 we find

$$\nabla^6 u_i=\frac{\gamma}{\nu}\left(\frac{\partial}{\partial x_i}+\frac{\partial}{\partial x_i}x_j\frac{\partial}{\partial x_j}-x_i\nabla^2\right)\nabla^2\theta, \quad . \quad . \quad . \quad (29)$$

or making use of eqn. (24), we have

$$\nabla^6 u_i=-\frac{2\beta\gamma}{\kappa\nu}\left(\frac{\partial}{\partial x_i}+\frac{\partial}{\partial x_i}x_j\frac{\partial}{\partial x_j}-x\nabla^2\right)(u_l x_l). \quad . \quad . \quad (30)$$

It can be readily verified that the operations x_i and ∇^2 are permutable when applied to a solenoidal vector. Therefore, multiplying eqns. (28) and (30) scalarly by x_i, we obtain :

$$\nabla^4(u_i x_i)=\frac{\gamma}{\nu}\left(x_i\frac{\partial}{\partial x_i}+x_i\frac{\partial}{\partial x_i}x_j\frac{\partial}{\partial x_j}-r^2\nabla^2\right)\theta \quad . \quad . \quad . \quad (31)$$

and

$$\nabla^6(u_i x_i)=-\frac{2\beta\gamma}{\kappa\nu}\left(x_i\frac{\partial}{\partial x_i}+x_i\frac{\partial}{\partial x_i}x_j\frac{\partial}{\partial x_j}-r^2\nabla^2\right)(u_l x_l). \quad . \quad (32)$$

The differential operator which occurs on the right-hand side of eqns. (31) and (32) is

$$r\frac{\partial}{\partial r}+r\frac{\partial}{\partial r}r\frac{\partial}{\partial r}-r^2\nabla^2=r^2\left(\frac{\partial^2}{\partial r^2}+\frac{2}{r}\frac{\partial}{\partial r}-\nabla^2\right)$$

$$=-\frac{1}{\sin\vartheta}\frac{\partial}{\partial\vartheta}\sin\vartheta\frac{\partial}{\partial\vartheta}-\frac{1}{\sin^2\vartheta}\frac{\partial^2}{\partial\varphi^2}=L^2 \text{ (say)}. \quad . \quad (33)$$

Hence, eqns. (31) and (32) can be written in the forms

$$\nabla^4(u_i x_i)=\frac{\gamma}{\nu}L^2\theta \quad . \quad . \quad . \quad . \quad . \quad . \quad . \quad (34)$$

and

$$\nabla^6(u_i x_i)=-\frac{2\beta\gamma}{\kappa\nu}L^2(u_i x_i). \quad . \quad . \quad . \quad . \quad . \quad . \quad (35)$$

It is apparent from the forms of eqns. (34) and (35) that the general solution of these equations must be expressible as a series in spherical harmonics. We, therefore, seek a solution of the form

$$\theta=\Theta(r)S_l(\vartheta,\varphi) \text{ and } u_i x_i=ru_r=W(r)S_l(\vartheta,\varphi), \quad . \quad . \quad . \quad (36)$$

where $S_l(\vartheta,\varphi)$ is a general spherical harmonic of order l and $\Theta(r)$ and $W(r)$ are functions of r only. Since

$$\left.\begin{aligned} L^2S_l(\vartheta,\varphi)&=l(l+1)S_l(\vartheta,\varphi)\\ \text{and}\qquad \nabla^2&=\frac{\partial^2}{\partial r^2}+\frac{2}{r}\frac{\partial}{\partial r}-\frac{L^2}{r^2},\end{aligned}\right\} \quad . \quad . \quad . \quad . \quad (37)$$

eqns. (34) and (35), for the assumed forms of θ and $u_i x_i$, reduce to

$$\left[\frac{d^2}{dr^2}+\frac{2}{r}\frac{d}{dr}-\frac{l(l+1)}{r^2}\right]^2 W=l(l+1)\frac{\gamma}{\nu}\Theta \quad . \quad . \quad . \quad . \quad . \quad (38)$$

and

$$\left[\frac{d^2}{dr^2}+\frac{2}{r}\frac{d}{dr}-\frac{l(l+1)}{r^2}\right] W=-\frac{2\beta\gamma}{\kappa\nu}l(l+1)W. \quad . \quad . \quad . \quad (39)$$

In the further discussion of eqns. (38) and (39) it is convenient to measure r in units of the radius R of the sphere. With this choice of unit, eqns. (38) and (39) become

$$\left[\frac{d^2}{dr^2}+\frac{2}{r}\frac{d}{dr}-\frac{l(l+1)}{r^2}\right]^2 W=l(l+1)R^4\frac{\gamma}{\nu}\Theta \quad . \quad . \quad . \quad (40)$$

and

$$\left[\frac{d^2}{dr^2}+\frac{2}{r}\frac{d}{dr}-\frac{l(l+1)}{r^2}\right] W=-l(l+1)C_l W, \quad . \quad . \quad . \quad (41)$$

where (cf. eqns. (2) and (11))

$$C_l=\frac{2\beta\gamma}{\kappa\nu}R^6=\frac{4\pi G\bar{\rho}\alpha\epsilon}{9\kappa^2\nu}R^6. \quad . \quad . \quad . \quad . \quad . \quad . \quad (42)$$

A subscript l has been attached to C to emphasize the fact that the characteristic values of this number will depend on the order of the spherical harmonic considered.

According to eqns. (16), (19), (23) and (40), the boundary conditions with respect to which we must seek a solution of eqn. (41) are that at $r=1$

$$\left.\begin{aligned} &W=\left[\frac{d^2}{dr^2}+\frac{2}{r}\frac{d}{dr}-\frac{l(l+1)}{r^2}\right]^2 W=0 \\ \text{and } \textit{either} \quad &\frac{dW}{dr} \quad \textit{or} \quad \frac{d^2W}{dr^2}=0 \qquad (r=1). \end{aligned}\right\} \quad . \quad . \quad . \quad . \quad (43)$$

Further, at $r=0$ none of the physical quantities must have a singularity; and it can be directly verified from eqn. (41) that this condition requires

$$W \text{ to behave like } r^l \text{ as } r\to 0. \quad . \quad . \quad . \quad . \quad . \quad . \quad (44)$$

A solution of eqn. (41) which satisfies the boundary conditions at $r=0$ and $r=1$ and is not zero everywhere is possible only when C_l takes one of a sequence of determinate characteristic values. In the present connection we are interested only in the lowest of these characteristic values.

§ 5. A Variational Procedure for Determining the Lowest Characteristic Numbers C_l

Letting

$$\left.\begin{aligned} G&=\left[\frac{d^2}{dr^2}+\frac{2}{r}\frac{d}{dr}-\frac{l(l+1)}{r^2}\right]W=\frac{1}{r^2}\left[\frac{d}{dr}\left(r^2\frac{d}{dr}\right)-l(l+1)\right]W, \\ F&=\left[\frac{d^2}{dr^2}+\frac{2}{r}\frac{d}{dr}-\frac{l(l+1)}{r^2}\right]^2 W=\frac{1}{r^2}\left[\frac{d}{dr}\left(r^2\frac{d}{dr}\right)-l(l+1)\right]G, \end{aligned}\right\} \quad . \quad (45)$$

we can rewrite the differential equation governing W in the form

$$\frac{1}{r^2}\left[\frac{d}{dr}\left(r^2\frac{dF}{dr}\right)-l(l+1)F\right]=-l(l+1)C_lW. \quad . \quad . \quad . \quad (46)$$

The boundary conditions (43) require that

$$F=W=0 \text{ and either } \frac{dW}{dr} \text{ or } \frac{d^2W}{dr^2}=0 \text{ at } r=1. \quad . \quad . \quad (47)$$

Multiply eqn. (46) by r^2F and integrate over the range of r. The right-hand side of the equation gives

$$\int_0^1 F\frac{d}{dr}\left(r^2\frac{dF}{dr}\right)dr-l(l+1)\int_0^1 F^2\,dr. \quad . \quad . \quad . \quad . \quad (48)$$

By integrating by parts the first of the two integrals in (48) and remembering that F vanishes at $r=1$ and is continuous at $r=0$, we obtain :

$$-\int_0^1\left\{r^2\left(\frac{dF}{dr}\right)^2+l(l+1)F^2\right\}dr. \quad . \quad . \quad . \quad . \quad . \quad (49)$$

Turning next to the left-hand side of eqn. (46), we have to consider (cf. eqns. (45))

$$\int_0^1 r^2WF\,dr=\int_0^1 W\frac{d}{dr}\left(r^2\frac{dG}{dr}\right)dr-l(l+1)\int_0^1 WG\,dr. \quad . \quad . \quad (50)$$

By integrating by parts the first of the two integrals on the left-hand side of (50) we get (cf. eqns. (44) and (47))

$$-\int_0^1\frac{dG}{dr}\left(r^2\frac{dW}{dr}\right)dr\,; \quad . \quad . \quad . \quad . \quad . \quad . \quad . \quad (51)$$

a further integration by parts yields

$$-\left(G\frac{dW}{dr}\right)_{r=1}+\int_0^1 G\frac{d}{dr}\left(r^2\frac{dW}{dr}\right)dr. \quad . \quad . \quad . \quad . \quad (52)$$

If $r=1$ is a rigid boundary $(dW/dr)_{r=1}=0$ and the integrated part vanishes. On the other hand, if $r=1$ is a free boundary, $(dW/dr)_{r=1}\neq 0$ and G will have the value (cf. eqns. (45)) $2(dW/dr)_{r=1}$ since $W_{r=1}=0$ and $(d^2W/dr^2)_{r=1}=0$. Hence in this latter case the integrated part in (52) will have the value $-2\,(dW/dr)^2_{r=1}$; we may clearly take this as the value of the integrated part in both cases. Thus, combining (50) and (52) we can write (cf. eqns. (45))

$$-2\left(\frac{dW}{dr}\right)^2_{r=1}+\int_0^1 r^2G^2\,dr. \quad . \quad . \quad . \quad . \quad . \quad . \quad (53)$$

Hence the result of multiplying eqn. (46) by r^2F and integrating is

$$l(l+1)C_l=\frac{\int_0^1\{r^2(dF/dr)^2+l(l+1)F^2\}dr}{-2(dW/dr)^2_{r=1}+\int_0^1 r^2G^2\,dr}=\frac{I_1}{I_2}\ \text{(say)}. \quad . \quad . \quad (54)$$

Consider now the effect on C_l of a variation δW in W compatible with the boundary conditions on W. To the first order, we have

$$l(l+1)\delta C_l = \frac{1}{I_2}\{\delta I_1 - l(l+1)C_l \delta I_2\}, \quad . \quad . \quad . \quad . \quad (55)$$

where δI_1 and δI_2 denote the corresponding variations in I_1 and I_2:

$$\delta I_1 = 2\int_0^1 \left\{r^2 \frac{dF}{dr}\frac{d}{dr}\delta F + l(l+1)F\delta F\right\} dr \quad . \quad . \quad . \quad . \quad (56)$$

and

$$\delta I_2 = -4\left(\frac{dW}{dr}\frac{d}{dr}\delta W\right)_{r=1} + 2\int_0^1 r^2 G\delta G\, dr. \quad . \quad . \quad . \quad (57)$$

The foregoing expressions for δI_1 and δI_2 can be reduced by one or more integrations by parts as follows:

$$\begin{aligned}\delta I_1 &= 2\left(r^2\frac{dF}{dr}\delta F\right)_{r=1} - 2\int_0^1 \left\{\frac{d}{dr}\left(r^2\frac{dF}{dr}\right) - l(l+1)F\right\}\delta F\, dr \\ &= -2\int_0^1 \left\{\frac{d}{dr}\left(r^2\frac{dF}{dr}\right) - l(l+1)F\right\}\delta F\, dr \quad . \quad . \quad . \quad . \quad . \quad . \quad (58)\end{aligned}$$

and

$$\begin{aligned}\delta I_2 &= -4\left(\frac{dW}{dr}\frac{d}{dr}\delta W\right) + 2\int_0^1 \left\{\frac{d}{dr}\left(r^2\frac{dW}{dr}\right) - l(l+1)W\right\}\delta G\, dr \\ &= -4\left(\frac{dW}{dr}\frac{d}{dr}\delta W\right) + 2\left(r^2\frac{dW}{dr}\delta G\right)_{r=1} - 2\left(Wr^2\frac{d}{dr}\delta G\right)_{r=1} \\ &\quad + 2\int_0^1 W\left\{\frac{d}{dr}\left(r^2\frac{d\,\delta G}{dr}\right) - l(l+1)\delta G\right\} dr \\ &= -4\left(\frac{dW}{dr}\frac{d}{dr}\delta W\right) + 2\left(\frac{dW}{dr}\delta G\right)_{r=1} + 2\int_0^1 r^2 W\,\delta F\, dr. \quad . \quad . \quad (59)\end{aligned}$$

The two terms besides the integral in this last expression for δI_2 vanish if $r=1$ is a rigid boundary (since in this case $dW/dr=0$). On the other hand, if $r=1$ is a free boundary then

$$(\delta G)_{r=1} = \left[\left\{\frac{d^2}{dr^2} + \frac{2}{r}\frac{d}{dr} - \frac{l(l+1)}{r^2}\right\}\delta W\right]_{r=1} = 2\left(\frac{d}{dr}\delta W\right)_{r=1} \quad . \quad . \quad (60)$$

and

$$-\left(4\frac{dW}{dr}\frac{d}{dr}\delta W\right)_{r=1} + 2\left(\frac{dW}{dr}\delta G\right)_{r=1} = 0. \quad . \quad . \quad . \quad . \quad (61)$$

Hence in both cases

$$\delta I_2 = 2\int_0^1 r^2 W\,\delta F\, dr. \quad . \quad . \quad . \quad . \quad . \quad . \quad . \quad (62)$$

Now combining eqns. (55), (58) and (62), we have

$$l(l+1)\delta C_l = -\frac{2}{I_2}\int_0^1 r^2\left\{\frac{1}{r^2}\frac{d}{dr}\left(r^2\frac{dF}{dr}\right) - \frac{l(l+1)}{r^2}F + l(l+1)C_l W\right\}\delta F\, dr. \quad (63)$$

Hence to the first order, $\delta C_l \equiv 0$ *for all small arbitrary variations* δF. It is evident that the converse of this proposition is also true. Further, it follows from (63) that the true solution of the problem gives an extremal

value for C_l. This last fact enables us to formulate the following variational procedure of solving eqn. (41) and satisfying the boundary conditions of the problem.

Assume for F an expression involving one or more parameters A_j which vanishes at $r=1$ and behaves like r^l as $r\to 0$. With the chosen form of F determine W as the solution of the differential equation

$$\left[\frac{d^2}{dr^2}+\frac{2}{r}\frac{d}{dr}-\frac{l(l+1)}{r^2}\right]^2 W=F, \quad . \quad . \quad . \quad . \quad . \quad (64)$$

which satisfies the conditions at $r=0$ and $r=1$. Then evaluate C_l according to formula (54) and minimize it with respect to the parameters A_j. In this way, we shall obtain the 'best' value of C_l for the chosen form of F.

The variational procedure as formulated above differs from that of Jeffreys and Bland (1951) in that they do not seek W (rather Θ in their connection) as a solution of a fourth order differential equation. It is necessary to do this since $\delta C_l=0$ only for arbitrary variations δF i.e., only for such variations δW which satisfy the differential equation

$$\left[\frac{d^2}{dr^2}+\frac{2}{r}\frac{d}{dr}-\frac{l(l+1)}{r^2}\right]^2 \delta W=\delta F, \quad . \quad . \quad . \quad . \quad . \quad (65)$$

where δF is arbitrary.

§ 6. The Determination of C_l for Various Values of l for the Cases (i) When the Bounding Surface is Free and (ii) When it is Rigid

The form of the equation to be solved for W suggests that we assume for F the trial function

$$F=\frac{1}{\sqrt{r}}\Sigma_j A_j J_{l+1/2}(\alpha_j r), \quad . \quad . \quad . \quad . \quad . \quad . \quad (66)$$

where $J_{l+1/2}$ denotes the Bessel function of order $l+\frac{1}{2}$, the α_j's ($j=1, 2, \ldots$) are its zeros and the A_j's are the variational parameters. With this choice, F vanishes at $r=1$ and behaves, as required, like r^l as $r\to 0$. Also, it may be recalled here that the functions $J_{l+1/2}(\alpha_j r)$ satisfy the orthogonality relations

$$\int_0^1 r\, J_{l+1/2}(\alpha_j r)\, J_{l+1/2}(\alpha_k r)\, dr=\tfrac{1}{2}\delta_{jk}\,[J'_{l+1/2}(\alpha_j)]^2, \quad . \quad . \quad (67)$$

where primes denote differentiation with respect to the argument and δ_{jk} is the usual Kronecker symbol.

With F given by (66) the equation to be solved for W is

$$\left[\frac{d^2}{dr^2}+\frac{2}{r}\frac{d}{dr}-\frac{l(l+1)}{r^2}\right]^2 W=\frac{1}{\sqrt{r}}\Sigma_j A_j J_{l+1/2}(\alpha_j r). \quad . \quad . \quad (68)$$

Since,

$$\left[\frac{d^2}{dr^2}+\frac{2}{r}\frac{d}{dr}-\frac{l(l+1)}{r^2}\right]\frac{J_{l+1/2}(\alpha r)}{\sqrt{r}}=-\frac{\alpha^2}{\sqrt{r}}J_{l+1/2}(\alpha r), \quad . \quad . \quad (69)$$

a particular integral of eqn. (68) is

$$\frac{1}{\sqrt{r}}\Sigma_j \frac{A_j}{\alpha_j^4} J_{l+1/2}(\alpha_j r). \quad . \quad . \quad . \quad . \quad . \quad . \quad . \quad . \quad (70)$$

Adding to (70) the complementary function Br^l+Cr^{l+2} which has no singularity at $r=0$, we obtain the general solution :

$$W=\frac{1}{\sqrt{r}}\Sigma_j \frac{A_j}{\alpha_j^4} J_{l+1/2}(\alpha_j r)+Br^l+Cr^{l+2}. \quad . \quad . \quad . \quad . \quad (71)$$

(In (71), B and C are constants of integration.) The condition $W=0$ at $r=1$ requires

$$B=-C, \quad . \quad . \quad . \quad . \quad . \quad . \quad . \quad . \quad . \quad . \quad (72)$$

and we have

$$W=\frac{1}{\sqrt{r}}\Sigma_j \frac{A_j}{\alpha_j^4} J_{l+1/2}(\alpha_j r)+B(r^l-r^{l+2}). \quad . \quad . \quad . \quad . \quad (73)$$

The constant B is determined by the remaining condition at $r=1$ namely, that here either dW/dr or d^2W/dr^2 must vanish (depending on whether the bounding surface at $r=1$ is rigid or free). We find that

$$B=\tfrac{1}{4}q\Sigma_j(A_j/\alpha_j^3)J'_{l+1/2}(\alpha_j), \quad . \quad . \quad . \quad . \quad . \quad . \quad (74)$$

where

$$\left.\begin{aligned} q&=2 \qquad \text{for a rigid boundary at } r=1 \\ &=-\frac{4}{2l+1} \qquad \text{for a free boundary at } r=1. \end{aligned}\right\} \quad . \quad . \quad (75)$$

Turning next to the evaluation of C_l according to formula (54), we find that for F and W given by eqns. (66) and (73) (cf. eqns. (48) to (53), (67) and (68)) :

$$\begin{aligned} &\int_0^1 \left\{r^2\left(\frac{dF}{dr}\right)^2+l(l+1)F^2\right\} dr \\ &\quad=-\int_0^1 r^2F\left\{\frac{d^2F}{dr^2}+\frac{2}{r}\frac{dF}{dr}-\frac{l(l+1)F}{r^2}\right\} dr \\ &\quad=+\int_0^1 r\Sigma_j A_j J_{l+1/2}(\alpha_j r)\Sigma_k A_k \alpha_k^2 J_{l+1/2}(\alpha_k r)\, dr \\ &\quad=\tfrac{1}{2}\Sigma_j A_j^2\alpha_j^2[J'_{l+1/2}(\alpha_j)]^2 \quad . \quad . \quad . \quad . \quad . \quad . \quad . \quad . \quad . \quad (76) \end{aligned}$$

and

$$\begin{aligned} &\int_0^1 r^2G^2\, dr-2\left(\frac{dW}{dr}\right)^2_{r=1}=\int_0^1 r^2WF\, dr \\ &\quad=\tfrac{1}{2}\Sigma_j(A_j^2/\alpha_j^4)[J'_{l+1/2}(\alpha_j)]^2+B\Sigma_j A_j\int_0^1 (r^{l+3/2}-r^{l+7/2})J_{l+1/2}(\alpha_j r)\, dr. \\ &\qquad . \quad . \quad . \quad (77)^* \end{aligned}$$

The remaining integral on the right-hand side of (77) can also be evaluated if proper use is made of the various recurrence relations satisfied by the Bessel functions. We find :

$$\int_0^1 r^2WF\, dr=\tfrac{1}{2}\Sigma_j(A_j^2/\alpha_j^4)[J'_{l+1/2}(\alpha_j)]^2+2B\Sigma_j(A_j/\alpha_j^2)J_{l+5/2}(\alpha_j). \quad . \quad . \quad (78)$$

* The transformations used in going from (48) to (49) and similarly from (50) to (53) can be used in the reverse fashion since these depend (apart from definitions) only on the boundary conditions of the problem.

The resulting expression for C_l is, therefore,

$$l(l+1)\,C_l = \frac{\Sigma_j A_j^2 \alpha_j^2 [J'_{l+1/2}(\alpha_j)]^2}{\Sigma_j (A_j^2/\alpha_j^4)[J'_{l+1/2}(\alpha_j)]^2 + q\Sigma_j (A_j/\alpha_j^3) J'_{l+1/2}(\alpha_j) \Sigma_k (A_k/\alpha_k^2) J_{l+5/2}(\alpha_k)} \quad . \quad . \quad . \quad . \quad . \quad . \quad . \quad (79)$$

where we have substituted for B according to (74). By minimizing this last expression with respect to the A_j's we shall obtain the ' best ' value for C_l for the chosen form of F.

The simplest trial function for F of the chosen form is

$$F = \frac{1}{\sqrt{r}} J_{l+1/2}(\alpha_1 r), \quad . \quad . \quad . \quad . \quad . \quad . \quad . \quad . \quad (80)$$

Table 1. The Characteristic Numbers C_l in Case the Bounding Surface if Free

l	First Approximation	A	Second Approximation
1	3094·0	−0·022022	3091·4
2	5227·4	−0·019119	5224·4
3	8778·6	−0·016639	8775·0
4	$1{\cdot}3986\times10^4$	−0·014618	$1{\cdot}3982\times10^4$
5	$2{\cdot}1209\times10^4$	−0·012977	$2{\cdot}1204\times10^4$
6	$3{\cdot}0853\times10^4$	−0·011630	$3{\cdot}0848\times10^4$
7	$4{\cdot}3360\times10^4$	−0·010511	$4{\cdot}3354\times10^4$
8	$5{\cdot}9203\times10^4$	−0·0095692	$5{\cdot}9196\times10^4$
9	$7{\cdot}8887\times10^4$	−0·0087674	$7{\cdot}8880\times10^4$
10	$1{\cdot}0295\times10^5$	−0·0080806	$1{\cdot}0294\times10^5$
11	$1{\cdot}3196\times10^5$	−0·0074825	$1{\cdot}3195\times10^5$
12	$1{\cdot}6650\times10^5$	−0·0069617	$1{\cdot}6649\times10^5$
13	$2{\cdot}0721\times10^5$	−0·0065003	$2{\cdot}0720\times10^5$
14	$2{\cdot}5475\times10^5$	−0·0060922	$2{\cdot}5474\times10^5$
15	$3{\cdot}0978\times10^5$	−0·0057276	$3{\cdot}0977\times10^5$

where α_1 is the first zero of $J_{l+1/2}$. For this choice of F there is no variational parameter with respect to which we have to minimize and eqn. (79) directly gives

$$l(l+1)C_l = \frac{\alpha_1^7 J'_{l+1/2}(\alpha_1)}{\alpha_1 J'_{l+1/2}(\alpha_1) + q J_{l+5/2}(\alpha_1)}, \quad . \quad . \quad . \quad . \quad (81)$$

where it may be recalled that q is given by eqns. (75). Values of C_l obtained with the aid of formula (81) are listed in tables 1 and 2.

The values given by (81) can be improved by including a second term in F. Thus, with the assumption

$$F = \frac{1}{\sqrt{r}} \{J_{l+1/2}(\alpha_1 r) + A J_{l+1/2}(\alpha_2 r)\}, \quad . \quad . \quad . \quad . \quad (82)$$

where α_2 denotes the second zero of $J_{l+1/2}$ and A is a variational parameter, eqn. (79), after some rearrangement, gives

$$C_l = \frac{{\alpha_1}^7}{l(l+1)} \{[J'_{l+1/2}(\alpha_1)]^2 + A^2(\alpha_2/\alpha_1)^2[J'_{l+1/2}(\alpha_2)]^2\}$$
$$\times [J'_{l+1/2}(\alpha_1)\{\alpha_1 J'_{l+1/2}(\alpha_1) + q J_{l+5/2}(\alpha_1)\} + 2q A(\alpha_1/\alpha_2)^3 J_{l+5/2}(\alpha_1) J'_{l+1/2}(\alpha_2)$$
$$+ A^2(\alpha_1/\alpha_2)^5 J'_{l+1/2}(\alpha_2)\{\alpha_2 J'_{l+1/2}(\alpha_2) + q J_{l+5/2}(\alpha_2)\}]^{-1} . \quad . \quad . \quad . \quad (83)$$

The values of C_l obtained after minimizing the foregoing expression with respect to A are also listed in tables 1 and 2 together with the values of A which give the minimum values.

Table 2. The Characteristic Numbers C_l in Case the Bounding Surface is Rigid

l	First Approximation	A	Second Approximation
1	8154·0	0·088804	8047·1
2	$1{\cdot}0559\times10^4$	0·098580	$1{\cdot}0403\times10^4$
3	$1{\cdot}5368\times10^4$	0·10409	$1{\cdot}5132\times10^4$
4	$2{\cdot}2352\times10^4$	0·10729	$2{\cdot}2006\times10^4$
5	$3{\cdot}1801\times10^4$	0·10914	$3{\cdot}1315\times10^4$
6	$4{\cdot}4117\times10^4$	0·11015	$4{\cdot}3459\times10^4$
7	$5{\cdot}9759\times10^4$	0·11062	$5{\cdot}8892\times10^4$
8	$7{\cdot}9221\times10^4$	0·11074	$7{\cdot}8108\times10^4$
9	$1{\cdot}0304\times10^5$	0·11061	$1{\cdot}0164\times10^5$
10	$1{\cdot}3176\times10^5$	0·11032	$1{\cdot}3004\times10^5$
11	$1{\cdot}6600\times10^5$	0·10991	$1{\cdot}6390\times10^5$
12	$2{\cdot}0637\times10^5$	0·10942	$2{\cdot}0384\times10^5$
13	$2{\cdot}5357\times10^5$	0·10888	$2{\cdot}5058\times10^5$
14	$3{\cdot}0814\times10^5$	0·10830	$3{\cdot}0462\times10^5$
15	$3{\cdot}7094\times10^5$	0·10770	$3{\cdot}6685\times10^5$

From a comparison of the results obtained in the first and the second approximations, it would appear that the second approximation gives values which are probably correct to one part in 10^4. As a confirmation of the precision reached by formula (83) we may note that according to Jeffreys and Bland (1951) the value of C_1 for the case of a free bounding surface obtained by an 'exact' solution of the characteristic value problem is 3091 ± 2 (±2 arising from rounding errors); and this value should be contrasted with the value 3091·4 given by eqn. (83).

Finally, we may compare the results obtained by the methods of this paper with those derived by Jeffreys and Bland (1951) from their formulation of the variational principle: The entries 3094·0, 5227·4, 8778·6, 8154·0 and 10559 in tables 1 and 2 should be compared with their values 3202, 5640, 9780, 8720 and 12600, respectively. The large discrepancy between these values is a reflection of the ineffectiveness of the variational procedure as used by Jeffreys and Bland.

§ 7. Concluding Remarks

As we have already stated in §1, the methods of this paper (in particular the variational procedure described in §§ 5 and 6) can be extended, quite readily, to determine the criterion for the onset of thermal instability in spherical shells. This latter problem has a direct bearing on the question of convection in the earth's mantle and on the interpretation of the feature of the earth's topography to which Vening Meinesz (1951) has recently drawn attention. For, as Vening Meinesz has pointed out (in this connection, see also Jeffreys 1952) in a spherical shell, we should expect that the mode of disturbance which will first become unstable will not be the one with $l=1$ (as in the case of a complete sphere) but rather one with a higher value of l. The results of calculations which are being undertaken to establish these features of convection in spherical shells in a quantitative fashion will be published in the near future. It might be added here that the writer's interest in these problems arose from an attempt to extend his recent discussion (Chandrasekhar 1952) of the magnetic inhibition of convection in a horizontal layer of fluid heated below to a spherical geometry with a view to applications to the earth's core (cf. Bullard 1948). But it was felt that before attempting to solve the problem of convection in a fluid sphere heated within and in the presence of a magnetic field, one must first solve the same problem in the absence of a magnetic field. The writer hopes to return to his original problem in the near future. A further problem which the writer also hopes to consider soon is the extension of the analysis of this paper to a rotating sphere.

In conclusion, I should like to express my thanks to Miss Donna Elbert for valuable assistance with the numerical work.

References

Benárd, H., 1900, *Rev. gén. Sci. por. appl.*, **12,** 1261, 1309.
Bullard, E. C., 1948, *Mon. Not. R. Astr. Soc., Geophys. Suppl.*, **5,** 248.
Chandrasekhar, S., 1952, *Phil. Mag.* [7], **43,** 501.
Jeffreys, H., 1952, *Mon. Not. R. Astr. Soc., Geophys. Suppl.*, **6,** 316.
Jeffreys, H., and Bland, M. E. M., 1951, *Mon. Not. R. Astr. Soc., Geophys. Suppl.*, **6,** 148.
Ramsey, A. S., 1949, *A Treatise on Hydromechanics, Part II, Hydrodynamics.* (London : Bell and Sons.)
Rayleigh, Lord, 1916, *Phil. Mag.* [6], **32,** 529 ; also *Scientific Papers*, **6,** 432.
Vening Meinesz, F. A., 1951, *Proc. Kon. Ned. Akad. v. Wet.*, Series B, **54,** 212 and 220.
Wasiutynski, J., 1946, *Astrophysica Norvegica*, **4.**

CXXXIII. *Magnetic Moments and Quadrupole Moments of Odd-mass Nuclei in jj-Coupling*

By B. H. Flowers*
Department of Mathematical Physics, The University, Birmingham†

[Received October 15, 1952]

Abstract

Magnetic moments and quadrupole moments of nuclei are treated in a model which considers all particles outside the core of completed levels on an equal footing. It is shown that in this way better agreement with experimental magnetic moments is obtained than from the simpler Schmidt model. The manner in which electric quadrupole moments arise in odd-neutron nuclei without the assumption of a deformable core is also discussed.

In considering the magnetic moments of odd-mass nuclei it is customary to follow the approach of Schmidt and to assume that the addition of a pair of like particles occupying the same orbit has no effect upon the properties of the nucleus. It is indeed true that the symmetry properties of the low-lying states, particularly the spins, are not changed by such an addition; but it is the purpose of this note to point out that for properties like the magnetic moment and the quadrupole moment, it is essential to consider *all* particles outside the completely occupied levels, whether these particles pair off or not.

In a recent paper Mizushima and Umezawa (1952) have shown that for a number of light nuclei better agreement between measured and calculated values of the magnetic moment can be obtained by taking into account the interaction between neutrons and protons in *jj*-coupling. They assume that each particle outside the core of closed shells possesses a magnetic moment equal to the usual one-particle value as used in the Schmidt diagram (and to which we shall refer simply as Schmidt values); but they combine all such particles, both neutrons and protons, into states classified by means of the isotopic spin T and the resultant angular momentum J. Energy calculations indicate (Flowers and Edmunds 1952) that for light nuclei, and for forces of reasonably short range, the lowest states are usually those having the smallest T consistent with the known $M_T=\frac{1}{2}(N-P)$, where N and P are the numbers of neutrons and protons outside the core. If the configuration is known, and the resultant angular momentum, it is then possible to calculate what the resultant magnetic moment should be. In general, as found by Mizushima and Umezawa, the values so obtained differ from the simple Schmidt limits.

---

* Now at the Atomic Energy Research Establishment, Harwell.
† Communicated by Professor R. E. Peierls, F.R.S.

Making use of the tables of fractional parentage coefficients calculated by Edmonds and Flowers (1952), which take into account also the new classification of states in jj-coupling according to their behaviour under symplectic transformation, the present author has been able to show that for three particles in the configuration j^3, in the usual ground state with $T=\frac{1}{2}$, $J=j$, and seniority 1, which arises from attractive forces of reasonably short range, the magnetic moment is given by

$$\left.\begin{aligned} &\mu=(6j+6)^{-1}\{(2j-1)\mu_n+(4j+5)\mu_p\} \text{ for an odd proton} \\ \text{and} \\ &\mu=(6j+6)^{-1}\{(4j+5)\mu_n+(2j-1)\mu_p\} \text{ for an odd neutron} \end{aligned}\right\} \quad . \quad . \quad (1)$$

where μ_n, μ_p are the Schmidt moments of neutron and proton, respectively, appropriate to the given values of l and j. Similar formulae exist for more than 3 particles, but for these we shall state only numerical results.

Table 1. Magnetic Moments of the Light Nuclei of Odd Mass

Nucleus	Configuration	Isotopic spin	Schmidt	Individual	Observed
$^{7}_{3}Li_4$	$(p_{3/2})^3$	$\frac{1}{2}$	3·79	3·04	3·26
$^{7}_{4}Be_3$	$(p_{3/2})^3$	$\frac{1}{2}$	−1·91	−1·16	?
$^{9}_{4}Be_5$	$(p_{3/2})^{-3}$	$\frac{1}{2}$	−1·91	−1·16	−1·18
$^{11}_{5}B_6$	$(p_{3/2})^{-1}$	$\frac{1}{2}$	3·79	3·79	2·69
	$(p_{3/2})^{-3}(p_{1/2})_n^2$	$\frac{1}{2}$	3·79	3·04	
$^{13}_{6}C_7$	$(p_{1/2})^1$	$\frac{1}{2}$	0·64	0·64	0·70
$^{15}_{7}N_8$	$(p_{1/2})^{-1}$	$\frac{1}{2}$	−0·26	−0·26	−0·28
$^{17}_{8}O_9$	$(d_{5/2})^1$	$\frac{1}{2}$	−1·91	−1·91	−1·89
$^{19}_{9}F_{10}$	$(d_{5/2})^2 2s_{1/2}$	$\frac{1}{2}$	2·79	2·79	2·63
$^{21}_{10}Ne_{11}$	$(d_{5/2})^5$	$\frac{1}{2}$	−1·91	−1·27	<0
$^{23}_{11}Na_{12}$	$(d_{5/2})^{-5}$	$\frac{1}{2}$	(2·87)	$\approx$2·0	2·22
$^{25}_{12}Mg_{13}$	$(d_{5/2})^{-3}$	$\frac{1}{2}$	−1·91	−0·64	−0·96
$^{27}_{13}Al_{14}$	$(d_{5/2})^{-1}$	$\frac{1}{2}$	4·79	4·79	3·64
	$(d_{5/2})^{-3}(s_{1/2})_n^2$	$\frac{1}{2}$	4·79	3·52	
$^{35}_{17}Cl_{18}$	$(d_{3/2})^3$	$\frac{1}{2}$	0·13	0·26	0·82
$^{37}_{17}Cl_{20}$	$(d_{3/2})^{-3}$	$\frac{3}{2}$	0·13	0·13	0·68
$^{45}_{21}Sc_{24}$	$(f_{7/2})^5$	$\frac{3}{2}$	5·79	5·10	4·76
$^{55}_{25}Mn_{30}$	$(f_{7/2})_p^{-3}(p_{3/2})_n^2$	—	(4·13)	$\approx$3·6	3·47

The results are shown in table 1 for odd mass nuclei of mass number $A\leqslant 55$. In all cases the experimental moments are taken from the recent compilation by Klinkenberg (1952). The following features are worthy of notice. The nuclei ^{13}C, ^{15}N, ^{17}O consisting of fully occupied orbits plus or minus one particle, have moments in excellent agreement with the Schmidt values. On the other hand, ^{11}B, and ^{27}Al, which are usually thought of as closed shell ± 1 nuclei, are not in such good agreement. In the case of ^{11}B one can improve matters by assuming that two neutrons are raised from the $p_{3/2}$ orbit into the nearby $p_{1/2}$ orbit, thus implying (not very surprisingly) that for such a light nucleus jj-coupling does not

strictly apply. Concerning ^{27}Al, it is known that the single-particle levels $d_{5/2}$ and $2s_{1/2}$ lie close together, and it is seen that the configuration $(d_{5/2})^{-3}(s_{1/2})^2$ now proposed for this nucleus yields a magnetic moment in good accord with experiment. It would clearly be of interest to obtain measured values for ^{11}C and ^{13}N in this connection. The nuclei ^{23}Na and ^{55}Mn are two of the three spin exceptions to the jj-coupling model, having $J=j-1$ rather than $J=j$ in the ground state. For these nuclei there properly exist no Schmidt limits, but the values shown in brackets in the fourth column are those derived from considering the proton configuration only, namely

$$\mu=\frac{j-1}{j}\mu_{\text{Schmidt}}.$$

The corresponding values in the fifth column have not been calculated completely because the necessary fractional parentage coefficients are not available, and are thus only rough estimates. For ^{25}Mg, Mizushima and Umezawa were able to state only that the magnetic moment should lie between $-1{\cdot}06$ and $2{\cdot}76$. Our unique value of $-0{\cdot}64$ is that appropriate to the state of seniority 1. The above authors calculate $-0{\cdot}48$ for the $T=\frac{1}{2}$ state of ^{35}Cl and $0{\cdot}80$ for the $T=3/2$ state, and conclude from the measured moment that this nucleus has $T=3/2$ in the ground state. Their values, however, appear to be in error in this case ; it is clear from formula (1) that since μ_n and μ_p are both positive for a $d_{3/2}$ orbit, the magnetic moment of the $T=\frac{1}{2}$ state is necessarily positive, as indeed experiment shows.

In all cases, values of the magnetic moment based upon the individual particle model are in much better accord with experiment than those based upon the naive Schmidt model. The importance of this result lies in the fact that, under favourable conditions, it is now possible to deduce from the measured moment not only the orbit of the odd particle, but the whole configuration giving rise to the moment. Moreover, it may not be necessary to appeal to quantized motions of the core, of the kind proposed by Aage Bohr (1952), or to large exchange moments as considered recently by Russek and Spruch (1952), to explain the very large deviations from the Schmidt limits. For the heavier nuclei, it is expected that a similar result will hold, and that much of the deviation from the Schmidt values can be explained in terms of the coupling between neutron and proton configurations. The case of ^{209}Bi, however, remains unsolved.

Regarding the electric quadrupole moments of odd mass nuclei, Rosenfeld (1951) has pointed out three striking features : (i) the quadrupole moment of a nucleus containing one hole (apart from filled levels) is approximately equal, but of opposite sign, to that of the corresponding nucleus having one particle in this level ; (ii) the quadrupole moment of an odd-neutron nucleus is roughly the same as that of a nearby odd-proton nucleus ; and (iii) heavy nuclei with $100<A<200$ have with very few

exceptions quadrupole moments about 10 times larger than one would expect on the basis of a single particle model.

The first feature follows immediately from the theory of holes, and we shall concern ourselves only with (ii) and (iii). We have calculated the quadrupole moments of configurations j^3 in the states $T=\frac{1}{2}$, $J=j$, and seniority 1, taking as individual particle values $Q_p=1$ and $Q_n=0$. We find

$$Q(1p+2n)=(4j+5)/(6j+6) \quad \text{and} \quad Q(1n+2p)=(2j+7)/(6j+6). \quad . \quad (2)$$

These expressions give $Q \approx 0{\cdot}7$ in both cases for small values of j. Thus the quadrupole moment "induced" upon the odd neutron by two protons is about equal to that of an odd proton in the presence of two neutrons, as observed by Rosenfeld.

The quadrupole moments of odd-neutron nuclei are therefore found to arise quite naturally from the coupling between neutrons and protons. It follows that a nucleus consisting of an odd neutron outside a *double* closed shell should have quadrupole moment zero (whatever the spin of the nucleus) for in this case there are no protons with which the neutron can readily interact. The only experimental evidence concerns ^{17}O which has $Q=-0{\cdot}005\times10^{-24}$ cm^2, or about 10–20 times less than those of nearby nuclei. It would be interesting to have experimental values for ^{91}Zr, and ^{209}Pb.

Further, we may enquire what effect the addition of two neutrons to an odd-proton nucleus may have upon the quadrupole moment. According to (2), the moment should be reduced by about 0·7. In table 2 are presented all such ratios known for masses less than 100 : all are found to be in the right direction and to be surprisingly consistent with the theoretical factor bearing in mind that in some cases the neutrons and protons occupy different orbits.

Table 2. Quadrupole Moments of Odd Mass Isotopes Differing by Two Neutrons

Nucleus	Proton configuration	Added neutron pair	$Q\times10^{24}$ cm^2	Ratio
$^{35}_{17}Cl$	$(d_{3/2})^1$	$(d_{3/2})^2$	−0·07894	0·79
$^{37}_{17}Cl$			−0·06213	
$^{63}_{29}Cu$	$(p_{3/2})^1$	$(p_{3/2})^2$ or $(f_{5/2})^2$	−0·13	0·92
$^{65}_{29}Cu$			−0·12	
$^{69}_{31}Ga$	$(p_{3/2})^{-1}$	$(f_{5/2})^2$ or $(p_{1/2})^2$	+0·2318	0·63
$^{71}_{31}Ga$			+0·1461	
$^{79}_{35}Br$	$(p_{3/2})^{-1}$	$(p_{1/2})^2$ or $(g_{9/2})^2$	+0·26	0·8
$^{81}_{35}Br$			+0·21	

Finally, concerning the third feature emphasized by Rosenfeld, it is clear that odd-neutron nuclei should have large quadrupole moments only when the *protons* are entering levels of high angular momentum.

There is only one odd-neutron nucleus known to have an excessively large Q: this is ^{173}Yb with a neutron configuration $(f_{5/2})^3$ according to Klinkenberg, and the proton configuration of this nucleus appears to contain either 6 or 4 holes in the $h_{11/2}$ orbit. We estimate very roughly that this could cause an increase in the Q for a single $f_{5/2}$ particle by a factor of as much as 5, which is at least of the right order of magnitude. Similarly, the large quadrupole moments observed for odd-proton nuclei in the mass region $A \approx 150$ all seem to be connected with the pairwise filling of the $h_{11/2}$ orbits by protons. One would expect similar results for the transuranic nuclei where the $i_{13/2}$ proton levels may be filling in pairs.

This work will appear in greater detail elsewhere, together with applications of the methods used here to the calculation of transition probabilities for electromagnetic radiation. It is a pleasure to thank Professor R. E. Peierls, F.R.S., for the interest he has shown in the work. The paper was written while the author was on leave of absence from the Atomic Energy Research Establishment, Harwell, and the Director's permission to publish it is gratefully acknowledged.

References

Bohr, A., 1951, *Phys. Rev.*, **81,** 134.
Edmonds, A. R., and Flowers, B. H., 1952, *Proc. Roy. Soc.* A, **214,** 514.
Flowers, B. H., and Edmonds, A. R., 1952, *A.E.R.E. T/R* 917.
Klinkenberg, P. F. A., 1952, *Rev. Mod. Phys.*, **24,** 63.
Mizushima, M., and Umezawa, M., 1952, *Phys. Rev.*, **85,** 37.
Rosenfeld, L., 1951, *Physica*, **17,** 461.
Russek, A., and Spruch, L., 1952, *Phys. Rev.*, **87,** 1111.

CXXXIV. CORRESPONDENCE

A Counter-Hodoscope Study of Associated Penetrating Particles Underground

By B. Leontic and A. W. Wolfendale
The Physical Laboratory, University of Manchester*

[Received September 29, 1952]

The production of pairs of associated penetrating particles (APP) has been examined using a counter hodoscope in a cave at Stockport under 26 metres water equivalent of rock.

The apparatus, shown in fig. 1, consisted of 18 counters arranged in two trays AB and C. The master pulse required to trigger the hodoscope was produced when at least one counter from each of the groups A, B and C, was discharged. Each counter then operated a corresponding neon lamp. The counters in the lower tray were separated by 1 cm lead slats in order to reduce the effects of knock-on electrons.

Events in which two counters in group C and one counter in each of groups A and B were discharged, were examined. Events have been observed which we interpret as pairs of APP originating in the roof and in Σ. Accidental coincidences, due to the passage of two unassociated particles through the apparatus, were negligible since the resolving time of the coincidence circuit was very short (1 μsec). The events are classified as follows : adjacent pairs, in which adjacent counters were discharged in C and AB ; separated pairs in which the counters discharged were not adjacent and the trajectories show that the particles diverged from a point in the roof or in Σ ; parallel pairs, where the trajectories are nearly parallel showing that the particles came from the roof. Our results are given in the table. The number of adjacent APP's has been corrected for the effects of successive knock-ons in the two trays, by using the knock-on frequencies observed for the individual trays.

The relatively small number of separated pairs compared with that of adjacent pairs is to be expected from the known approximate angular distribution of the secondary about the direction of the primary, as observed in cloud chamber experiments (Braddick *et al.* 1951) and the geometrical bias of the split-tray arrangement.

The absorption of particles from the roof, measured by putting $\Sigma=0$ and comparing the rates with $t=16$ cm and $t=6$ cm, leads to a value for the interaction length of the secondary particles

$$L=14\pm4 \text{ cm Pb.}$$

* Communicated by Professor P. M. S. Blackett, F.R.S.

This value agrees with that calculated by us from the results given by Amaldi *et al.* (1952) which lead to

$$L=10\pm4 \text{ cm Pb.}$$

The conclusion from this experiment is that the secondary is a nuclear interacting particle—possibly a π-meson.

Fig. 1

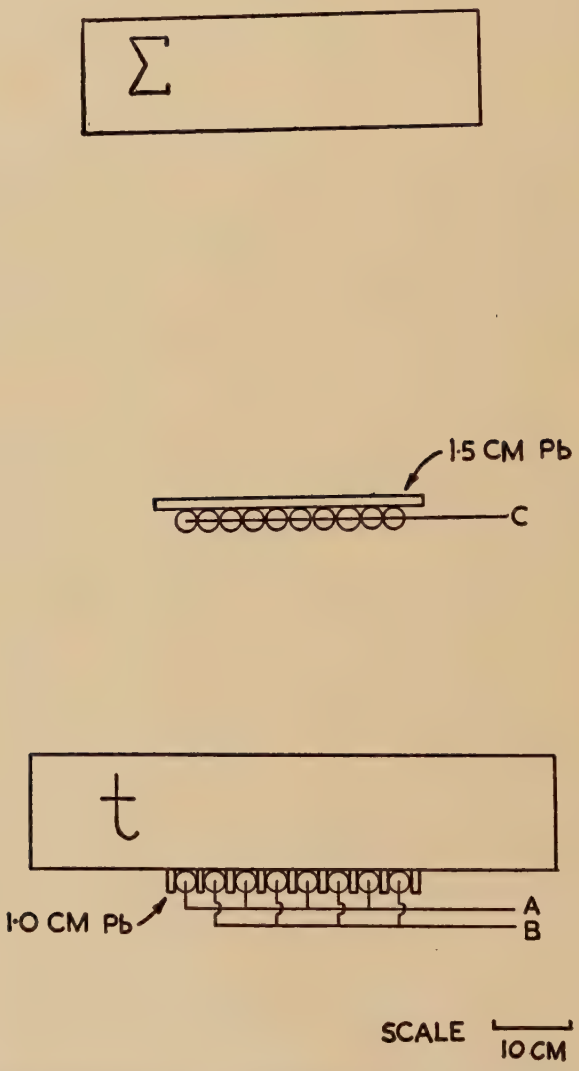

Appapillai, Mailvaganam and Wolfendale, in work not yet published, have found cloud chamber evidence in support of this conclusion.

The lack of sufficiently accurate knowledge of the angular distribution of the secondary about the direction of the primary makes it impossible to derive a cross-section for production.

Σ (cm Pb)	t (cm Pb)	Time (hours)	Number of adjacent coinci-dences	Corrected number of adjacent pairs	Separated pairs	Parallel pairs
15	16	448	221	82	4	0
15	6	253	274	196	17	5
0	16	383	219	101	4	2
0	6	330	321	219	11	14

Fig. 2

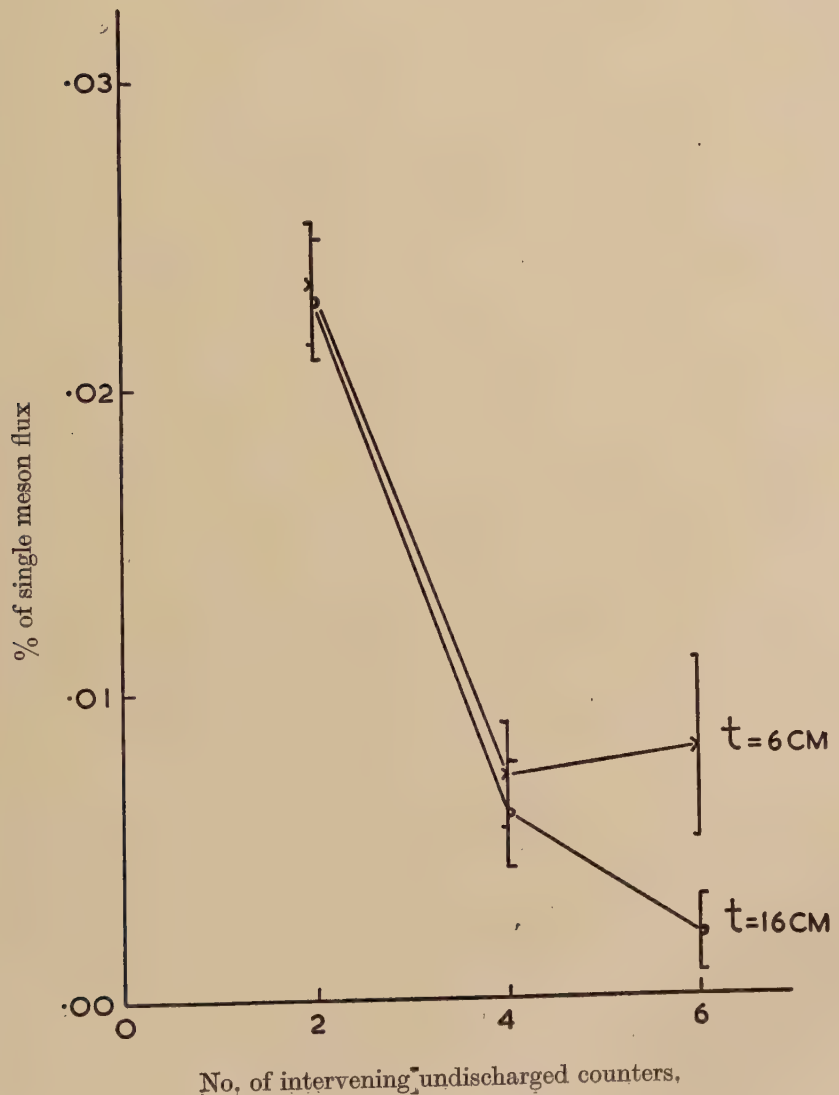

Events have also been recorded in which one counter in C and two non-adjacent counters in AB were discharged. Similar events have been observed by George and Trent (1951) who ascribe them to the production of APP's. An alternative explanation in terms of a simpler phenomenon is given here.

Figure 2 shows the distribution of the counting rate of these 3-fold coincidences as a function of the number of intervening undischarged counters in the AB tray (simple geometrical corrections have been applied to the rates). It will be seen that the rates for $t=6$ cm Pb and $t=16$ cm Pb are virtually the same. The mechanism suggested for these events is that a penetrating meson produces near the bottom of t a knock-on shower from which low energy photons of energy in the region of 3 MEV penetrate the absorber and a counter is discharged by a locally produced Compton-recoil electron (c.f. Greisen (1949)). The number of photons crossing any counter will decrease with increasing distance from the parent meson and so the rate of events will decrease with increasing number of undischarged counters. An approximate theoretical analysis has been carried out which gives rough numerical agreement with the experimental result for both thicknesses of absorber.

A contribution to these events by the production of APP's in t is to be expected but this is small due to the relatively small number of secondaries emitted at large angles.

REFERENCES

AMALDI, E., CASTAGNOLI, C., GIGLI, A., and SCIUTI, S., 1952, *Nuovo Cimento*, **9**, 453.

BRADDICK, H. J. J., NASH, W. F., and WOLFENDALE, A. W., 1951, *Phil. Mag.*, **42**, 1277.

GEORGE, E. P., and TRENT, P. T., 1951, *Proc. Phys. Soc.* A, **64**, 1134.

GREISEN, K., 1949, *Phys. Rev.*, **75**, 1071.

The Existence of a Macroscopic Shear in the Transformation in Cobalt

By T. R. ANANTHARAMAN and J. W. CHRISTIAN
The Inorganic Chemistry Laboratory, Oxford*

[Received September 18, 1952]

A REGION of f.c.c. crystal may be transformed into a single crystal having a h.c.p. structure by the movement of an imperfect dislocation, of type $\frac{a}{6}\langle 112\rangle$, through every alternate plane of a series of $\{111\}$ planes. The martensitic transformations in cobalt and in iron-manganese alloys probably occur in this way, since half-dislocations are present in a stable

---

* Communicated by the Authors.

f.c.c. lattice at the boundaries of extended dislocations (stacking faults) in {111} planes. There are six possible ⟨110⟩ slip directions in a given set of {111} planes, and the corresponding $\frac{a}{2}\langle 110\rangle$ lattice dislocations will dissociate to give three different $\frac{a}{6}\langle 112\rangle$ dislocations in these planes. An identical atomic arrangement is produced by the motion of any one of these imperfect dislocations across a glide plane. Transformation might occur by the independent extension of stacking fault nuclei, assuming there are sufficient dislocations to give ~ 1 region of stacking fault on each atomic plane, or by the propagation of a half dislocation down a series of {111} planes. Bilby (1951) pointed out that the existence or non-existence of a macroscopic shear should be a valuable indication of the mode of reaction Independent extension of nuclei should produce random averaging over the three shear directions, giving zero macroscopic shear. If, however, the hexagonal crystal is produced from a single stacking fault nucleus, the Burger's vector of the transformation dislocation would be identical in a series of planes, and the formation of the crystal would involve a macroscopic shear of magnitude $\tan^{-1}(\sqrt{2}/4)$. This corresponds to the original proposal for transformation (Burgers 1934), and implies the production of plate-shaped hexagonal crystals with a definite habit plane, as in other martensitic transformations. Barrett and Hess (1952) have reported that such plates are visible in thermally polished cobalt, after cooling to room temperature.

We have observed the electropolished surface of a polycrystalline specimen of pure cobalt under the microscope, while heating in hydrogen through the transformation range. At about 415° C thin plates began to appear, the specimen surface being tilted about the line of intersection of the plates. The plates were similar in appearance to Neumann bands in iron, and although very narrow they could occasionally be seen to have a lenticular shape ; their number increased until transformation was complete. In a single grain there were at most four different directions of traces in the surface ; traces were often observed parallel to the sides of {111} cubic annealing twins. On cooling to room temperature the traces did not disappear completely, presumably because transformation in a polycrystalline specimen involves some non-reversible plastic deformation. The appearance of a typical microsection after heating and cooling is shown in fig. 1.

To identify the habit plane, both stereographic analysis and x-ray examination were used. In fig. 2 (*a*), a stereographic solution for the grain shown in fig. 1 is given ; the four trace directions are consistent with the habit plane being {111}. The same grain (~ 2 mm in diameter) was photographed in an oscillation camera using a narrow x-ray beam. By setting each trace vertical in turn, two hexagonal (00·1) poles were located exactly and the other two within a range of angles (because of the specimen thickness which limited the range of oscillation). The

results are shown in fig. 2 (*b*), and the (00·1) poles fall on the {111} poles of fig. 2 (*a*) to within 1°. It follows that a single cubic grain forms four sets of plate-like hexagonal crystals, the habit plane being {111}.

The observations appear to prove the existence of a macroscopic shear, and thus suggest that independent spreading of stacking fault nuclei cannot account for the transformation. This conclusion is supported by unpublished results we have obtained for the variation with grain size of the proportion of stacking faults in hexagonal cobalt. The mechanism of transformation is still undetermined : Bilby and Cottrell (1951) showed that internal climbing of an $\frac{a}{6}\langle 112\rangle$ dislocation is impossible in a f.c.c. lattice, and the calculations of Leibfried (1950) and Nabarro (1951) show that the reflexion mechanism (Christian 1951) is very improbable.

Fig. 1

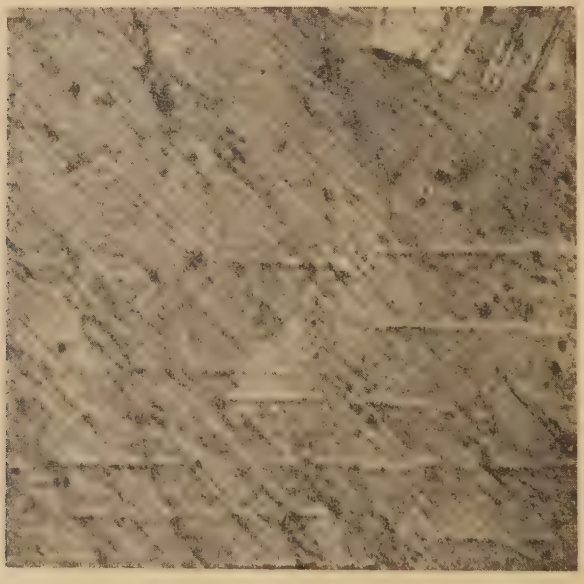

Surface of electropolished cobalt after heating and cooling through the transformation. ×900.

An alternative possibility, suggested to us by Dr. N. Thompson, is that the dislocation movements would be random in a strain-free material, but have locally preferred directions in our experiments, because of varying internal shear stresses. We do not think this very probable, since in many regions of our photographs three intersecting sets of plates are visible, but it is obviously important to establish whether there is a macroscopic shear when a single crystal transforms. The successful production of single crystals of hexagonal cobalt (e.g. Myers and Sucksmith 1951) implies that the dislocation movements can be confined to

one set of {111} planes, but there is no evidence whether or not the relative movements of these planes occur randomly in the possible ⟨112⟩ directions.

Fig. 2

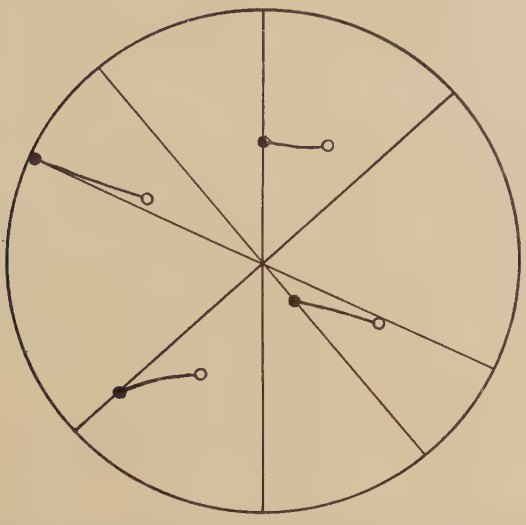

(*a*) Stereographic projection of area shown in fig. 1. Lines are normal to trace directions, open circles are {111} poles of standard projection, and filled circles are {111} poles after rotation through 36°.

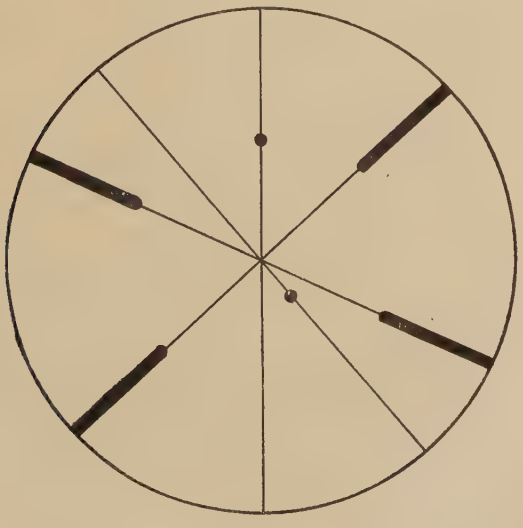

(*b*) Position of (00·1) poles from oscillation photographs. Two of the poles could only be located within the angular range represented by the thickened lines.

In some martensitic transformations wide plate-like crystals are formed, and the transformation is complete in a small temperature interval. It seems probable that in these cases either or both of the following conditions must be satisfied: (1) the transformation shear is small, so that deformation of the matrix is not unduly large; (2) the transformation can proceed by reversing the shear, allowing the strain in the matrix to be periodically relaxed. Neither condition is fulfilled in cobalt, so that the martensitic plates are thin, and complete transformation is very difficult. In fine-grained cobalt, it seems virtually impossible to transform more than $\sim 70\%$ of the metal, except by cold-working. There are so many possible explanations for the faulted structure of hexagonal cobalt that we shall not discuss this here.

We wish to thank Dr. B. A. Bilby for helpful discussion, and Dr. W. Hume-Rothery, F.R.S. for his interest.

References

Bilby, B. A., 1951, *Brit. J. Appl. Phys.*, **2**, 316.
Burgers, W. G., 1934, *Physica*, **1**, 561.
Christian, J. W., 1951, *Proc. Roy. Soc.* A, **206**, 51.
Cottrell, A. H., and Bilby, B. A., 1951, *Phil. Mag.*, **42**, 573.
Hess, J. B., and Barrett, C. S., 1952, *J. Metals*, **4**, 645.
Leibfried, G., 1950, *Z. Physik*, **126**, 790.
Myers, H. P., and Sucksmith, W., 1951, *Proc. Roy. Soc.* A, **207**, 427.
Nabarro, F. R. N., 1951, *Proc. Roy. Soc.* A, **209**, 278.

Note on Thermal Radiation at Low Temperatures

By D. Bijl
Clarendon Laboratory, Oxford*

[Received October 3, 1952]

A fundamental result of statistical mechanics and quantum theory is the conclusion that, for any system at sufficiently low temperatures, the usual thermodynamic concepts (in which energy and temperature are regarded as simultaneously determinable quantities) become meaningless. Statistical concepts, however, remain significant (Tolman 1938).

The case of an ideal crystal was discussed many years ago (Planck 1921, Schaefer 1921) and it was clear that this situation could in general be expected only at exceedingly low temperatures at present inaccessible. In rather exceptional cases (a cube of diamond with edges of 0·01 cm) these temperatures are within the range attainable by adiabatic demagnetization (Simon 1939).

---

* Communicated by the Author.

The case of thermal radiation enclosed in a cavity can be discussed in exactly the same way as an ideal crystal. This does not seem to have been done and it is the purpose of this note to fill this gap.

Let us consider the electromagnetic radiation enclosed in a cavity in thermodynamic equilibrium at a temperature T. Treating this radiation in the usual way as a system of harmonic oscillators we can at once write down the partition function of the radiation. We have

$$\log Z = -\sum_i \log \{1-\exp(h\nu_i/kT)\}. \quad . \quad . \quad . \quad . \quad . \quad (1)$$

The summation must be carried out over all the electromagnetic modes of vibration of the cavity, the energy is measured relative to the state of the system in which every oscillator is in its lowest state.

With increasing quantum numbers the frequency density increases, ultimately becoming practically continuous. At sufficiently high temperatures these high states virtually determine the properties of the system. In this case it is possible to determine a continuous frequency density function (which is independent of the shape of the cavity) and the summation in (1) can be replaced by an integration. This leads to a manageable expression for $\log Z$ and the subsequent straightforward calculations of thermodynamic quantities can be found in any book on statistical mechanics.

This procedure is certainly legitimate if for any pair of adjacent frequencies ν' and ν''

$$|\, h(\nu'-\nu'')/kT \,| \ll 1. \quad . \quad . \quad . \quad . \quad . \quad . \quad . \quad (2)$$

Let us consider the lowest possible frequencies in some details. These are of the order $q/v^{1/3}$; q is the velocity of propagation of the radiation in the enclosure which is of the order of the velocity of light *in vacuo*, and v is the volume of the enclosure. The differences $\nu'-\nu''$ are also of the same order of magnitude. The actual values of the frequencies depend on the shape of the enclosure, but here we need consider only the order of magnitude.

For these frequencies condition (2) becomes

$$T \gg hq/kv^{1/3},$$

where $hq/k \simeq 1$ cm degree. For a cavity with a volume of 1 cm^3 the usual procedure is certainly correct for temperatures much higher than 1° K. At temperatures of the order of 1° K or lower condition (2) is no longer fulfilled for the lowest frequencies. In this case, however, these frequencies virtually determine the properties of the system, as follows from the expression for their average number $\bar{n}_i$ in a state i

$$\bar{n}_i = 1/\{\exp(h\nu_i/kT)-1\}.$$

For the lowest state of our example is of the order 1 and for higher states $\bar{n}_i$ decreases rapidly. The system behaves as if the number of degrees of freedom is small. Consequently thermodynamic considerations which are important for discussing the properties of thermal radiation at

high temperatures are no longer relevant, and typical results of the thermodynamic treatment such as Kirchhoff's, Wien's and Stefan's law are no longer significant. All properties depend upon the shape of the enclosure, and, moreover, deviations from Planck's law must be expected.

An entirely similar analysis has been given by Planck and Schaefer for an ideal crystal. In this case the velocity q is about a factor 10^5 smaller. Therefore the temperature below which thermodynamic concepts break down is a factor 10^5 smaller than in the case of thermal radiation in an enclosure of the same size as the crystal.

I am indebted to the Pressed Steel Company Limited for a Research Fellowship during the tenure of which this note was written.

References

Planck, M., 1923, *Vorlesungen über die Theorie der Wärmestrahlung*. Leipzig, 5th edition, 184.
Schaefer, C., 1921, *Zeit. f. Phys.*, **7**, 287.
Simon, F., 1939, *Science Progress*, No. 133.
Tolman, R. C., 1938, *The Principles of Statistical Mechanics* (Oxford) Chap. xiv.

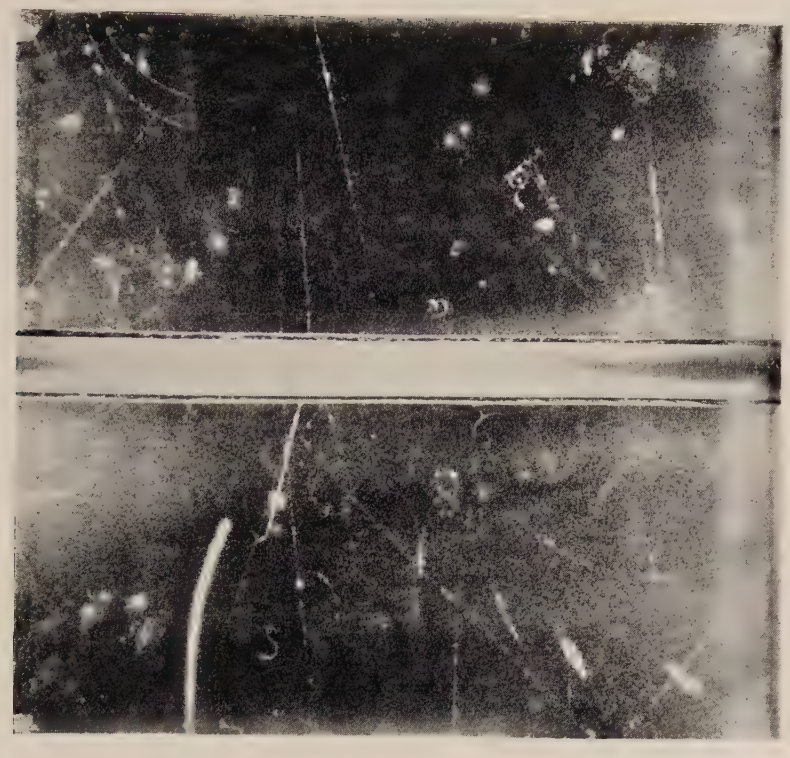

(*a*) Decay event 3. The heavily ionizing particle from the lead plate decays in the gas and the charged secondary particle travels away from the camera out of the illuminated region. There is marked distortion of the tracks (see table 2).

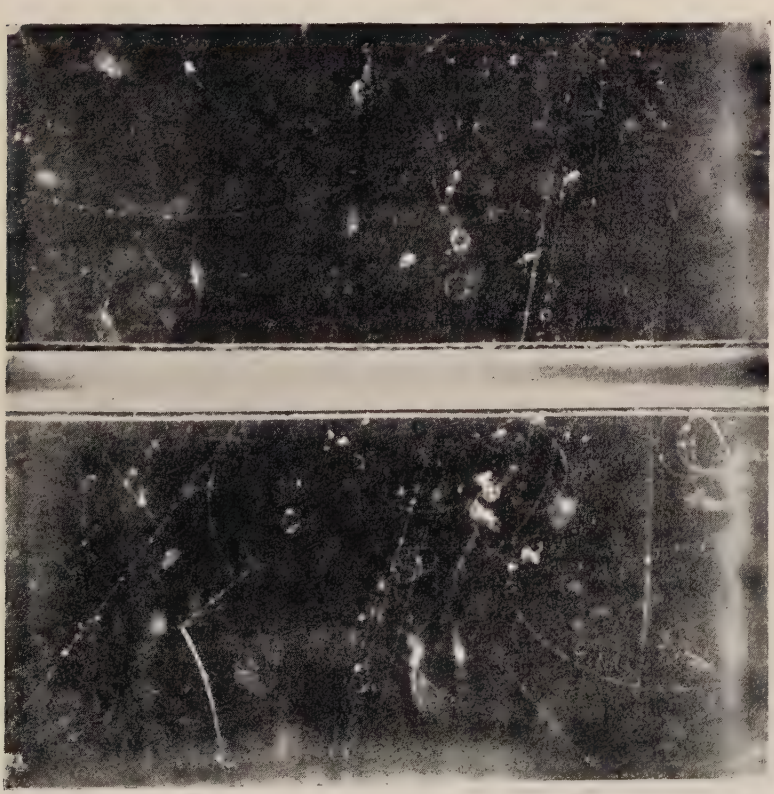

(*b*) Decay event 4. The primary particle comes from behind the cloud chamber and decays into a slow light meson in the lower half of the chamber. Interpretation as the decay of an upward moving V_2^0 is also possible (see text).

(*a*) Decay event 6. A heavily ionizing negative particle decays after a flight in the chamber of $2{\cdot}3\times10^{-9}$ sec. The secondary charged particle has a specific ionization $<2{\cdot}5\times$ minimum.

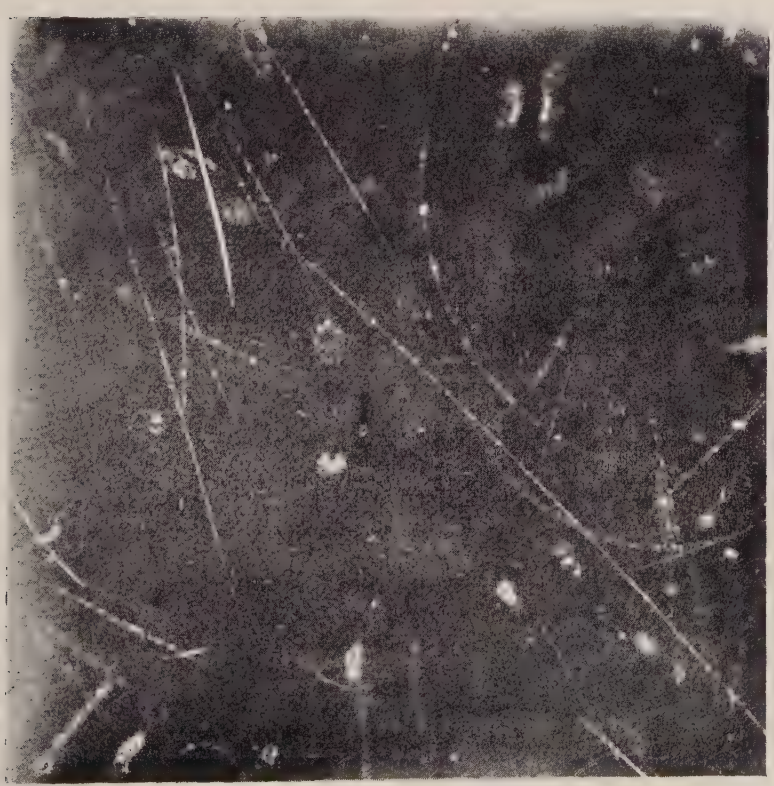

(*b*) Decay event 11. A lightly ionizing positive particle decays after a flight in the chamber of $<4{\cdot}1\times10^{-10}$ sec. The charged secondary has specific ionization $<2{\cdot}5\times$ minimum.

Figs. 1–4

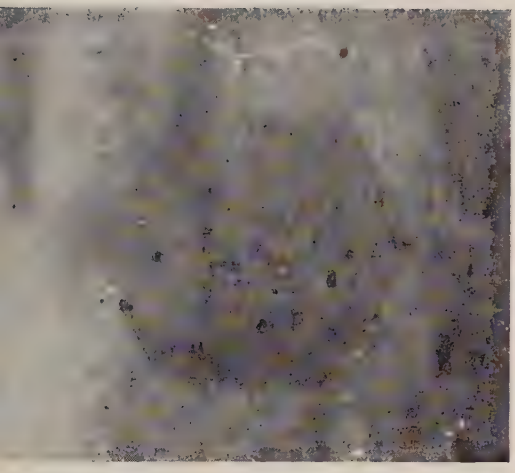

2

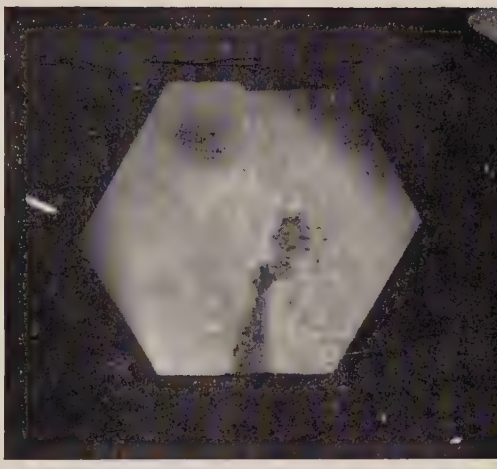

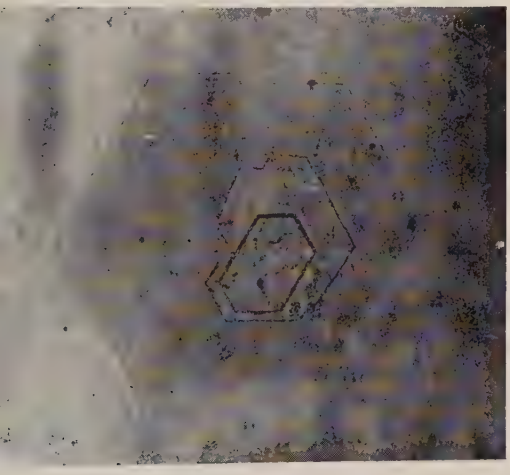

4

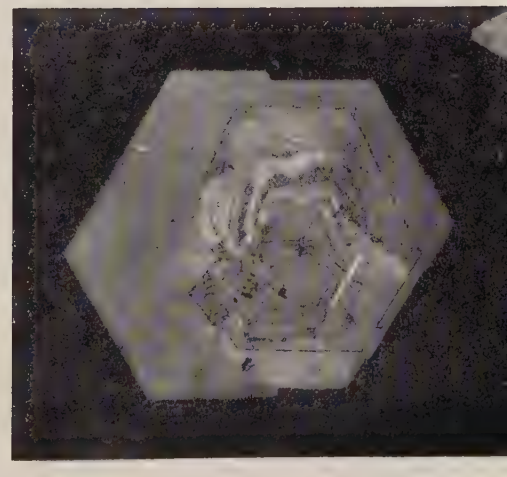

Figs. 5–8

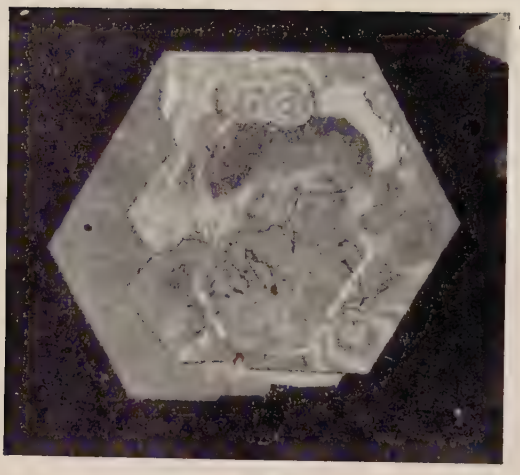

6

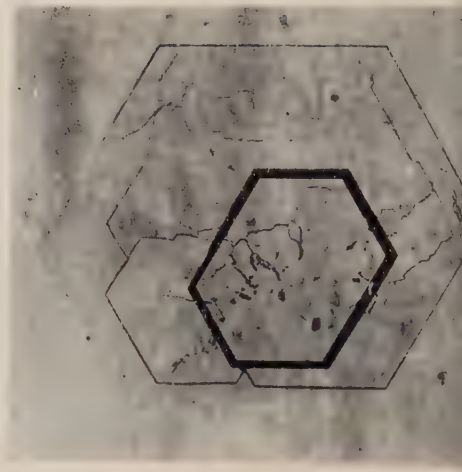

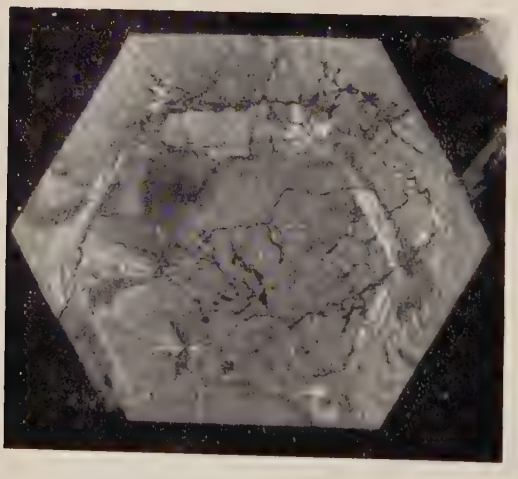

8

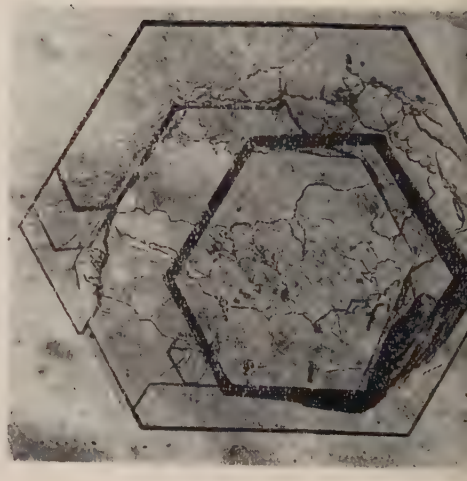

Figs. 9–14

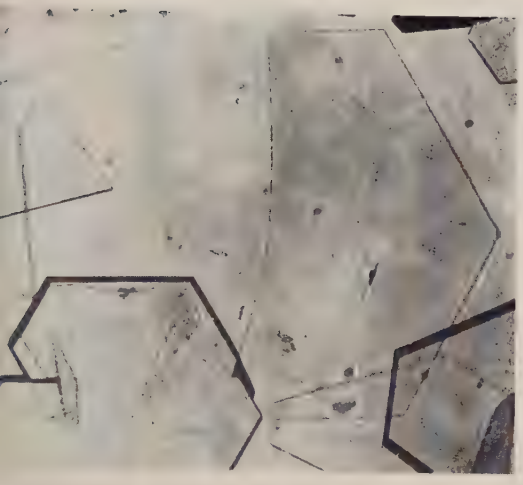

10

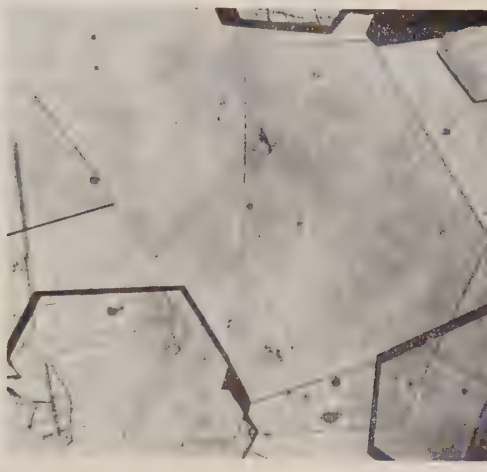

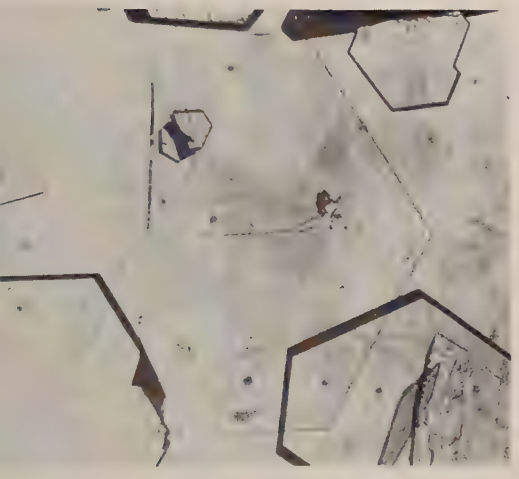

12

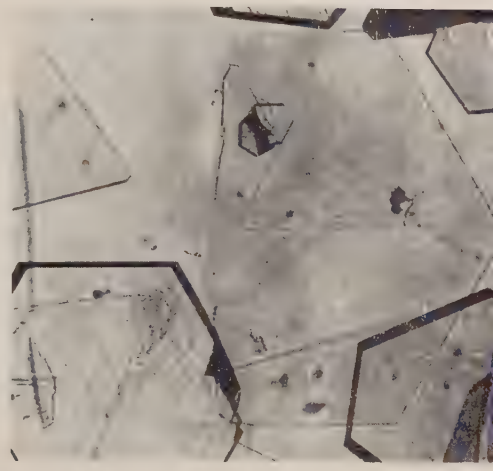

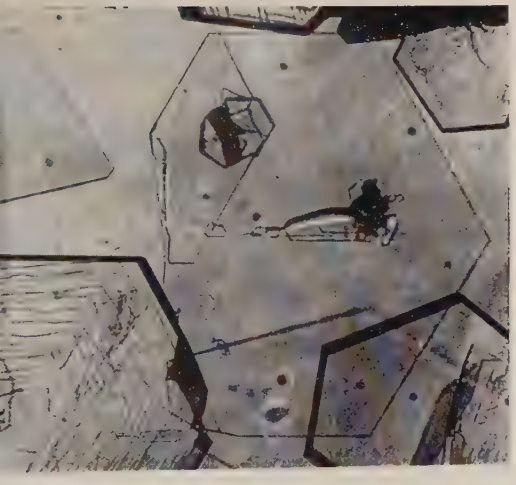

14

Figs. 15–20

15

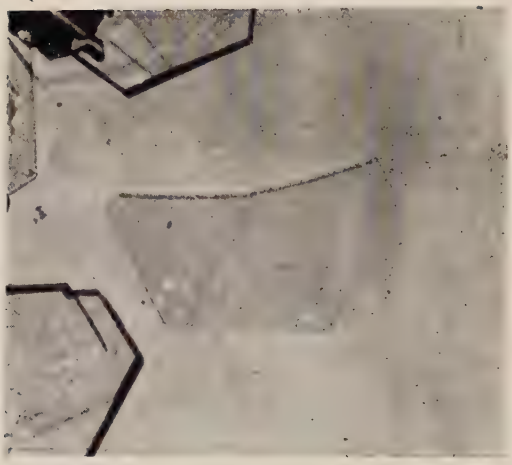

16

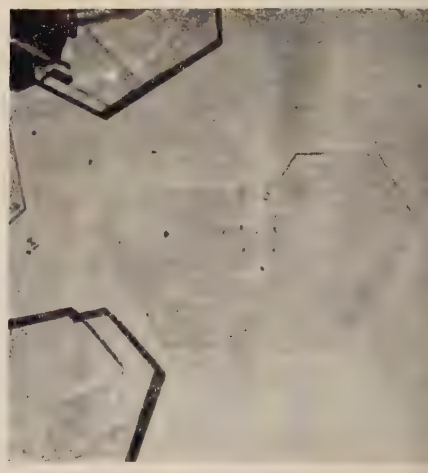

17

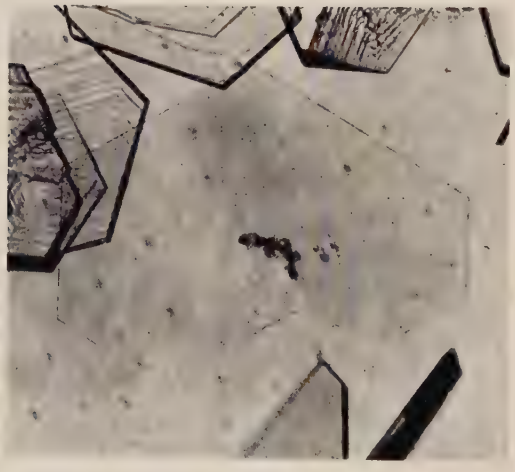

18

19

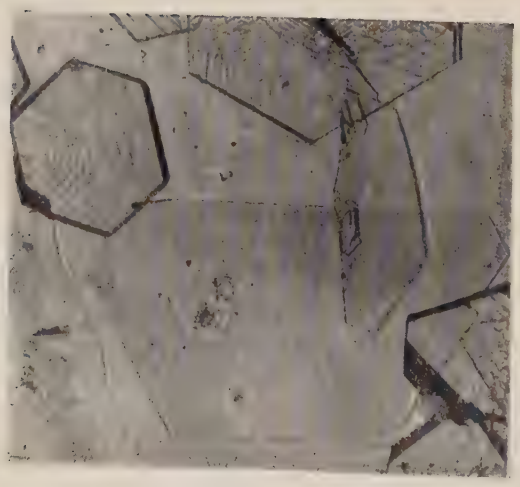

20

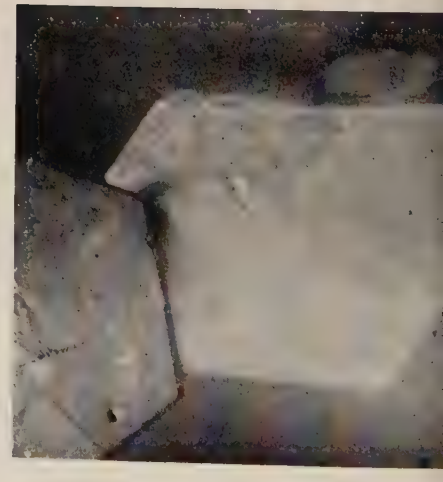

INDEX TO VOL. XLIII.

END OF THE FORTY-THIRD VOLUME

Printed by Taylor & Francis, Ltd.
Red Lion Court, Fleet Street, London, E.C.4